

**Synergistic impact of simultaneously assimilating radar- and radiometer-based soil moisture retrievals on the performance of numerical weather prediction systems**

Yonghwan Kwon<sup>a\*</sup>, Sanghee Jun<sup>a</sup>, Hyunglok Kim<sup>b</sup>, Kyung-Hee Seol<sup>a</sup>, In-Hyuk Kwon<sup>a</sup>,  
Eunkyu Kim<sup>a</sup>, Sujeong Cho<sup>a</sup>

<sup>a</sup>Korea Institute of Atmospheric Prediction System, Seoul 07071, South Korea

<sup>b</sup>~~Department of Environment and Energy Engineering School of Earth Sciences and Environmental Engineering~~, Gwangju Institute of Science and Technology (GIST), Gwangju 61005, South Korea

\*To whom correspondence may be addressed (yhwon@kiaps.org).

Revised manuscript submitted to *Hydrology and Earth System Sciences*

Submitted to *Journal of Hydrology*

1 **Abstract**

2 The combined use of independent soil moisture data from radar and radiometer  
3 measurements in data assimilation (DA) systems is expected to yield synergistic performance  
4 gains due to their complementary strengths. This study evaluates the impact of  
5 simultaneously assimilating soil moisture (~~SM~~) retrievals from ASCAT (Advanced  
6 SCATterometer) and SMAP (Soil Moisture Active Passive) into the Korean Integrated Model  
7 (KIM) using a weakly coupled ~~data assimilation (DA)~~ framework based on the National  
8 Aeronautics and Space Administration's Land Information System (LIS). The Noah land  
9 surface model (LSM) within LIS, which is the same as that used in KIM, is used to simulate  
10 land surface states and assimilate soil moisture~~SM~~ retrievals. The impact of soil moisture~~SM~~  
11 DA is evaluated using independent reference datasets, assessing its influence on soil  
12 moisture~~SM~~ analysis and numerical weather prediction (~~NWP~~) performance. Overall,  
13 assimilating ASCAT or SMAP soil moisture~~SM~~ data into the LSM improves global soil  
14 moisture~~SM~~ analysis accuracy by 4.0% and 10.5%, respectively, compared to the control  
15 case without soil moisture~~SM~~ DA, achieving the most significant enhancements in croplands.  
16 Relative to single-sensor soil moisture~~SM~~ DA, multi-sensor soil moisture~~SM~~ DA yields more  
17 balanced skill enhancements for both specific humidity and air temperature analyses and  
18 forecasts. The most pronounced synergistic improvements by simultaneously assimilating  
19 both soil moisture~~SM~~ products are observed in the 2-m air temperature analysis and forecast,  
20 especially when both soil moisture~~SM~~ products have a positive impact. The results also  
21 demonstrate that precipitation forecast skill, particularly in predicting precipitation events,  
22 can be enhanced by constraining the modeled soil moisture~~SM~~ with multiple soil moisture~~SM~~

23 retrievals from different sources. This paper discusses remaining issues for future studies to  
24 further improve the weather prediction performance of the KIM-LIS multi-sensor soil  
25 moistureSM DA system.

26  
27 **Key words:** soil moisture data assimilation, multi-sensor, Korean Integrated Model, Land  
28 Information System, numerical weather prediction, land-atmosphere coupled system

## 29 30 **1. Introduction**

31 Soil moisture (~~SM~~) is one of the decisive land surface state variables that control land-  
32 atmosphere interactions associated with water and energy cycles (Gentine et al., 2011; Koster  
33 et al., 2004; Tuttle and Salvucci, 2016) and that determine surface water infiltration,  
34 percolation, and runoff (Assouline, 2013; Orth and Seneviratne, 2013). Many studies  
35 underline the importance of accurate knowledge of the spatial and temporal soil moistureSM  
36 variability for various hydrometeorological applications (e.g., Jalilvand et al., 2019; Shin and  
37 Jung, 2014; Wanders et al., 2014; Yuan et al., 2011). Because of the long-memory effect of  
38 soil moistureSM, proper soil moistureSM initialization is a prominent part of numerical  
39 weather prediction (NWP), particularly in the lower atmosphere (Dirmeyer and Halder, 2016;  
40 Drusch and Viterbo, 2007; Jun et al., 2021; Koster et al., 2010; Kwon et al., 2024; van den  
41 Hurk et al., 2012).

42 As a viable method to produce spatially and temporally complete, observation-constrained  
43 estimates of soil moistureSM profiles (Bolten et al., 2010; Reichle et al., 2002a), assimilating  
44 satellite-based soil moistureSM data into land surface models (LSMs) (~~hereafter SM-DA~~) has

45 been widely explored. Soil moisture<sup>SM</sup> data assimilation (DA) optimally merges remotely-  
46 sensed near-surface soil moisture<sup>SM</sup> observations with modeled soil moisture<sup>SM</sup> estimates  
47 based on their respective uncertainties (Kumar et al., 2008a; Reichle et al., 2008), and it can  
48 generate soil moisture<sup>SM</sup> estimates superior to either observations or models alone when the  
49 relative size of the uncertainties is properly characterized (Liu et al., 2011; Blyverket et al.,  
50 2019). A number of studies have applied soil moisture<sup>SM</sup> DA to improve flood and drought  
51 forecasts (e.g., Azimi et al., 2020; Gavahi et al., 2022; Laiolo et al., 2016), streamflow and  
52 runoff predictions (e.g., Baugh et al., 2020; Brocca et al., 2010; Lievens et al., 2016),  
53 irrigation characterization (e.g., Kwon et al., 2022; Nair and Indu, 2019), and evaporative  
54 flux estimates (e.g., Li et al., 2020; Pipunic et al., 2013). In particular, it has been  
55 demonstrated that the assimilation of satellite-based soil moisture<sup>SM</sup> retrievals into LSMs  
56 that are coupled to atmospheric models has a positive impact on weather forecast skill (e.g.,  
57 Draper and Reichle, 2019; Jun et al., 2021; Kwon et al., 2024; Lin and Pu, 2020; Lodh et al.,  
58 2022; Yin et al., 2019).

59 In addition to DA methods, a variety of alternative data fusion techniques have been  
60 widely explored to integrate soil moisture information from different sources, including  
61 remote sensing products, in-situ measurements, model simulations, and reanalysis datasets.  
62 One group of approaches relies on statistical methods (e.g., Min et al., 2022; Wang et al.,  
63 2021; Xie et al., 2022), such as unweighted averaging, linear weight fusion, and emergent  
64 constraint. Another group leverages machine learning (e.g., Huang et al., 2023; Lamichhane  
65 et al., 2025; Long et al., 2019; Zhang et al., 2022, Zeng et al., 2024) and deep learning  
66 techniques (e.g., Fuentes et al., 2022; Huang et al., 2022; Jiang et al., 2025; Singh and Gaurav,

67 2023; van der Schalie et al., 2018). These machine learning and deep learning approaches are  
68 rapidly gaining prominence because of their ability to incorporate diverse data sources and to  
69 capture complex, nonlinear relationships between datasets (Huang et al, 2022; Zeng et al.,  
70 2024). While different fusion approaches have distinct strengths and limitations, this study is  
71 devoted to DA methods, with the goal of improving model-based soil moisture estimates that  
72 interact with atmospheric processes in operational land-atmosphere coupled systems, thereby  
73 enhancing weather forecasts.

74 Microwave satellite systems provide useful information to retrieve surface soil  
75 moisture<sup>SM</sup> data at the global scale owing to their sensitivity to soil dielectric properties that  
76 mainly depend on soil water content and surface roughness (Schmugge et al., 1986). Many  
77 satellite soil moisture<sup>SM</sup> products have been generated from microwave observations at  
78 different frequencies (i.e., X, C and L-band) using various retrieval algorithms in different  
79 systems during the past several decades (Kumar et al., 2019; Nair and Indu, 2018). Among  
80 them, the Advanced SCATterometer (ASCAT) (e.g., Bartalis et al., 2007; Wagner et al.,  
81 2013), Soil Moisture Active Passive (SMAP) (e.g., Chan et al., 2018; O'Neill et al., 2021),  
82 and Soil Moisture and Ocean Salinity (SMOS) (e.g., Kerr et al., 2012) are relatively modern  
83 sensors that have been widely used in soil moisture<sup>SM</sup> DA studies (e.g., Blyverket et al.,  
84 2019; Jun et al., 2021; Khaki and Awange, 2019; Kolassa et al., 2017; Kumar et al., 2019;  
85 Kwon et al., 2022, 2024; Nair and Indu, 2019; Renzullo et al., 2014; Seo et al., 2021;  
86 Tangdamrongsub et al., 2020). In addition, most recently, Nguyen et al. (2025) have  
87 demonstrated the usefulness of soil moisture<sup>SM</sup> retrievals based on signals from the Global  
88 Navigation Satellite Systems. Kumar et al. (2019) report that soil moisture<sup>SM</sup> retrievals from

89 these modern sensors exhibit better performance in ~~data-assimilation~~ (DA) systems than those  
90 from older sensors.

91 The present study focuses on the use of the ASCAT and SMAP soil moisture<sup>SM</sup> products  
92 to improve modeled soil moisture<sup>SM</sup> estimates via assimilation. The ASCAT soil  
93 moisture<sup>SM</sup> product is generated from active microwave backscatter measurements at C-  
94 band (5.3 GHz) while the SMAP soil moisture<sup>SM</sup> data is based on passive microwave  
95 satellite systems, which utilize naturally emitted brightness temperature ( $T_B$ ) from the Earth's  
96 surface at an L-band (1.4 GHz) frequency. The C-band (i.e., ASCAT) and L-band (i.e.,  
97 SMAP) sensors typically provide soil moisture<sup>SM</sup> information for soil depth of 0–2 cm and  
98 0–5 cm, respectively (Kim et al., 2018). Compared to passive radiometers, radar observations  
99 (i.e., ASCAT) have smaller footprint sizes (i.e., finer spatial resolutions) and thus provide  
100 better spatial details of soil moisture<sup>SM</sup> (Nair and Indu, 2019). However, ASCAT has large  
101 uncertainties over regions of complex topography due to multiple scattering effects (Dobson  
102 and Ulaby, 1986). In contrast, radiometer (SMAP) observations are more sensitive to the  
103 presence of soil moisture<sup>SM</sup> than active radars (Kolassa et al., 2017), but the accuracy of  
104 their soil moisture<sup>SM</sup> products is strongly influenced by vegetation water content and surface  
105 temperature (Paloscia and Pampaloni, 1988).

106 Because of their complementary advantages, better soil moisture<sup>SM</sup> estimates can be  
107 obtained by assimilating the soil moisture<sup>SM</sup> data from multiple sources into the model-  
108 simulated soil moisture<sup>SM</sup> within a DA system. There have been some efforts to  
109 synergistically combine multiple active and passive observations for spatially and temporally  
110 improved soil moisture<sup>SM</sup> retrievals such as the European Space Agency Climate Change

111 Initiative (ESA CCI; Dorigo et al., 2017). In addition, one of the key goals of the SMAP  
112 mission was to utilize both active and passive sensors on the same satellite platform to  
113 retrieve high spatial resolution global near-surface soil moistureSM data with great accuracy  
114 (Entekhabi et al., 2010). However, due to mechanical malfunction of the SMAP radar,  
115 alternative radar observations from other satellites (e.g., Sentinel-1) have been combined with  
116 the SMAP radiometer data to maintain data continuity (Das et al., 2019). Meanwhile, Kolassa  
117 et al. (2017) and Nair and Indu (2019) demonstrate that simultaneously assimilating  
118 individual radar- and radiometer-based soil moistureSM retrievals achieves comparable  
119 overall performance to the assimilation of the blended (i.e., radar + radiometer) soil  
120 moistureSM products. In this study, we do not aim to retrieve or assimilate blended soil  
121 moistureSM products from multiple satellite measurements. Instead, we independently utilize  
122 soil moistureSM data from each sensor (i.e., ASCAT and SMAP) within a land-atmosphere  
123 coupled DA system, while also incorporating both observations separately rather than  
124 combining them spatially. This approach may provide a more effective way to account for the  
125 relative reliability of each sensor in soil moistureSM assimilation (Kolassa et al., 2017), and  
126 offers greater flexibility for assimilating various soil moistureSM products simultaneously in  
127 different combinations.

128 This study is built on a land-atmosphere coupled DA system, which consists of the  
129 Korean Integrated Model (KIM; Hong et al., 2018) and the National Aeronautics and Space  
130 Administration (NASA) Land Information System (LIS; Kumar et al., 2006, 2008b; Peters-  
131 Lidard et al., 2007). Hereafter, this system is referred to as the KIM-LIS coupled system. As  
132 an operational global NWP model at the Korea Meteorological Administration-(~~KMA~~), KIM

133 has been developed by the Korea Institute of Atmospheric Prediction Systems (KIAPS). KIM  
134 has capabilities of conducting short-to-medium-range and extended-range weather forecasts,  
135 and of implementing atmospheric DA to generate improved atmospheric initial conditions for  
136 the forecasts (Kwon et al., 2018). Land DA in the current [Korea Meteorological](#)  
137 [Administration](#)KMA's operational NWP system is based on the KIM-LIS coupled system  
138 and ingests the ASCAT [soil moisture](#)SM retrievals to constrain the modeled [soil moisture](#)SM  
139 (Jun et al., 2021). Recently Kwon et al. (2024) have demonstrated the feasibility of  
140 assimilating the SMAP [soil moisture](#)SM retrievals into the Noah LSM (Ek et al., 2003)  
141 within the KIM-LIS system to enhance the global [soil moisture](#)SM estimates and weather  
142 forecast performance of KIM.

143 [While several studies have explored the simultaneous use of radar and radiometer-based](#)  
144 [soil moisture data in offline land DA systems, mainly to improve soil moisture estimates and](#)  
145 [associated hydrological processes \(e.g., Draper et al., 2012; Khaki and Awange, 2019; Khaki](#)  
146 [et al., 2019, 2020; Kolassa et al., 2017; Kumar et al., 2019; Nair and Indu, 2019; Renzullo et](#)  
147 [al., 2014; Seo et al., 2021; Tangdamrongsub et al., 2020\), only a few have investigated their](#)  
148 [impacts on atmospheric forecasts in land-atmosphere coupled NWP systems \(e.g., de Rosnay](#)  
149 [et al., 2022; Draper and Reichle, 2019; Fairbairn et al., 2024\). Even among studies using](#)  
150 [coupled forecast systems, most assimilate only ASCAT and SMOS together, despite evidence](#)  
151 [that SMAP provides high-quality soil moisture data \(e.g., Bhuiyan et al., 2018; Chan et al.,](#)  
152 [2018; Colliander et al., 2017\) and often outperforms other sensors \(Kumar et al., 2018\). In](#)  
153 [this regard, the novelty of this study is the combined use of ASCAT and SMAP soil moisture](#)

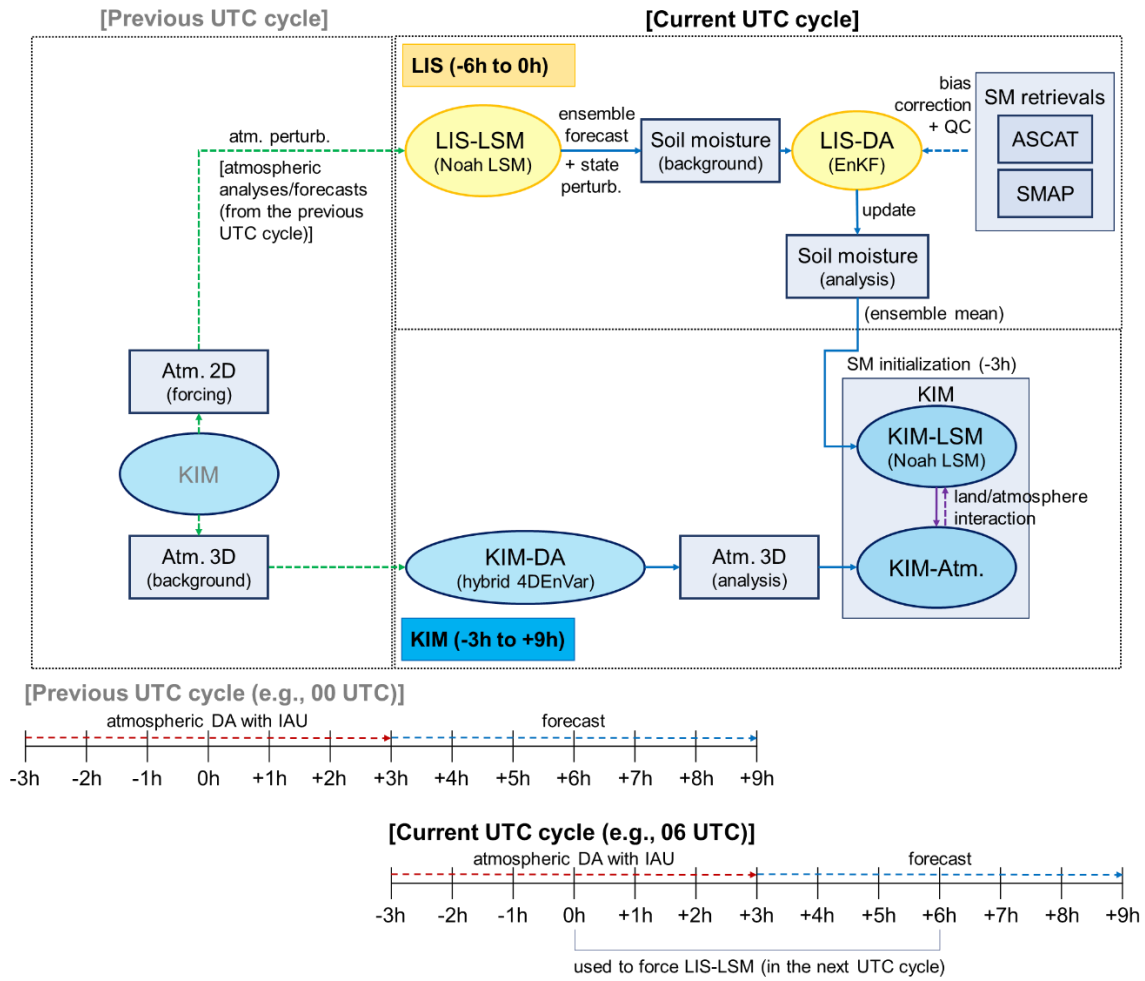
154 products in the KIM-LIS-based land-atmosphere coupled DA system, demonstrating their  
155 feasibility.

156 The present study aims to evaluate the relative (individual) and combined performance of  
157 C-band radar-based (i.e., ASCAT) and L-band radiometer-based (i.e., SMAP) surface soil  
158 moisture<sup>SM</sup> products in improving the global soil moisture<sup>SM</sup> analysis and atmospheric  
159 analysis/forecast via assimilation within the KIM-LIS coupled system. We first assimilate  
160 each soil moisture<sup>SM</sup> product individually into the Noah LSM in the KIM-LIS system over  
161 the global domain, and compare their respective performance gains. The synergistic impacts  
162 of simultaneously assimilating the ASCAT and SMAP soil moisture<sup>SM</sup> retrievals on the  
163 global estimates of lower atmospheric variables are then investigated.

## 164

## 165 **2. KIM-LIS-based weakly coupled DA system**

166 The KIM-LIS system (Jun et al., 2021; Kwon et al., 2024) is a weakly coupled DA  
167 system, in which the land analysis and atmospheric analysis are implemented independently  
168 (Figure 1). The present study uses the KIM version 3.9 and LIS version 7.4, the same  
169 versions as those used in Kwon et al. (2024). KIM (Hong et al., 2018) is composed of a  
170 global non-hydrostatic dynamical core using a cubed-sphere grid system with up to 91  
171 vertical levels on a hybrid-sigma coordinate system (Song et al., 2017; Kwon et al., 2018).  
172 LIS (Kumar et al., 2006, 2008b; Peters-Lidard et al., 2007) is a land surface hydrological  
173 modeling and DA system where various LSMs, DA schemes, and surface coordinate systems  
174 are available for different applications. In this study, the latitude-longitude grid system is  
175 used for LIS.



177  
178  
179  
180  
181  
182

**Figure 1.** Schematic diagram of the KIM-LIS-based land-atmosphere weakly coupled data assimilation (DA) system. The figure outlines the process flow between KIM and LIS in one UTC cycle that is performed four times (i.e., 00, 06, 12, and 18 UTC cycles) a day. (IAU: incremental analysis update, QC: quality control)

183  
184  
185  
186  
187

KIM and LIS employ separate versions of the Noah LSM, referred to as KIM-LSM and LIS-LSM, respectively, in Figure 1 to simulate land-surface hydrological processes. In the Noah LSM (Ek et al., 2003), a soil column (2-m total depth) is discretized into four layers with the standard thickness of 0.1 m, 0.3 m, 0.6 m, and 1.0 m from surface to bottom for estimation of soil moisture<sup>SM</sup> and soil temperature. The Noah LSM estimates soil

188 moisture<sup>SM</sup> and soil temperature based on the diffusivity form of the Richards equation and  
189 one-dimensional thermal diffusion equation, respectively. Surface water infiltration is  
190 estimated following Schaake et al. (1996) by considering the frozen soil effects. Simulations  
191 of latent heat flux and evapotranspiration rely on the formulation of the Penman equation.  
192 The original Noah version of KIM-LIS is 2.7.1, but it has undergone many updates based on  
193 later versions of the Noah LSM with additional modifications to physical parameterizations  
194 and land surface inputs to achieve optimal performance of KIM (Koo et al., 2017). As in Jun  
195 et al. (2021) and Kwon et al. (2024), the Noah LSM version 3.3 implemented within LIS is  
196 used for LIS-LSM by applying the same modifications to ensure consistency between KIM-  
197 LSM and LIS-LSM.

198 The KIM-LIS coupled system conducts a forecast/analysis cycle every 6 hours [(i.e., 00,  
199 06, 12, and 18 Coordinated Universal Time (UTC) cycles)] where KIM and LIS run for time  
200 windows of 12 hours (i.e.,  $-3$  h to  $+9$  h) and 6 hours (i.e.,  $-6$  h to 0 h), respectively, as  
201 outlined in Figure 1. LIS-LSM (i.e., Noah LSM) creates an ensemble of background (prior)  
202 soil moisture<sup>SM</sup> estimates forced by atmospheric fields from the previous UTC cycle (0 h to  
203  $+6$  h) KIM analysis/forecast, which are remapped from the cubed-sphere grid to the latitude-  
204 longitude grid and perturbed by adding Gaussian random perturbations. Additional random  
205 perturbations are imposed on the prior soil moisture<sup>SM</sup> estimates, which are then merged  
206 with remotely-sensed soil moisture<sup>SM</sup> retrievals using the ensemble Kalman filter (EnKF)  
207 method (Evensen, 1994; Reichle et al., 2002b) to generate the soil moisture<sup>SM</sup> analysis. This  
208 sequential EnKF procedure (i.e., soil moisture<sup>SM</sup> forecast and analysis) is performed from  $-6$   
209  $h$  to 0 h in the current UTC cycle, and LIS writes land outputs every 3 hours (i.e.,  $-3$  h

210 and 0 h) and generates a restart files at 0 h. The restart file contains the complete set of model  
211 state variables at that time, enabling LIS-LSM to be consistently re-initialized in the  
212 subsequent UTC cycle. The soil moisture<sup>SM</sup> analysis from LIS at -3 h is remapped from the  
213 latitude-longitude grid to the cubed-sphere grid, and is used to initialize the soil moisture<sup>SM</sup>  
214 conditions of KIM-LSM that provides land boundary conditions for the KIM forecast and  
215 analysis from -3 h to +9 h in the current UTC cycle. The atmospheric analysis is performed  
216 based on the hybrid four-dimensional ensemble variational (hybrid 4D<sub>EnVar</sub>) DA method  
217 (Song et al., 2017; Kwon et al., 2018). To minimize the initialization shock resulting from the  
218 atmospheric DA, the four-dimensional incremental analysis update (4DIAU; Lorenc et  
219 al.,2015) is employed within an atmospheric assimilation window (i.e., -3 h to +3h). KIM is  
220 further run without DA until +9 h, and the KIM analysis/forecasts from 0 h to +6 h ~~and the~~  
221 ~~LIS-LSM restart file at 0 h~~ in the current UTC cycle are then used for the next UTC cycle  
222 LIS implementation.

223 Although the remapping procedures required to share information between KIM and LIS  
224 may introduce some error, Jun et al. (2021) and Kwon et al. (2024) have demonstrated that  
225 soil moisture<sup>SM</sup> DA based on the KIM-LIS system provides beneficial impacts on improving  
226 the weather forecast performance of KIM. ~~In addition, the KIM-LIS coupled system has~~  
227 ~~advantages in terms of flexibility and extensibility for implementing new land DA~~  
228 ~~capabilities within LIS in a land-atmosphere coupled system.~~ In addition, the KIM-LIS  
229 coupled system, which employs the LIS-based land DA, has several advantages: (1) it can  
230 readily leverage the existing land DA functions of LIS, and (2) it allows straightforward  
231 implementation of new land DA developments due to LIS's extensible framework.

232

### 233 3. Satellite-based soil moisture<sup>SM</sup> retrievals

234 We assimilate the satellite-based near-surface soil moisture<sup>SM</sup> retrievals from ASCAT  
235 and SMAP individually and together into the Noah LSM to constrain the modeled soil  
236 moisture<sup>SM</sup> estimates. A brief explanation of the soil moisture<sup>SM</sup> products is given below.

#### 237 3.1. Active soil moisture<sup>SM</sup> product: ASCAT

238 ASCAT is a real aperture radar onboard the Meteorological Operational (MetOp)  
239 satellites (i.e., MetOp-A, MetOp-B, and MetOp-C), and measures radar backscatter at C-band  
240 (5.3 GHz) VV (vertical transmit vertical receive) polarization (Wagner et al., 2013). The  
241 MetOp satellites follow a near-polar sun-synchronous orbit, and their equator crossing times  
242 are 9:30 am/pm local solar time (LST) for the descending and ascending overpasses,  
243 respectively, with a revisit frequency of 1–3 days. Although ASCAT was originally designed  
244 to monitor wind direction and speed over the ocean, it has also been effectively utilized to  
245 retrieve soil moisture<sup>SM</sup> over land due to its multiple-viewing capabilities and its sensitivity  
246 to soil moisture<sup>SM</sup> variability (Wagner et al., 2013). The ASCAT soil moisture<sup>SM</sup> is  
247 retrieved based on the Vienna University of Technology (TU Wien) change detection  
248 algorithm (Wagner et al., 1999, 2010), and provides an estimate of the degree of water  
249 saturation (ranging between 0 and 100%) of the top 0–2 cm soil layer.

250 We use the MetOp-B/C ASCAT near-real time (~~NRT~~) soil moisture<sup>SM</sup> product at 12.5  
251 km swath grid. The soil moisture<sup>SM</sup> product used in this study was obtained directly from  
252 the European Organisation for the Exploitation of Meteorological Satellites (EUMETSAT)  
253 for use in the ~~KMA~~ Korea Meteorological Administration's operational weather prediction

254 system while the same product can be downloaded from the EUMETSAT Earth Observation  
255 Portal (<https://eoportal.eumetsat.int>).

256

### 257 **3.2. Passive soil moisture<sup>SM</sup> product: SMAP**

258 Unlike ASCAT, the SMAP mission is specifically designed for global soil moisture<sup>SM</sup>  
259 monitoring based on L-band (1.4 GHz) passive microwave radiometer measurements  
260 (Entekhabi et al., 2010). The SMAP satellite is in sun-synchronous orbits at approximately  
261 685 km altitudes with a local equator-crossing time of 6 am (descending) and 6 pm  
262 (ascending) and a revisit cycle of 2–3 days. It provides volumetric soil moisture (in  $\text{m}^3 \text{m}^{-3}$ )  
263 for a soil depth of 0–5 cm from the surface.

264 The present study uses the SMAP Level 2 (L2) Radiometer Half-Orbit 36 km Equal Area  
265 Scalable Earth (EASE)–Grid soil moisture<sup>SM</sup> data (SPL2SMP version 9, O’Neill et al.,  
266 2021), which is obtained from the National Snow and Ice Data Center (NSIDC,  
267 <https://n5eil01u.ecs.nsidc.org/SMAP/SPL2SMP.009/>). The SMAP soil moisture<sup>SM</sup> retrievals  
268 based on the Dual Channel Algorithm (DCA, Chaubell et al., 2020) are assimilated. DCA  
269 uses both horizontally (H) and vertically (V) polarized  $T_B$ -brightness temperature  
270 measurements and is the current baseline retrieval algorithm of the SMAP soil moisture<sup>SM</sup>  
271 product (Chan and Dunbar, 2021).

272

### 273 **3.3. Bias correction of the soil moisture<sup>SM</sup> data**

274 Typical DA algorithms are designed to correct random errors under the assumption of  
275 unbiased state estimates between models and observations (Dee and da Silva, 1998).

276 However, there are generally large systematic discrepancies between modeled and satellite-  
277 retrieved soil moisture<sup>SM</sup> because of their different representations of soil moisture<sup>SM</sup>  
278 associated with the geophysical definition and horizontal/vertical scales (Koster et al., 2009;  
279 Kumar et al., 2019). Therefore, soil moisture<sup>SM</sup> DA systems essentially employ appropriate  
280 bias correction strategies to remove these systematic biases prior to assimilation, and thus to  
281 comply with the DA assumption of unbiased models and observations (Kolassa et al., 2017;  
282 Reichle and Koster, 2004). In this study, bias correction is implemented differently for the  
283 ASCAT and SMAP soil moisture<sup>SM</sup> products. That is, we apply cumulative distribution  
284 function (CDF) matching (Reichle and Koster 2004) and anomaly correction methods (Kwon  
285 et al., 2022) to assimilate the ASCAT and SMAP soil moisture<sup>SM</sup> retrievals, respectively,  
286 into the Noah LSM within the KIM-LIS coupled system. The use of the anomaly correction  
287 method for SMAP follows our previous investigations (Kwon et al., 2022, 2024) aiming to  
288 minimize the loss of useful information from the original data through bias correction. In  
289 contrast, traditional CDF matching is applied to ASCAT, since the anomaly correction  
290 method is not applicable due to difference in soil moisture data type between ASCAT (soil  
291 wetness index) and the model (volumetric soil moisture in  $\text{m}^3 \text{m}^{-3}$ ). Further details are  
292 provided in the following two paragraphs.

293 The CDF matching is a commonly used bias correction method in soil moisture<sup>SM</sup> DA.  
294 Through the CDF matching, in this study, the ASCAT soil wetness index (~~SWI~~) data are  
295 transformed to volumetric soil moisture<sup>SM</sup> ( $\text{m}^3 \text{m}^{-3}$ ) by correcting all the statistical moments  
296 of the original ASCAT data to those of the Noah-simulated soil moisture<sup>SM</sup>. Existing soil  
297 moisture<sup>SM</sup> DA studies use two different CDF matching approaches. One uses a lumped

298 CDF computed using all seasons data (i.e., pixel-wise single CDF for each data type) (e.g.,  
299 Draper et al., 2011, 2012; Kumar et al., 2009, 2014; Reichle et al., 2007) while the other uses  
300 monthly-stratified CDFs (i.e., pixel-wise 12 CDFs for each data type) (e.g., Jun et al., 2021;  
301 Kumar et al., 2015; Kwon et al., 2022, 2024; Santanello Jr et al., 2016). Kumar et al. (2015)  
302 and Santanello Jr et al., (2016) suggest using the monthly CDF rather than the lumped CDF  
303 to mitigate spurious statistical artifacts in the bias-corrected soil moisture<sup>SM</sup> by the CDF  
304 matching. Kwon et al. (2024) show that abnormal fluctuations are witnessed in the lumped  
305 CDF-based rescaled soil moisture<sup>SM</sup>, particularly in dry periods, and Kwon et al. (2022)  
306 demonstrate that soil moisture<sup>SM</sup> DA employing the monthly CDF achieves better soil  
307 moisture<sup>SM</sup> analysis than that applying the lumped CDF matching. Based on these previous  
308 findings, we implement the monthly CDF matching for the ASCAT soil moisture<sup>SM</sup> DA.

309 The anomaly correction method, proposed by Kwon et al. (2022), is a simpler alternative  
310 to traditional bias correction approaches. It aims to reduce the reliance of DA systems on  
311 rescaling methods like the CDF matching, which is known to cause significant information  
312 loss in the original soil moisture<sup>SM</sup> data, especially when human-induced processes (e.g.,  
313 irrigation activities), poorly represented in models, are the dominant source of systematic  
314 discrepancies between observations and models (Kumar et al., 2015; Nearing et al., 2018).

315 Instead of rescaling the SMAP soil moisture<sup>SM</sup> retrievals, the anomaly correction approach  
316 obtains the soil moisture<sup>SM</sup> temporal variability (i.e., anomaly) information by subtracting  
317 the long-term soil moisture<sup>SM</sup> mean from the original SMAP data. The extracted SMAP soil  
318 moisture<sup>SM</sup> anomaly is added to the long-term mean of the modeled soil moisture<sup>SM</sup>, which  
319 is then assimilated into the LSM. The anomaly correction assumes that the systematic bias

320 between observations and models is dominated by the climatological mean difference and  
321 higher moment (e.g., standard deviation) differences are negligible. Kwon et al. (2022) and  
322 Kwon et al. (2024) demonstrate that the SMAP soil moisture<sup>SM</sup> data and Noah-simulated  
323 soil moisture<sup>SM</sup> satisfy this underlying assumption over the continental United States  
324 (~~CONUS~~) and global domain, respectively. In particular, Kwon et al. (2024) show that the  
325 anomaly correction-based SMAP soil moisture<sup>SM</sup> DA is effective in improving the global  
326 soil moisture<sup>SM</sup> estimates and weather forecast skill of the KIM-LIS coupled system that  
327 employs the Noah LSM.

328

#### 329 **3.4. Quality control (~~QC~~) of the soil moisture<sup>SM</sup> data**

330 The ASCAT and SMAP soil moisture<sup>SM</sup> retrievals undergo quality control (~~QC~~) before  
331 DA by removing inaccurate or uncertain soil moisture<sup>SM</sup> observations based on strategies  
332 employed in previous soil moisture<sup>SM</sup> DA studies (e.g., Blyverket et al., 2019; Draper et al.,  
333 2012; Ferguson et al., 2020; Jun et al., 2021; Kolassa et al., 2017; Kumar et al., 2014, 2019;  
334 Kwon et al., 2022, 2024; Nair and Indu, 2019). Firstly, before bias correction, the soil  
335 moisture<sup>SM</sup> data are discarded when the data quality flags provided with each soil  
336 moisture<sup>SM</sup> product indicate that the data accuracy is impacted by open water bodies, dense  
337 vegetation, urban areas, precipitation, snow cover, frozen ground, complex topography, or  
338 anthropogenic Radio Frequency Interference (RFI). Especially, the ASCAT soil moisture<sup>SM</sup>  
339 retrievals are assimilated only when the Estimated ~~SM-Soil Moisture~~ Error (ESME) is less  
340 than 16%, and the topographic complexity and wetland fraction are below 20% and 15%,  
341 respectively, as applied in Jun et al. (2021). These uncertainty thresholds are slightly higher

342 than those used in Draper et al. (2012) and Kolassa et al. (2017) for the purpose of utilizing  
343 more data in a near-real time~~an-NRT~~ operational DA system.

344 Secondly, the model-based quality control~~QC~~ is additionally applied to both ASCAT and  
345 SMAP after bias correction. Specifically, assimilation of ASCAT and SMAP soil  
346 moisture~~SM~~ into the Noah LSM is not performed in the case that (1) model background  
347 estimates indicate active precipitation events or frozen/snow-covered soil conditions, that (2)  
348 the model land cover type and green vegetation fraction ~~(GVF)~~ inputs from the Moderate  
349 resolution imaging spectroradiometer (MODIS) International Geosphere-Biosphere  
350 Programme (IGBP) data (Friedl et al., 2002) and the National Centers for Environmental  
351 Prediction (NCEP), respectively, indicate that a grid cell is classified as forests or has green  
352 vegetation fraction~~GVF~~ greater than 0.7, or that (3) bias-corrected soil moisture~~SM~~ retrievals  
353 are close to wilting point or saturation.

354

## 355 **4. DA methods**

### 356 **4.1. Atmospheric DA**

357 Atmospheric DA in KIM is based on a hybrid four-dimensional ensemble variational  
358 (hybrid 4D<sub>En</sub>Var) DA method as described in Kwon et al. (2018) and Song et al. (2017).  
359 KIM's 4D<sub>En</sub>Var DA system consists of deterministic and stochastic (ensemble) components  
360 whose atmospheric analyses are generated using the KIM VARIational DA (KVAR, Song  
361 and Kwon, 2015) and four-dimensional local ensemble transform Kalman filter (LETKF,  
362 Shin et al., 2016) schemes, respectively. KIM LETKF independently performs analysis  
363 updates by assimilating almost the same atmospheric observations as used in the

364 deterministic component (i.e., KVAR), but the main function of LETKF in the KIM DA  
365 system is currently to construct ensemble background error covariance ~~(BEC)~~ of KVAR  
366 (Kwon et al., 2018). The relative contribution of the ensemble background error  
367 covariance~~BEC~~ gradually increases from 45% at the poles to 70% at the equator in the  
368 troposphere and then gently decreases above the troposphere. Three-dimensional spatial  
369 localizations are implemented using the Gaspari and Cohn ~~(GC)~~ Gaussian-like localization  
370 function (Gaspari and Cohn, 1999). To obtain an appropriate ensemble spread in LETKF, an  
371 additive inflation (Shin et al., 2018) and relaxation-to-prior perturbation (~~RTPP~~, Whitaker  
372 and Hamill, 2012) are applied together.

373 In this study, we assimilate both conventional and non-conventional atmospheric data  
374 including the Advanced Microwave Sounding Unit-A (AMSU-A), Atmospheric Motion  
375 Vectors (AMVs), Microwave Humidity Sounder (MHS), Global Positioning System Radio  
376 Occultation (GPS-RO), Infrared Atmosphere Sounding Interferometer (IASI), Advanced  
377 Technology Microwave Sounder (ATMS), Cross-track Infrared Sounder (CrIS), and  
378 observations obtained from surface, aircraft, and sonde. The KIM Package of Observation  
379 Processing (KPOP, Kang et al., 2019) is employed to preprocess (e.g., quality control~~QC~~ and  
380 bias correction) the observations before assimilation.

381

## 382 4.2. Land soil moisture~~SM~~ DA

383 In the KIM-LIS coupled system, land DA is conducted by the LIS-DA subsystem (Figure  
384 1) in which various DA schemes are available. The current study applies a 1-dimensional ~~(1D)~~  
385 EnKF method (Reichle et al., 2002b) to assimilate satellite soil moisture~~SM~~ retrievals (i.e.,

386 ASCAT and SMAP) into the Noah LSM. The EnKF is one of the widely used DA schemes  
387 for nonlinear hydrological applications (e.g., Cho et al., 2023; Crow and Van den Berg, 2010;  
388 Draper and Reichle, 2019; Kim et al., 2021a; Kwon et al., 2019, 2021; Reichle et al., 2023;  
389 Renzullo et al., 2014; Xu et al., 2021) because of its relatively flexible and computationally  
390 efficient nature (Keppenne, 2000).

391 Within the EnKF-based DA system, model forecasts and analysis updates are performed  
392 alternately. That is, the ensemble forecasts of model prognostic state variables are propagated  
393 forward in time until observations are available, and the forecasted states are updated in the  
394 assimilation step when and where observations exist. The resulting analysis ensemble is then  
395 used as the initial condition for the next model forecast. In this study, the control vectors that  
396 are directly updated by assimilating the ASCAT and SMAP soil moisture<sup>SM</sup> retrievals  
397 include the Noah LSM estimates of soil moisture<sup>SM</sup> at four soil layers while other related  
398 hydrometeorological variables are adjusted through model physics in subsequent model  
399 integrations. As we conduct the 1-~~D~~dimensional EnKF, the soil moisture<sup>SM</sup> analysis in a  
400 given grid is produced independently of neighboring grids.

401 The EnKF increments are determined depending on the relative uncertainties (error  
402 variances) of model and observation. The model uncertainty (background error covariance) is  
403 represented by the ensemble forecast spread (ensemble size of 20), which is obtained at each  
404 grid by randomly perturbing the atmospheric variables from KIM including shortwave  
405 radiation-~~(SW)~~, longwave radiation-~~(LW)~~, and precipitation-~~(P)~~, and by additionally  
406 (randomly) perturbing the Noah LSM-simulated soil moisture<sup>SM</sup> estimates. Shortwave  
407 radiation<sup>SW</sup> and precipitation<sup>P</sup> are perturbed by applying log-normally distributed

408 multiplicative perturbations with standard deviations of 0.3 and 0.5, respectively, while  
 409 normally distributed additive perturbations are applied to longwave radiationLW (with a  
 410 standard deviation of  $50 \text{ W m}^{-2}$ ) and the soil moisture (SM) estimates at four soil layers  
 411 [with standard deviations of 0.01, 0.006, 0.003, and  $0.0015 \text{ m}^3 \text{ m}^{-3}$  for SM1 (top layer), SM2,  
 412 SM3, and SM4 (bottom layer), respectively]. First-order autoregressive temporal correlations  
 413 and cross-variable correlations are also considered during the perturbation (Table 1), whereas  
 414 horizontal error correlations are neglected. The perturbation parameters used in this study are  
 415 determined based on Kumar et al. (2017, 2019) and Reichle et al. (2008), and have also been  
 416 effectively applied in Jun et al. (2021) and Kwon et al. (2024).

417 **Table 1.** Perturbation parameter values used for autoregressive temporal correlation and cross  
 418 correlations between different variables (SW: shortwave radiation, LW: longwave radiation,  
 419 P: precipitation, SM1: top layer soil moisture ~~(SM)~~, SM2: second layer soil moistureSM,  
 420 SM3: third layer soil moistureSM, and SM4: bottom layer soil moistureSM).

Perturbed variables	Time scale of first-order autoregressive temporal correlations (hour)	Cross correlations with perturbations in			
		SW	LW	P	
<u>KIM atmospheric forcing</u>					
SW	24	1.0	<u>-0.5</u>	<u>-0.8</u>	
LW	24	<u>-0.5</u>	1.0	0.5	
P	24	<u>-0.8</u>	0.5	1.0	
<u>Noah LSM soil moisture</u>					
SM1	12	1.0	0.6	0.4	0.2
SM2	12	0.6	1.0	0.6	0.4
SM3	12	0.4	0.6	1.0	0.6
SM4	12	0.2	0.4	0.6	1.0

421

422 The spatially and temporally constant observation error standard deviations of 10% and  
 423  $0.02 \text{ m}^3 \text{ m}^{-3}$  are applied for ASCAT and SMAP soil moistureSM retrievals, respectively,  
 424 based on previous DA studies (e.g., Dorigo et al., 2010; Draper et al., 2012; Ferguson et al.,  
 425 2020; Kolassa et al., 2017; Kwon et al. 2022, 2024). In the KIM-LIS coupled system, the  
 426 ASCAT-derived soil wetness indexSWI data are scaled into the Noah LSM soil moistureSM

427 climatology (in  $\text{m}^3\cdot\text{m}^{-3}$ ) through the CDF matching (see Section 3.3) to remove the  
428 systematic bias between the ASCAT soil moisture<sup>SM</sup> and Noah-simulated soil moisture<sup>SM</sup>.  
429 Correspondingly the 10% ASCAT soil moisture<sup>SM</sup> error standard deviation is also locally  
430 scaled by the ratio of the Noah LSM and ASCAT soil moisture<sup>SM</sup> time series standard  
431 deviations following Draper et al. (2012) and Jun et al. (2021). Unlike ASCAT, the SMAP  
432 soil moisture<sup>SM</sup> data are provided in the same unit as the Noah LSM soil moisture<sup>SM</sup>, and  
433 only the climatological mean biases between the SMAP soil moisture<sup>SM</sup> and modeled soil  
434 moisture<sup>SM</sup> are corrected during the bias correction procedure (see Section 3.3). Therefore,  
435 the observation error standard deviation of SMAP is not scaled in this study.

436 Note that there is a mismatch in the surface soil layer depth between the soil moisture<sup>SM</sup>  
437 observations (i.e., 0–2 cm for ASCAT and 0–5 cm for SMAP) and Noah LSM (i.e., 0–10 cm).  
438 However, Shellito et al. (2016, 2018) and Nair and Indu (2019) have demonstrated that  
439 changing the surface layer depth in the model from 10 cm to 2 cm or 5 cm has only a  
440 marginal impact on the simulated soil moisture<sup>SM</sup>. Moreover, because we apply the  
441 systematic bias correction of the soil moisture<sup>SM</sup> retrievals before assimilation, the impact of  
442 the surface soil layer depth difference on the DA performance is assumed to be negligible.

443

## 444 5. Experiments

445 Land-atmosphere coupled DA experiments (with a 6-hour cycling frequency) using the  
446 active radar (i.e., ASCAT) and passive radiometer (i.e., SMAP) soil moisture<sup>SM</sup> retrievals  
447 are designed as summarized in Table 2. CTL, a control case serving as a baseline experiment,  
448 only assimilates atmospheric observations while an open-loop ensemble simulation of the

449 Noah LSM is performed without soil moisture<sup>SM</sup> assimilation. SG\_AT and SG\_SP are  
450 single-sensor soil moisture<sup>SM</sup> DA experiments where the near-surface soil moisture<sup>SM</sup> data  
451 from individual sensors (ASCAT or SMAP, respectively) are assimilated into the Noah LSM  
452 using the 1-dimensional EnKF with an ensemble size of 20. MT\_ATSP, a multi-sensor soil  
453 moisture<sup>SM</sup> DA experiment, jointly assimilates both ASCAT and SMAP soil moisture<sup>SM</sup>  
454 products to investigate the synergistic impact of assimilating the radar- and radiometer-based  
455 soil moisture<sup>SM</sup> retrievals together on improving the atmospheric analysis/forecast of the  
456 KIM-LIS coupled system. As explained in Section 3.3, the CDF matching and anomaly  
457 correction methods are applied for bias correction of the ASCAT and SMAP soil moisture<sup>SM</sup>  
458 retrievals, respectively, in the single- and multi-sensor soil moisture<sup>SM</sup> DA experiments.  
459 Atmospheric DA is performed identically in all experiments.

460  
461 **Table 2.** Summary of land-atmosphere coupled data assimilation (DA) experiments  
462 conducted in this study (SM: soil moisture; see Appendix A for additional abbreviations).

	CTL*	SG_AT	SG_SP*	MT_ATSP
<b><u>Land</u></b>				
SM DA	X	O	O	O
SM data	-	ASCAT	SMAP	ASCAT + SMAP
SM bias correction method	-	CDF matching	anomaly correction	CDF matching (ASCAT); anomaly correction (SMAP)
SM DA scheme	-	EnKF	EnKF	EnKF
LSM	Noah LSM v2.7.1 (KIM-LSM) and v3.3 (LIS-LSM)			
LSM horizontal resolution	25 km			
LSM ensemble size	20			
<b><u>Atmosphere</u></b>				
KIM	KIM v3.9			
KIM horizontal resolution	deterministic component (25 km); ensemble component (50 km)			
Atmospheric DA scheme	deterministic component (4DEnVar); ensemble component (LETKF)			

---

Experimental period ~~1~~April 1 to ~~31~~July 31, 2022 (DA spin-up: ~~1~~to ~~31~~March 1 to 31, 2022)

---

463 \*Note that CTL and SG\_SP are the same experiments as those presented in Kwon et al.  
 464 (2024).

465  
 466 This study uses the same model setup and experimental period as in Kwon et al. (2024).

467 We use the Shuttle Radar Topography Mission (SRTM) elevation (Farr et al., 2007),  
 468 MODIS-IGBP land cover (Friedl et al., 2002), National Centers for Environmental Prediction  
 469 (NCEP) green vegetation fraction~~GVP~~ and surface albedo, and the blended State Soil  
 470 Geographic (STATSGO, Miller and White, 1998)/Food and Agriculture Organization (FAO)  
 471 soil texture (Reynolds et al., 2000) as land inputs for the Noah LSM. The LSM and KIM  
 472 deterministic component are run over the global domain at a horizontal resolution of 25 km  
 473 while the KIM ensemble component is run at a 50 km horizontal resolution due to its high  
 474 computational cost in the 6-hourly cycling experiments. All 6-hourly cycling experiments are  
 475 conducted from March to July 2022 while the first month is excluded from evaluation as it is  
 476 used as the assimilation spin-up (burn-in) period. To obtain LSM initial conditions at the  
 477 beginning of the experiments (i.e., ~~1~~March 1, 2022), an offline spin-up of the Noah LSM is  
 478 first run from 2008 to April 2020 forced by the meteorological forcing fields from the Global  
 479 Land Data Assimilation System (GLDAS, Rodell et al., 2004), followed by additional spin-  
 480 up until ~~1~~March 1, 2022 using the KIM atmospheric forcing, which is available only from  
 481 May 2020 for the LSM offline simulation. The KIM atmospheric model is initialized by the  
 482 fifth generation of the European Centre for Medium-Range Weather Forecasts (ECMWF)  
 483 atmospheric reanalysis (ERA5, Hersbach et al., 2020). In addition to the cycling runs in each

484 experimental case, 5-day forecasts are performed every 00 UTC and 12 UTC cycle after  
485 being initialized by the land and atmospheric analyses from DA.

486

487

## 488 **6. Performance evaluation**

489 Due to the difficulty in acquiring a global ground truth reference dataset, we perform  
490 global-scale performance evaluations of the [soil moisture<sup>SM</sup>](#) DA for different  
491 hydrometeorological variables using datasets from various sources such as satellite-based  
492 observations and analysis fields from different systems. The four experiments (i.e., CTL,  
493 SG\_AT, SG\_SP, and MT\_ATSP) listed in Table [4-2](#) are assessed in terms of generating the  
494 [soil moisture<sup>SM</sup>](#) analysis, specific humidity and air temperature analyses/forecasts, and  
495 precipitation forecasts. Methodologies and datasets employed in this study for the evaluation  
496 are described below.

497

### 498 **6.1. Soil moisture**

499 A triple collocation analysis (TCA, Stoffelen, 1998; Scipal et al., 2008), a statistical  
500 random error estimation method, is applied to evaluate the global [soil moisture<sup>SM</sup>](#) analysis  
501 from the [soil moisture<sup>SM</sup>](#) DA experiments. TCA has been initially proposed by Stoffelen  
502 (1998) to quantify the error of near-surface ocean wind speed estimates, and it is now one of  
503 the most commonly used method for estimating uncertainties in satellite-based [soil](#)  
504 [moisture<sup>SM</sup>](#) retrievals (e.g., Dorigo et al., 2010; Gruber et al., 2016; Kim et al., 2021b, 2023;  
505 Scipal et al., 2008) or for evaluating large-scale [soil moisture<sup>SM</sup>](#) simulations of

506 computational models (e.g., Kim et al., 2021a; Kwon et al., 2024; Nair and Indu, 2019;  
507 Renzullo et al., 2014) due to no requirement of reliable ground truth reference data that is  
508 hard to be obtained at large scales.

509 The TCA approach is based on the assumption of a linear relationship between  
510 hypothetical true soil moistureSM and individual soil moistureSM estimates as expressed in  
511 Equation (1):

512

$$513 \quad \theta_k = \alpha_k + \beta_k \theta_{true} + \varepsilon_k \quad (1)$$

514

515 where  $\theta_k$  is independent collocated soil moistureSM datasets (i.e., triplet components,  $k \in [x,$   
516  $y, z]$ );  $\alpha_k$  and  $\beta_k$  are additive and multiplicative systematic biases of  $\theta_k$ , respectively, with  
517 respect to the unknown hypothetical true soil moistureSM signal ( $\theta_{true}$ ); and  $\varepsilon_k$  represents  
518 the additive random noise in each soil moistureSM data ( $\theta_k$ ). The random error (noise)  
519 variance ( $\sigma_{\varepsilon_k}^2$ ) of three collocated soil moistureSM triplets [Equations (2) to (4)] can be  
520 derived from variance and covariance equations by introducing additional assumptions, i.e.,  
521 error orthogonality (independence between the random error of the soil moistureSM datasets  
522 and the unknown soil moistureSM truth) and zero error-cross correlation (independence of  
523 the random errors between the soil moistureSM datasets) (Gruber et al., 2016).

524

$$525 \quad \sigma_{\varepsilon_x}^2 = \sigma_x^2 - \frac{\sigma_{xy}\sigma_{xz}}{\sigma_{yz}} \quad (2)$$

526

527 
$$\sigma_{\varepsilon_y}^2 = \sigma_y^2 - \frac{\sigma_{yx}\sigma_{yz}}{\sigma_{xz}} \quad (3)$$

528

529 
$$\sigma_{\varepsilon_z}^2 = \sigma_z^2 - \frac{\sigma_{zx}\sigma_{zy}}{\sigma_{xy}} \quad (4)$$

530

531 where  $\sigma_k^2$  and  $\sigma_{\varepsilon_k}^2$  ( $k \in [x, y, z]$ ) are the variance and random error variance, respectively, of  
 532 each soil moistureSM data; and  $\sigma_{xy}$ ,  $\sigma_{xz}$ , and  $\sigma_{yz}$  are the covariances of two soil  
 533 moistureSM triplet components. In this study, the fractional mean-square error ( $fMSE_k =$   
 534  $\frac{\sigma_{\varepsilon_k}^2}{\sigma_k^2}$ , Draper et al., 2013), ranging from 0 (free-of-noise soil moistureSM data) to 1 (no  
 535 meaningful soil moistureSM signal), is computed using Equation (5). This metric is  
 536 employed as a TCA-based global soil moistureSM evaluation metric following procedures  
 537 implemented by Kim et al. (2020 and 2021a) and Kwon et al. (2024).

538

539 
$$fMSE_k = \frac{\sigma_{\varepsilon_k}^2}{\sigma_k^2} \quad (5)$$

540

541 In order to meet the zero error-cross correlation assumption, we select two independent  
 542 satellite-based soil moistureSM products, i.e., ASCAT and Advanced Microwave Scanning  
 543 Radiometer 2 (AMSR2) [or Soil Moisture and Ocean Salinity (SMOS)], derived from  
 544 different microwave sensors using different retrieval algorithms for the first and second soil  
 545 moistureSM triplet components while the soil moistureSM simulations from the experiments  
 546 (CTL, SG\_AT, and SG\_SP) are used for the third triplet component (Table 3). Due to the

547 TCA assumptions, it is hard to compose the same reference frame for all experimental cases,  
548 especially for the multi-sensor [soil moisture<sup>SM</sup>](#) DA experiment. Therefore, for a fair  
549 comparison, we only evaluate the relative improvement in the [soil moisture<sup>SM</sup>](#) estimates by  
550 comparing fMSE of the single-sensor [soil moisture<sup>SM</sup>](#) DA with fMSE of CTL that are  
551 computed using the same first and second triplet components (i.e., satellite [soil moisture<sup>SM</sup>](#)  
552 retrievals that are not assimilated in the [soil moisture<sup>SM</sup>](#) DA experiment) as shown in Table  
553 3. The effects of the multi-sensor [soil moisture<sup>SM</sup>](#) DA (MT\_ATSP) are assessed only for  
554 atmospheric variables (see Sections 6.2 and 6.3).

555

556 **Table 3.** [Triple collocation analysis \(TCA\)](#) triplet composition to quantify the relative  
557 improvement in the [soil moisture<sup>SM</sup>](#) estimates by [soil moisture<sup>SM</sup> data assimilation \(DA\)](#) as  
558 compared to CTL. The CTL [soil moisture<sup>SM</sup>](#) estimates are also evaluated using the same  
559 satellite-based reference [soil moisture<sup>SM</sup>](#) products as used for each single-sensor [soil](#)  
560 [moisture<sup>SM</sup>](#) DA experiment (EXP: SG\_AT and SG\_SP).

Experiments	Triples for EXP	Triples for CTL
SG_AT	AMSR2, SMOS, SG_AT	AMSR2, SMOS, CTL
SG_SP	AMSR2, ASCAT, SG_SP	AMSR2, ASCAT, CTL

561

562 The ASCAT, SMOS, and AMSR2 [soil moisture<sup>SM</sup>](#) data used in TCA are the 12.5-km  
563 ASCAT [soil moisture<sup>SM</sup>](#) Climate Data Record (CDR) version 7 product (H119 and extended  
564 H120) based on the TU-Wien change detection algorithm (Wagner et al., 2013), the SMOS-  
565 INRA-CESBIO (SMOS-IC) version 2 product, and the AMSR2 X-band Land Parameter  
566 Retrieval Model (LPRM) product, respectively. The original datasets are preprocessed by  
567 conducting [quality control<sup>QC</sup>](#) based on quality flags provided in each data product, and  
568 spatial resampling using the nearest neighbor distance method to match the spatial resolution  
569 of the datasets with that of the LSM outputs (i.e., 25-km latitude-longitude grids). Due to the

570 different local overpass time between the satellite soil moistureSM products [i.e., 09:30  
571 am/pm LST for ASCAT, 01:30 am/pm LST for ASMR2, and 06:00 am/pm LST for SMOS],  
572 the UTC-based Noah-LSM outputs at 04:00 am/pm LST and 11 am/pm LST are extracted for  
573 TCA that uses AMSR2/SMOS/SG\_AT(or CTL) and AMSR2/ASCAT/SG\_SP(or CTL),  
574 respectively. We select model outputs at the approximate midpoint time (e.g., 04:00) between  
575 the overpass times of two other satellite-based soil moisture triplet components (e.g., 01:30  
576 AMSR2 and 06:00 SMOS) for a fair comparison. While some errors may still arise due to  
577 sampling-time mismatches between the triplet components, we assume these errors are  
578 acceptable since the same sampling time was applied to both CTL and DA experimental  
579 outputs to evaluate their relative performance. Please refer to Kwon et al. (2024) and Kim et  
580 al. (2023) for more detailed procedures.

581

## 582 **6.2. Specific humidity and air temperature**

583 Evaluations of the specific humidity and air temperature analyses/forecasts are performed  
584 using the ECMWF Integrated Forecasting System (IFS) analysis (ECMWF, 2017) as  
585 reference data. The IFS components have undergone continuous evolution since 1979,  
586 leading to a steady enhancement in the precision of the IFS analyses and forecasts (Ben  
587 Bouallègue et al., 2024). Extensive studies have used the ECMWF-IFS analysis for various  
588 purposes such as an atmospheric forcing to drive offline models (e.g., Manco et al., 2023;  
589 Ricker et al., 2024), initial and boundary conditions for other forecasting systems (e.g.,  
590 Federico et al., 2024; Sacchetti et al., 2024; Torcasio et al., 2023), and a reference data to  
591 evaluate modeling systems (e.g., Ben Bouallègue et al., 2024; Kwon et al., 2024; Lee et al.,

592 2020; Polichtchouk et al., 2023; Reichle et al., 2023). The root mean square difference  
593 (RMSD) between the atmospheric variables (i.e., specific humidity and air temperature) from  
594 each experiment and those from the IFS analysis is computed.

595

### 596 **6.3. Precipitation**

597 Local variations in soil moisture modify boundary-layer heat and moisture fluxes, thereby  
598 altering water–energy budgets and influencing convective triggering (Findell and Eltahir,  
599 2003; Pal and Eltahir, 2003) and subsequently influence large-scale dynamics (Cook et al.,  
600 2006; Pal and Eltahir, 2003), both of which play key roles in determining precipitation  
601 processes. A number of studies have investigated the complex interaction mechanisms  
602 between soil moisture and precipitation, referred to as the ‘soil moisture-precipitation  
603 feedback’, using observational analyses (e.g., Catalano et al., 2016; Yang et al., 2018) and  
604 computational modeling systems (e.g., Beljaars et al., 1996; Bosilovich and Sun, 1999;  
605 Hohenegger et al., 2009; Lin et al., 2023; Pal and Eltahir, 2003). Although these studies  
606 generally agree on a predominant positive feedback, the sign and strength vary depending on  
607 modeling systems and spatiotemporal scales (Hohenegger et al., 2009; Lin et al., 2023).  
608 Differences in the sign of soil moisture-precipitation feedback can be attributed to the  
609 complexity of representing the soil moisture–evapotranspiration relationship (Yang et al.,  
610 2018) and convective development (Hohenegger et al., 2009). Considerable debate and  
611 uncertainty remain regarding the physical mechanisms determining the sign of the feedback  
612 (Hohenegger et al., 2009). Nevertheless, there is no doubt that soil moisture and precipitation  
613 are reciprocally linked, implying that better characterization of soil moisture conditions

614 through soil moisture DA can enhance precipitation forecasts in land-atmosphere coupled  
 615 systems.

616 — We assess the impact of soil moisture<sup>SM</sup> DA on precipitation forecast skill using a well-  
 617 established metrics such as the frequency bias (FB) and equitable threat score (ETS) based on  
 618 recommendations by the World Meteorological Organization (WMO, 2008). Calculations of  
 619 the FB and ETS metrics are based on a  $2 \times 2$  contingency table (Table 4), which consists of  
 620 *Hits*, *Misses*, *FalseAlarms*, and *CorrectNegatives*. Gauge-based global daily precipitation  
 621 analyses from the National Oceanic and Atmospheric Administration (NOAA) Climate  
 622 Prediction Center (CPC) (Chen et al., 2008; Xie et al., 2007) are used as reference data for  
 623 precipitation evaluation.

625 **Table 4.** Contingency table for computing precipitation forecast evaluation metrics

		Observation (reference data)	
		Yes	No
Forecast (model data)	Yes	<i>Hits</i>	<i>FalseAlarms</i>
	No	<i>Misses</i>	<i>CorrectNegatives</i>

627 FB [Equation (~~65~~)] assesses the ratio of the frequency of precipitation occurrence in the  
 628 forecast to that in the observation:

$$629 \quad FB = \frac{Hits+FalseAlarms}{Hits+Misses} \quad (65)$$

630  
 631 where *Hits*, *FalseAlarms*, and *Misses* are the number of model grid points with correct  
 632 forecasts, false alarms, and missed forecasts of precipitation occurrence, respectively. The FB  
 633 metric ranges from zero to infinity where the ideal FB score is 1.0, indicating that the number

634 of the forecasted precipitation events is the same as that of the observed events. Note that FB  
635 does not consider the timing of precipitation events.

636 ETS [Equation (76)] quantifies the fraction of the forecasted or observed precipitation  
637 events that are captured correctly after excluding random hits ( $Hits_{rnd}$ ), which is the number  
638 of correct forecasts by random chance computed using Equation (87):

639

$$640 \quad ETS = \frac{Hits - Hits_{rnd}}{Hits + Misses + FalseAlarms - Hits_{rnd}} \quad (76)$$

641

$$642 \quad Hits_{rnd} = \frac{(Hits + Misses)(Hits + FalseAlarms)}{N} \quad (87)$$

643

644 where  $N$  is the total number of events defined as  $N = Hits + Misses + FalseAlarms +$   
645  $CorrectNegatives$ .  $CorrectNegatives$  denotes the number of correct forecasts of no  
646 precipitation. The ETS metric ranges from  $-1/3$  to 1, where values below 0 and 1 represent  
647 “no skill” and “perfect skill” (no  $Misses$  or  $FalseAlarms$ ), respectively.

648

649

## 650 7. Results

651 In this section, we first examine the performance of the KIM-LIS coupled system in  
652 producing enhanced global [soil moisture<sup>SM</sup>](#) estimates when the system is informed by  
653 satellite-based [soil moisture<sup>SM</sup>](#) retrievals from ASCAT and SMAP via assimilation. Next,  
654 the impacts of assimilating the ASCAT and SMAP [soil moisture<sup>SM</sup>](#) data, both individually

655 and simultaneously, on atmospheric analyses and forecasts are assessed. Finally, we evaluate  
656 the added skill of the KIM-LIS system in forecasting precipitation when using initialized soil  
657 moisture<sup>SM</sup> conditions from multi-sensor soil moisture<sup>SM</sup> DA.

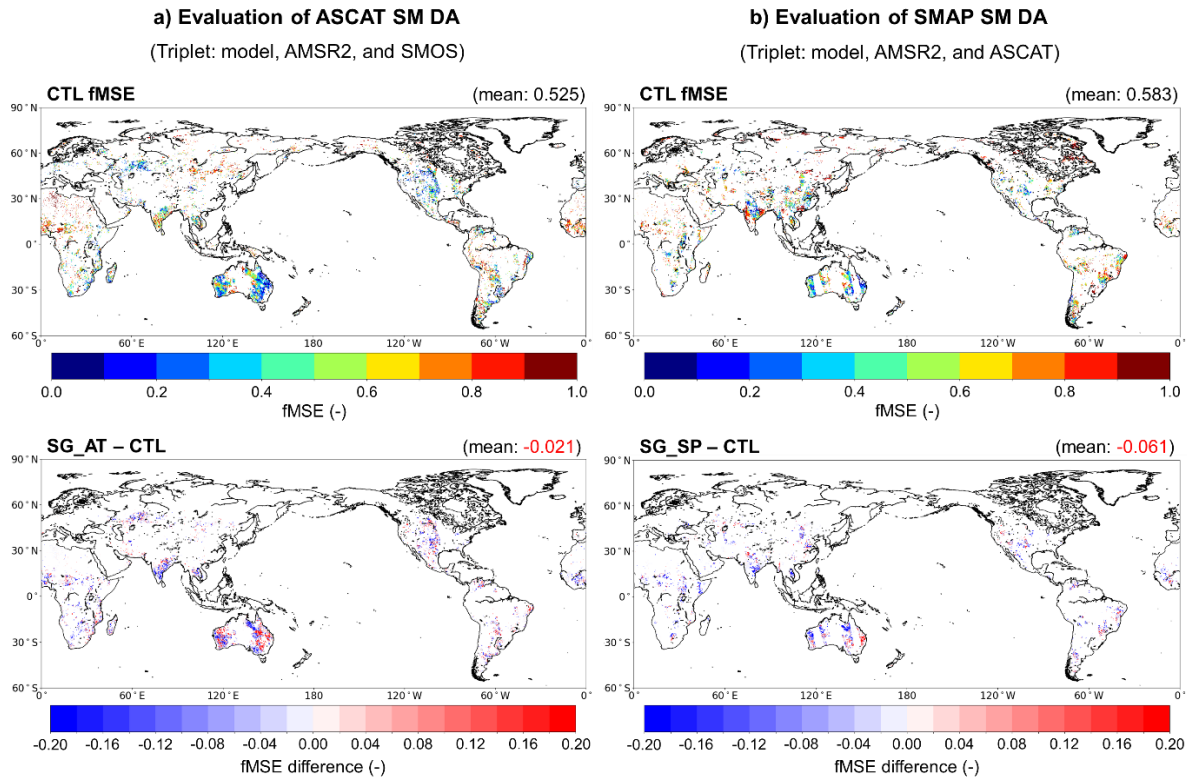
## 659 7.1. Soil moisture analysis

660 The impact of single-sensor soil moisture<sup>SM</sup> assimilation (i.e., SG\_AT and SG\_SP) on  
661 the global soil moisture<sup>SM</sup> estimates is evaluated using the TCA method (see Section 6.1).  
662 Figure 2 presents the spatial distribution of fMSE obtained from TCA during the  
663 experimental period from April to July 2022. Both ASCAT and SMAP are seen to have an  
664 overall positive impact on the surface soil moisture<sup>SM</sup> estimates of the Noah LSM through  
665 assimilation. Compared to the CTL experiment, which does not assimilate soil moisture<sup>SM</sup>  
666 data, SG\_AT and SG\_SP reduce the global mean fMSE by 4.0% (Figure 2a) and 10.5%  
667 (Figure 2b), respectively. In both single-sensor soil moisture<sup>SM</sup> DA cases, obvious  
668 improvements in soil moisture<sup>SM</sup> are observed in Asia while a decrease in skill is mostly  
669 found in the Australian and North American continents where CTL already exhibits a  
670 relatively good performance in estimating soil moisture<sup>SM</sup>.

671 Note that we use identical first and second triplet components for DA and CTL (Table 3),  
672 replacing only the CTL soil moisture estimates with those from the DA experiments (SG\_AT  
673 and SG\_SP) to assess the relative performance gain from soil moisture DA. This approach  
674 (i.e., replacing one triplet member) may alter the fMSE calculation of the other two triplet  
675 components and thus influence the comparison results between DA and CTL. However,  
676 because the soil moisture estimates from DA and CTL share the same spatial and temporal

677 coverage and climatology, as they are generated from the identical modeling system, the  
 678 impact of replacing the model-based triplet member is negligible, as shown in Figure S1.  
 679 Therefore, the fMSE comparison results (Figure 2) can be considered reliable.

680

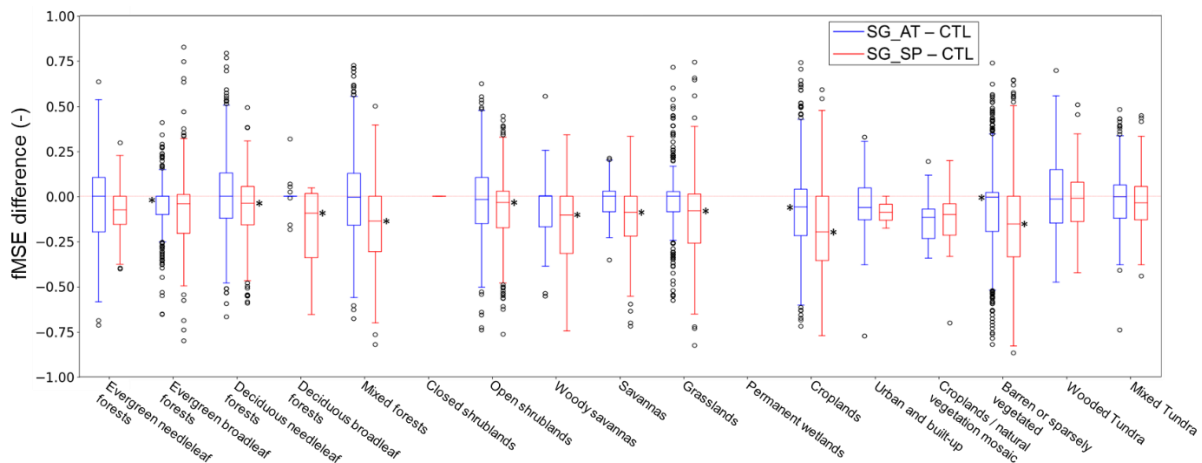


681 **Figure 2.** Global maps of the soil moisture<sup>SM</sup> triple collocation analysis (TCA) results for (a)  
 682 ASCAT (i.e., SG\_AT) and (b) SMAP soil moisture<sup>SM</sup> data assimilation (i.e., SG\_SP). Upper  
 683 panels show the fractional mean-square error (fMSE) of CTL soil moisture<sup>SM</sup> at 04:00  
 684 am/pm local solar time (LST) (left panel) and 11:00 am/pm LST (right panel), respectively.  
 685 Lower panels show the soil moisture<sup>SM</sup> fMSE difference between SG\_AT and CTL (left  
 686 panel) and between SG\_SP and CTL (right panel) where the negative fMSE difference  
 687 indicates the improved soil moisture<sup>SM</sup> estimates by ASCAT and SMAP soil moisture<sup>SM</sup>  
 688 DA, respectively.  
 689  
 690

691 Because land surface characteristics affect the soil moisture<sup>SM</sup> skill of models and  
 692 observations (Draper et al., 2012), the TCA results are also plotted for the MODIS-IGBP land  
 693 cover types. Figure 3 shows that for all land cover types, both SG\_AT and SG\_SP enhance

694 the skill of the modeled soil moisture<sub>SM</sub> relative to CTL in terms of the median fMSE, with  
 695 SG\_SP achieving greater skill gains. The soil moisture<sub>SM</sub> estimates are significantly  
 696 improved by SG\_AT for evergreen broadleaf forests and croplands, and by SG\_SP for  
 697 deciduous needleleaf forests, deciduous broadleaf forests, mixed forests, open shrublands,  
 698 woody savannas, savannas, grasslands, croplands, and barren or sparsely vegetated land  
 699 cover types. In both SG\_AT and SG\_SP experiments, the highest skill improvements, in  
 700 terms of the median fMSE, are observed for croplands. This implies that the land DA system  
 701 effectively utilizes soil moisture<sub>SM</sub> signals related to agricultural practices from satellite  
 702 observations, especially in the case of SMAP soil moisture<sub>SM</sub> DA (SG\_SP), which employs  
 703 the anomaly-based bias correction approach.

704



705

706 **Figure 3.** Differences in the soil moisture<sub>SM</sub> fractional mean-square error (fMSE) between  
 707 the single-sensor soil moisture<sub>SM</sub> data assimilation (i.e., SG\_AT and SG\_SP) and control  
 708 [(without soil moisture<sub>SM</sub> data assimilation (DA); i.e., CTL)] experiments depending on land  
 709 cover types. A dominant land cover type in each model grid is obtained from the MODIS-  
 710 IGBP land cover classifications (Friedl et al., 2002). The asterisk symbol (\*) indicates  
 711 statistical significance at  $p < 0.05$ . Negative values represent the improved soil moisture<sub>SM</sub>  
 712 estimates by soil moisture<sub>SM</sub> DA. Results are not plotted for closed shrublands and  
 713 permanent wetlands because of missing triplet data.

714

715 Figures 2 and 3 indicate that SMAP DA shows higher skill than ASCAT DA for the soil  
716 moisture<sup>SM</sup> analysis. The superior performance of SMAP over ASCAT within a land DA  
717 system is also reported in Seo et al. (2021) where SMAP and ASCAT soil moisture<sup>SM</sup> DA  
718 results are evaluated against *in situ* measurements in the continental United States<sup>CONUS</sup>.  
719 These results can be supported by the fact that L-band brightness temperature measurements  
720 have higher sensitivity to soil moisture<sup>SM</sup> variations than C-band backscatter measurements  
721 (Kolassa et al., 2017), and thus the SMAP soil moisture<sup>SM</sup> retrievals have better accuracy  
722 (Al-Yaari et al., 2019; Kumar et al., 2018). However, note that in this study, a direct  
723 comparison of the global soil moisture<sup>SM</sup> analysis between SG\_AT and SG\_SP is not made  
724 because the model soil moisture<sup>SM</sup> outputs used in TCA are extracted at different LST—  
725 specifically, 04:00 am/pm for SG\_AT and 11:00 am/pm for SG\_SP—due to the different  
726 local overpass times of the satellite soil moisture<sup>SM</sup> data used for TCA-based assessment  
727 (see Section 6.1).

728 As shown in Figure 2, soil moisture<sup>SM</sup> performance gains and losses by each single-  
729 sensor soil moisture<sup>SM</sup> DA are locally dependent. Thus, some previous studies (e.g., Draper  
730 et al., 2012; Kolassa et al., 2017) have shown that simultaneously assimilating soil  
731 moisture<sup>SM</sup> retrievals from both passive and active sensors achieves higher model soil  
732 moisture<sup>SM</sup> accuracy than assimilating a single product. However, ~~because due to the~~  
733 ~~difficulty in obtaining soil moisture<sup>SM</sup>~~ triplets that ~~do not violate fully satisfy~~ the TCA  
734 assumptions (see Section 6.1) are difficult to obtain over the global domain for the multi-  
735 sensor soil moisture<sup>SM</sup> DA experiment, the combined effects of ASCAT and SMAP DA are

736 discussed only ~~for~~ in terms of atmospheric variables, which are the ultimate objective of this  
737 study, in the subsequent sections.

## 739 7.2. Analysis and forecast of specific humidity and air temperature

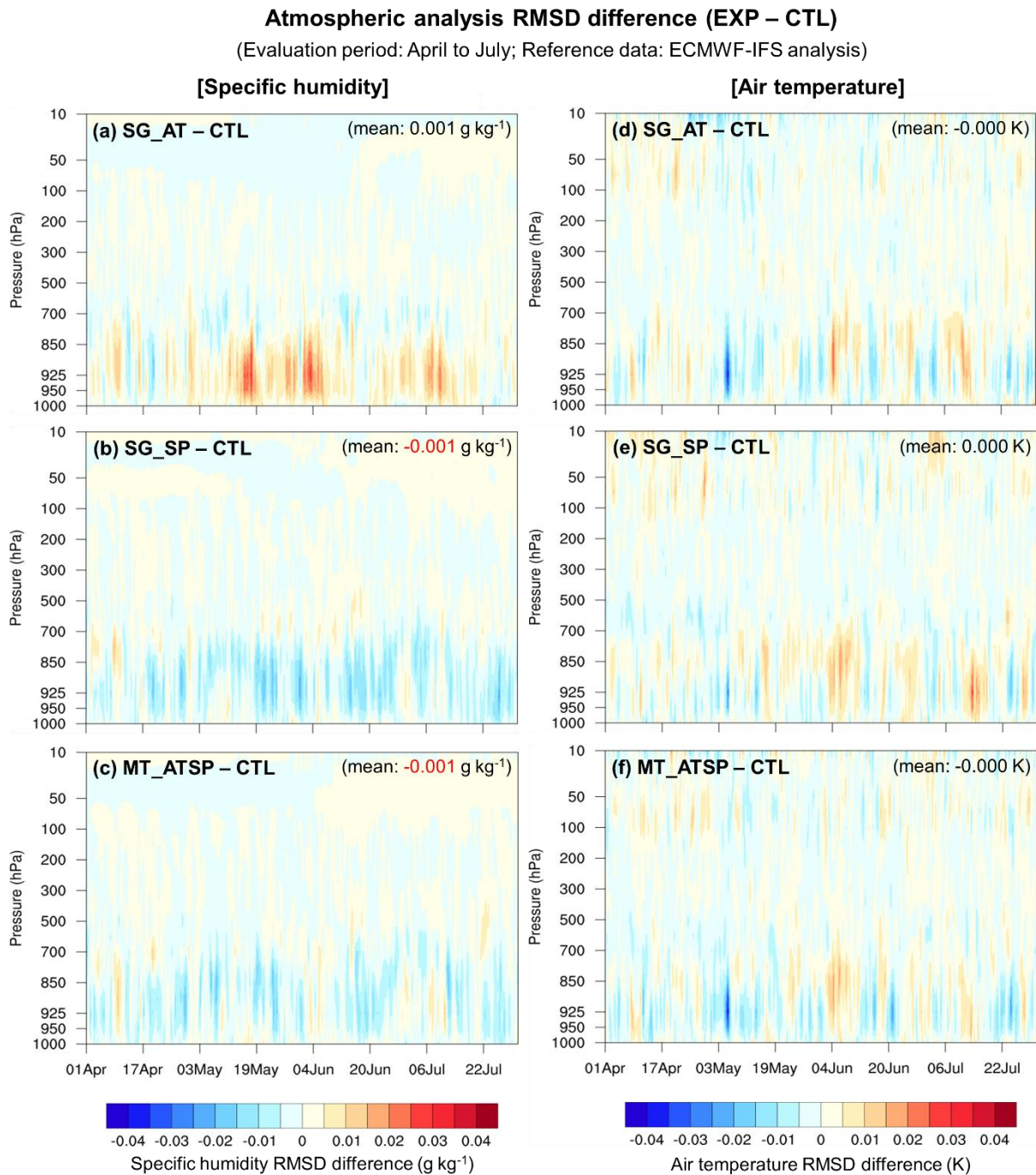
740 Domain-averaged RMSD differences (i.e.,  $\text{RMSD}_{\text{EXP}}$  minus  $\text{RMSD}_{\text{CTL}}$ ) in the specific  
741 humidity analysis (Figures 4a to 4c) and air temperature analysis (Figures 4d to 4f) are  
742 evaluated across atmospheric levels and over time. Compared to CTL (without soil  
743 moisture<sup>SM</sup> DA), ASCAT DA (i.e., SG\_AT) has more beneficial impacts on the air  
744 temperature analysis (Figure 4d) while SMAP DA (i.e., SG\_SP) has more beneficial impacts  
745 on the specific humidity analysis (Figure 4b). Figures 4c and 4f show that the simultaneous  
746 assimilation of ASCAT and SMAP soil moisture<sup>SM</sup> retrievals (i.e., MT\_ATSP) improves the  
747 analysis of both atmospheric variables relative to CTL. Notably, degradations in the specific  
748 humidity and air temperature analyses by SG\_AT and SG\_SP, respectively, are compensated  
749 by additionally assimilating other soil moisture<sup>SM</sup> products.

750 Figure 5 more clearly demonstrates that multi-sensor soil moisture<sup>SM</sup> DA enhances the  
751 performance of the specific humidity (Figure 5a) and air temperature analyses (Figure 5d)  
752 compared to the single-sensor soil moisture<sup>SM</sup> DA cases (i.e., SG\_AT and SG\_SP,  
753 respectively). Although MT\_ATSP exhibits somewhat reduced performance in the air  
754 temperature (Figure 5c) and specific humidity analyses (Figure 5b) compared to SG\_AT and  
755 SG\_SP, respectively, it achieves a more balanced improvement ~~in both atmospheric variables~~  
756 ~~is achieved~~, meaning that neither variable is degraded while both show moderate gains  
757 compared to CTL, by assimilating radar- and radiometer-based soil moisture<sup>SM</sup> data together.

758 Tables 5 and 6 summarize the domain-averaged RMSD differences between the [soil](#)  
759 [moistureSM](#) DA experiments and CTL for the analyses and forecasts of 2-m atmospheric  
760 variables (i.e., specific humidity and air temperature) from the 00 UTC cycle (Table 5) and  
761 the 12 UTC cycle (Table 6). In the global domain, SG\_SP generally achieves better domain-  
762 averaged analysis and forecast skills for both 2-m atmospheric variables compared to SG\_AT  
763 (Tables 5 and 6), except for the 2-m air temperature forecast of the 12 UTC cycle, where  
764 SG\_AT performs slightly better (Table 6). During the experimental period, all [soil](#)  
765 [moistureSM](#) DA cases are more effective in improving the 2-m air temperature analysis and  
766 forecast than those of specific humidity, especially for the 00 UTC cycle. Overall, they  
767 perform better in the Northern Hemisphere than in the Southern Hemisphere (Tables 5 and 6),  
768 although they achieve greater 2-m air temperature forecast skill during the 00 UTC cycle in  
769 the Southern Hemisphere (Table 5). The lower analysis and forecast skills of [soil moistureSM](#)  
770 DA in the Southern Hemisphere can be attributed to the use of spatially and temporally  
771 constant observations errors (see Section 4.2), which do not adequately reflect the relatively  
772 higher uncertainties in winter-period [soil moistureSM](#) data.

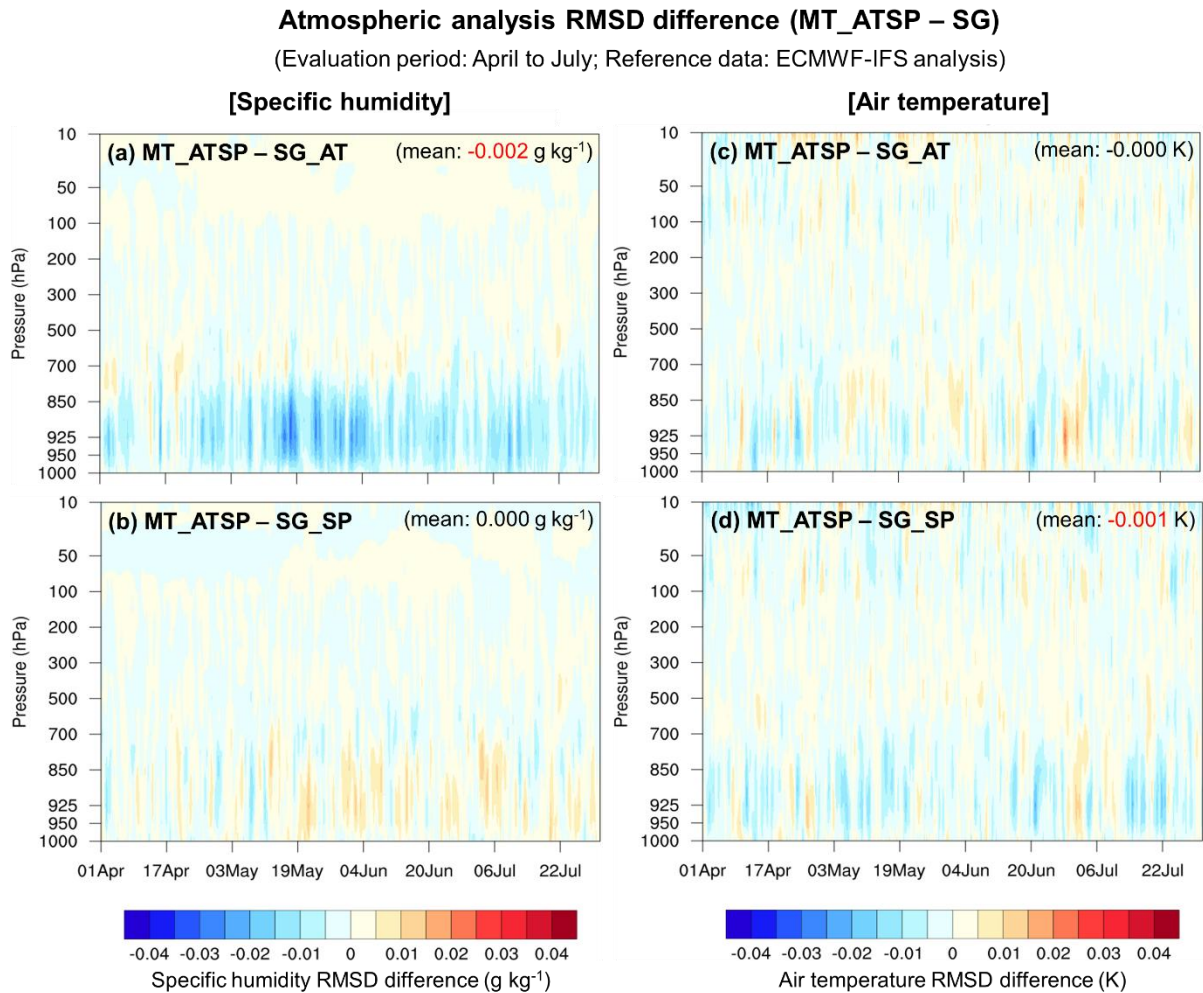
773 For the 2-m specific humidity estimates, the assimilation of SMAP [soil moistureSM](#)  
774 retrievals alone (SG\_SP) achieves the best domain-averaged performance (Tables 5 and 6).  
775 MT\_ATSP reduces RMSD compared to SG\_AT by additionally assimilating the SMAP [soil](#)  
776 [moistureSM](#) data, but it exhibits relatively lower skill in specific humidity than SG\_SP.  
777 However, in Europe and tropical regions, MT\_ATSP provides improved 2-m specific  
778 humidity forecasts compared to SG\_SP, particularly when both ASCAT and SMAP have a

779 positive impact. The synergistic impacts of the combined assimilation of ASCAT and SMAP  
 780 are evident in the 2-m air temperature analysis and forecast of the 00 UTC cycle (Table 5).  
 781



782

783 **Figure 4.** Vertical profile time series of RMSD differences in the specific humidity analysis  
 784 (left column) and air temperature analysis (right column) between the soil moisture<sup>SM</sup> data  
 785 assimilation (DA) and CTL experiments. The RMSD is calculated using the ECMWF-IFS  
 786 analysis as reference data. Negative RMSD differences indicate improved estimates of the  
 787 atmospheric variables by assimilating the soil moisture<sup>SM</sup> retrievals.  
 788



789 **Figure 5.** Vertical profile time series of RMSD differences in the specific humidity analysis  
 790 (left column) and air temperature analysis (right column) between the multi-sensor soil  
 791 moisture<sup>SM</sup> data assimilation (DA) (MT\_ATSP) and single- sensor soil moisture<sup>SM</sup> DA  
 792 [SG\_AT (a and c) and SG\_SP (b and d)] experiments. The RMSD is calculated using the  
 793 ECMWF-IFS analysis as reference data. Negative RMSD differences indicate improved  
 794 estimates of the atmospheric variables by additionally assimilating the SMAP or ASCAT soil  
 795 moisture<sup>SM</sup> retrievals.  
 796  
 797  
 798  
 799



801 **Table 5.** Domain-averaged ARMSD-RMSD differences ( $\Delta\text{RMSD} = \text{RMSD}_{\text{EXP}} - \text{RMSD}_{\text{CTL}}$ ) for the 2-m specific humidity and air temperature  
802 analyses and (5-day) forecasts across six domains [i.e., global domain (GLOB), Northern Hemisphere (NH), Southern Hemisphere (SH), ~~Aisa~~  
803 Asia (ASIA), Europe (EU), and tropical area (TROP)]. The RMSD is calculated for the 00 UTC cycle from April to July 2022 (whole  
804 experimental period) using the ECMWF-IFS analysis as reference data. Negative  $\Delta\text{RMSD}$  indicates improved estimates of the atmospheric  
805 variables by assimilating the soil moistureSM retrievals.

April to July 2022 (00 UTC)																				2-m specific humidity $\Delta\text{RMSD}$ (EXP – CTL) [g kg <sup>-1</sup> ]								
Domain	Analysis						Forecast																					
	1-day lead time			2-day lead time			3-day lead time			4-day lead time			5-day lead time															
	SG_ AT	SG_ SP	MT_ ATSP	SG_ AT	SG_ SP	MT_ ATSP	SG_ AT	SG_ SP	MT_ ATSP																			
GLOB	0.011	<b>-0.001</b>	0.001	0.012	0.001	0.002	0.014	0.004	0.005	0.013	0.004	0.004	0.014	0.004	0.006	0.017	0.004	0.010										
NH	0.005	<b>-0.006</b>	<b>-0.005</b>	0.005	<b>-0.004</b>	<b>-0.004</b>	0.006	<b>-0.002</b>	<b>-0.001</b>	0.006	<b>-0.002</b>	<b>-0.001</b>	0.005	<b>-0.004</b>	0.000	0.009	<b>-0.005</b>	0.001										
SH	0.046	0.025	0.040	0.029	0.011	0.016	0.026	0.010	0.012	0.017	0.006	0.007	0.018	0.007	0.009	0.022	0.016	0.025										
ASIA	0.004	<b>-0.004</b>	<b>-0.002</b>	0.003	<b>-0.001</b>	0.000	0.006	0.002	0.003	0.008	0.004	0.004	0.009	0.003	0.006	0.009	0.006	0.010										
EU	0.016	<b>-0.001</b>	0.003	0.012	<b>-0.002</b>	<b>-0.004</b>	0.010	<b>-0.000</b>	<b>-0.005</b>	0.004	<b>-0.001</b>	<b>-0.006</b>	0.002	0.006	0.000	0.002	0.003	0.001										
TROP	0.008	<b>-0.001</b>	<b>-0.004</b>	0.016	0.005	0.005	0.021	0.011	0.010	0.022	0.012	0.011	0.023	0.013	0.013	0.025	0.014	0.017										

2-m air temperature $\Delta\text{RMSD}$ (EXP – CTL) [K]																			
Domain	Analysis						Forecast												
	1-day lead time			2-day lead time			3-day lead time			4-day lead time			5-day lead time						
	SG_ AT	SG_ SP	MT_ ATSP	SG_ AT	SG_ SP	MT_ ATSP													
GLOB	0.001	0.000	<b>-0.003</b>	<b>-0.000</b>	<b>-0.014</b>	<b>-0.013</b>	0.001	<b>-0.013</b>	<b>-0.011</b>	0.001	<b>-0.011</b>	<b>-0.010</b>	0.003	<b>-0.010</b>	<b>-0.008</b>	0.005	<b>-0.009</b>	<b>-0.003</b>	
NH	0.001	<b>-0.008</b>	<b>-0.007</b>	0.002	<b>-0.005</b>	<b>-0.005</b>	0.007	0.002	0.002	0.010	0.006	0.006	0.013	0.009	0.011	0.015	0.008	0.017	
SH	0.016	0.002	<b>-0.003</b>	0.006	<b>-0.012</b>	<b>-0.009</b>	<b>-0.006</b>	<b>-0.027</b>	<b>-0.022</b>	<b>-0.016</b>	<b>-0.028</b>	<b>-0.028</b>	<b>-0.019</b>	<b>-0.033</b>	<b>-0.029</b>	<b>-0.012</b>	<b>-0.021</b>	<b>-0.024</b>	
ASIA	<b>-0.000</b>	<b>-0.007</b>	<b>-0.003</b>	<b>-0.001</b>	<b>-0.009</b>	<b>-0.025</b>	<b>-0.003</b>	<b>-0.009</b>	<b>-0.029</b>	<b>-0.003</b>	<b>-0.007</b>	<b>-0.029</b>	0.002	<b>-0.003</b>	<b>-0.020</b>	0.005	<b>-0.009</b>	<b>-0.015</b>	
EU	<b>-0.005</b>	<b>-0.011</b>	<b>-0.010</b>	<b>-0.009</b>	<b>-0.033</b>	<b>-0.027</b>	<b>-0.001</b>	<b>-0.027</b>	<b>-0.019</b>	<b>-0.000</b>	<b>-0.026</b>	<b>-0.019</b>	<b>-0.003</b>	<b>-0.026</b>	<b>-0.019</b>	<b>-0.012</b>	<b>-0.038</b>	<b>-0.022</b>	
TROP	<b>-0.005</b>	0.012	0.001	<b>-0.005</b>	<b>-0.027</b>	<b>-0.027</b>	<b>-0.006</b>	<b>-0.030</b>	<b>-0.028</b>	<b>-0.008</b>	<b>-0.032</b>	<b>-0.029</b>	<b>-0.007</b>	<b>-0.030</b>	<b>-0.029</b>	<b>-0.005</b>	<b>-0.030</b>	<b>-0.027</b>	

806  
807  
808  
809

810 **Table 6.** Same as Table 5 but for the 12 UTC cycle from April to July 2022 (whole experimental period).

April to July 2022 (12 UTC)				2-m specific humidity $\Delta$ RMSD (EXP – CTL) [g kg <sup>-1</sup> ]														
Domain	Analysis			Forecast														
	SG_ AT	SG_ SP	MT_ ATSP	1-day lead time			2-day lead time			3-day lead time			4-day lead time			5-day lead time		
				SG_ AT	SG_ SP	MT_ ATSP	SG_ AT	SG_ SP	MT_ ATSP	SG_ AT	SG_ SP	MT_ ATSP	SG_ AT	SG_ SP	MT_ ATSP	SG_ AT	SG_ SP	MT_ ATSP
<b>GLOB</b>	0.014	0.004	0.006	0.015	0.008	0.010	0.019	0.010	0.014	0.018	0.011	0.015	0.017	0.011	0.016	0.019	0.012	0.019
<b>NH</b>	0.003	<b>-0.006</b>	<b>-0.005</b>	0.005	<b>-0.009</b>	<b>-0.006</b>	0.007	<b>-0.007</b>	<b>-0.001</b>	0.006	<b>-0.004</b>	0.002	0.005	<b>-0.004</b>	0.002	0.008	<b>-0.006</b>	0.003
<b>SH</b>	0.052	0.026	0.036	0.064	0.040	0.050	0.060	0.033	0.045	0.053	0.029	0.041	0.046	0.027	0.042	0.046	0.030	0.046
<b>ASIA</b>	0.006	0.002	0.003	0.007	<b>-0.002</b>	0.001	0.011	<b>-0.000</b>	0.007	0.009	0.004	0.014	0.009	0.005	0.014	0.011	0.000	0.016
<b>EU</b>	<b>-0.003</b>	<b>-0.007</b>	<b>-0.009</b>	<b>-0.003</b>	<b>-0.005</b>	<b>-0.009</b>	<b>-0.004</b>	0.000	<b>-0.007</b>	<b>-0.008</b>	0.000	<b>-0.008</b>	<b>-0.011</b>	0.005	<b>-0.005</b>	<b>-0.014</b>	0.003	0.003
<b>TROP</b>	0.018	0.013	0.013	0.013	0.022	0.019	0.021	0.026	0.026	0.023	0.027	0.026	0.027	0.028	0.029	0.026	0.030	0.033

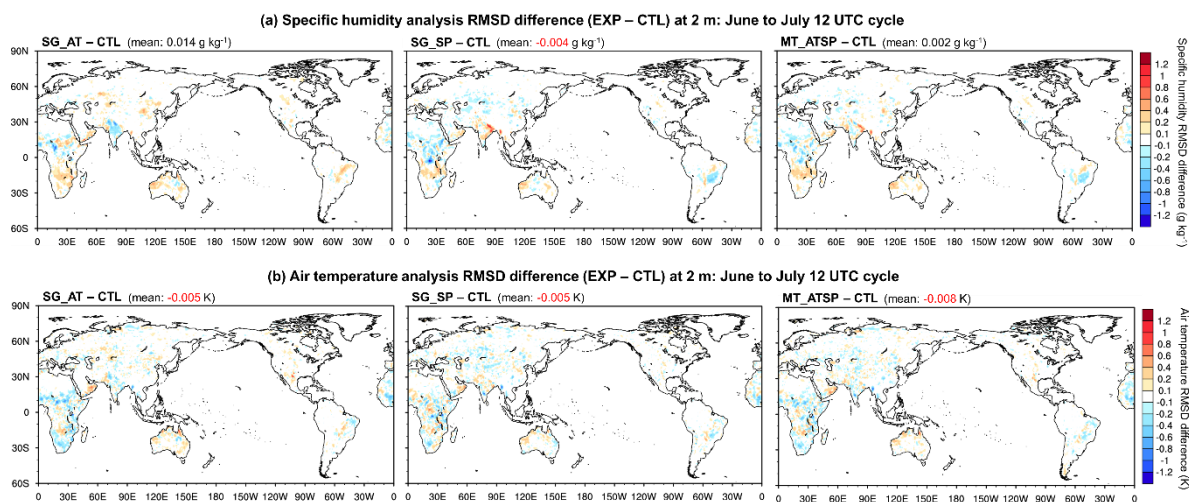
  

				2-m air temperature $\Delta$ RMSD (EXP – CTL) [K]														
Domain	Analysis			Forecast														
	SG_ AT	SG_ SP	MT_ ATSP	1-day lead time			2-day lead time			3-day lead time			4-day lead time			5-day lead time		
				SG_ AT	SG_ SP	MT_ ATSP	SG_ AT	SG_ SP	MT_ ATSP	SG_ AT	SG_ SP	MT_ ATSP	SG_ AT	SG_ SP	MT_ ATSP	SG_ AT	SG_ SP	MT_ ATSP
<b>GLOB</b>	<b>-0.007</b>	<b>-0.010</b>	<b>-0.015</b>	0.005	0.018	0.012	0.008	0.018	0.012	0.009	0.019	0.015	0.007	0.017	0.011	0.008	0.018	0.011
<b>NH</b>	0.002	<b>-0.004</b>	<b>-0.007</b>	<b>-0.002</b>	<b>-0.008</b>	<b>-0.008</b>	<b>-0.000</b>	<b>-0.012</b>	<b>-0.009</b>	<b>-0.003</b>	<b>-0.015</b>	<b>-0.011</b>	<b>-0.004</b>	<b>-0.018</b>	<b>-0.018</b>	<b>-0.002</b>	<b>-0.018</b>	<b>-0.017</b>
<b>SH</b>	0.008	<b>-0.001</b>	<b>-0.004</b>	0.070	0.037	0.051	0.082	0.045	0.060	0.087	0.050	0.071	0.091	0.060	0.079	0.082	0.056	0.073
<b>ASIA</b>	<b>-0.006</b>	<b>-0.010</b>	<b>-0.018</b>	0.002	<b>-0.004</b>	<b>-0.002</b>	0.011	<b>-0.003</b>	0.004	0.010	<b>-0.007</b>	0.004	0.009	<b>-0.016</b>	<b>-0.006</b>	0.015	<b>-0.017</b>	0.001
<b>EU</b>	0.000	<b>-0.003</b>	<b>-0.000</b>	<b>-0.021</b>	<b>-0.004</b>	<b>-0.008</b>	<b>-0.026</b>	<b>-0.001</b>	<b>-0.011</b>	<b>-0.031</b>	0.003	<b>-0.015</b>	<b>-0.032</b>	0.008	<b>-0.020</b>	<b>-0.033</b>	0.018	<b>-0.009</b>
<b>TROP</b>	<b>-0.024</b>	<b>-0.021</b>	<b>-0.029</b>	<b>-0.007</b>	0.049	0.026	<b>-0.003</b>	0.053	0.027	<b>-0.000</b>	0.058	0.033	<b>-0.003</b>	0.054	0.031	<b>-0.000</b>	0.058	0.031

811

812 Local performance differences in the 2-m atmospheric analysis between the single-sensor  
813 [soil moisture<sup>SM</sup>](#) DA cases are clearly illustrated in Figure 6, which is plotted for the 12 UTC  
814 cycle from June to July 2022. SG\_AT and SG\_SP exhibit opposite impacts on the  
815 atmospheric analysis, especially on specific humidity, over India, Eurasia, and Brazil.  
816 ASCAT DA (SG\_AT) generally leads to the improved analyses of specific humidity and air  
817 temperature over India while SMAP DA (SG\_SP) performs better in Eurasia (except for  
818 India and the southern part of West Asia) and Brazil. These discrepancies in the local  
819 performance of 2-m specific humidity between ASCAT and SMAP DA may contribute to the  
820 reduced domain-averaged skill of MT\_ATSP relative to SG\_SP, as shown in Tables 5 and 6.  
821 In Africa, SG\_AT yields better air temperature analysis than SG\_SP, whereas SG\_SP  
822 outperforms SG\_AT in the specific humidity analysis. It can be noted from Figure 6 that,  
823 locally, the joint assimilation of the ASCAT and SMAP [soil moisture<sup>SM</sup>](#) retrievals yields the  
824 best estimates of the 2-m atmospheric variables when both [soil moisture<sup>SM</sup>](#) products have  
825 positive impacts.

826



827

828 **Figure 6.** Difference in the 2-m atmospheric analysis RMSD [i.e., specific humidity (upper  
829 panels) and air temperature (lower panels)] between the soil moisture<sup>SM</sup> data assimilation  
830 (DA) and CTL experiments. Evaluation results for the 12 UTC cycle from June to July 2022  
831 (a two-month period) are presented with domain-averaged values in parenthesis. The RMSD  
832 is calculated using the ECMWF-IFS analysis as reference data. Negative RMSD differences  
833 indicate improved estimates of the atmospheric variables by assimilating the soil moisture<sup>SM</sup>  
834 retrievals.  
835

### 836 7.3. Precipitation

837 The potential added value of multi-sensor soil moisture<sup>SM</sup> DA for precipitation forecasts  
838 is assessed using categorical skill score metrics, including the FB and ETS, as detailed in  
839 Section 6.3. Daily precipitation rates ( $\text{mm day}^{-1}$ ) are computed from the KIM forecasts at 0-  
840 24 h, 24-48 h, and 48-72 h lead times, and compared against reference data using seven  
841 conventional thresholds (0.5, 1.0, 5.0, 10.0, 15.0, 20.0, and 25.0  $\text{mm day}^{-1}$ ). The numbers of  
842 model grid points classified as *Hits*, *FalseAlarms*, *Misses*, and *CorrectNegatives* in the  
843 contingency table (Table 4) are then counted, and FB and ETS are calculated for six domains  
844 (i.e., global domain, Northern Hemisphere, Southern Hemisphere, Asia, Europe, and tropical  
845 area). Figure 7S2 presents the FB and ETS of daily precipitation forecasts from KIM,  
846 averaged accumulated over the three lead times, 0-24 h, 24-48 h, and 48-72 h, in the for CTL  
847 and the three soil moisture<sup>SM</sup> DA experiments (SG\_AT, SG\_SP, and MT\_ATSP) during the  
848 00 UTC cycle in July 2022. The corresponding differences ( $\Delta\text{FB} = |\text{FB}_{\text{EXP}} - 1| -$   
849  $|\text{FB}_{\text{CTL}} - 1|$ ,  $\Delta\text{ETS} = \text{ETS}_{\text{EXP}} - \text{ETS}_{\text{CTL}}$ ) are shown in Figure 7.

850 In the global domain, CTL (without soil moisture<sup>SM</sup> DA) tends to overestimate  
851 precipitation frequency ( $\text{FB} > 1.0$ ), simulating excessive precipitation events, except for the  
852 precipitation threshold of  $25.0 \text{ mm day}^{-1}$  (Figure 7S2a). The model significantly

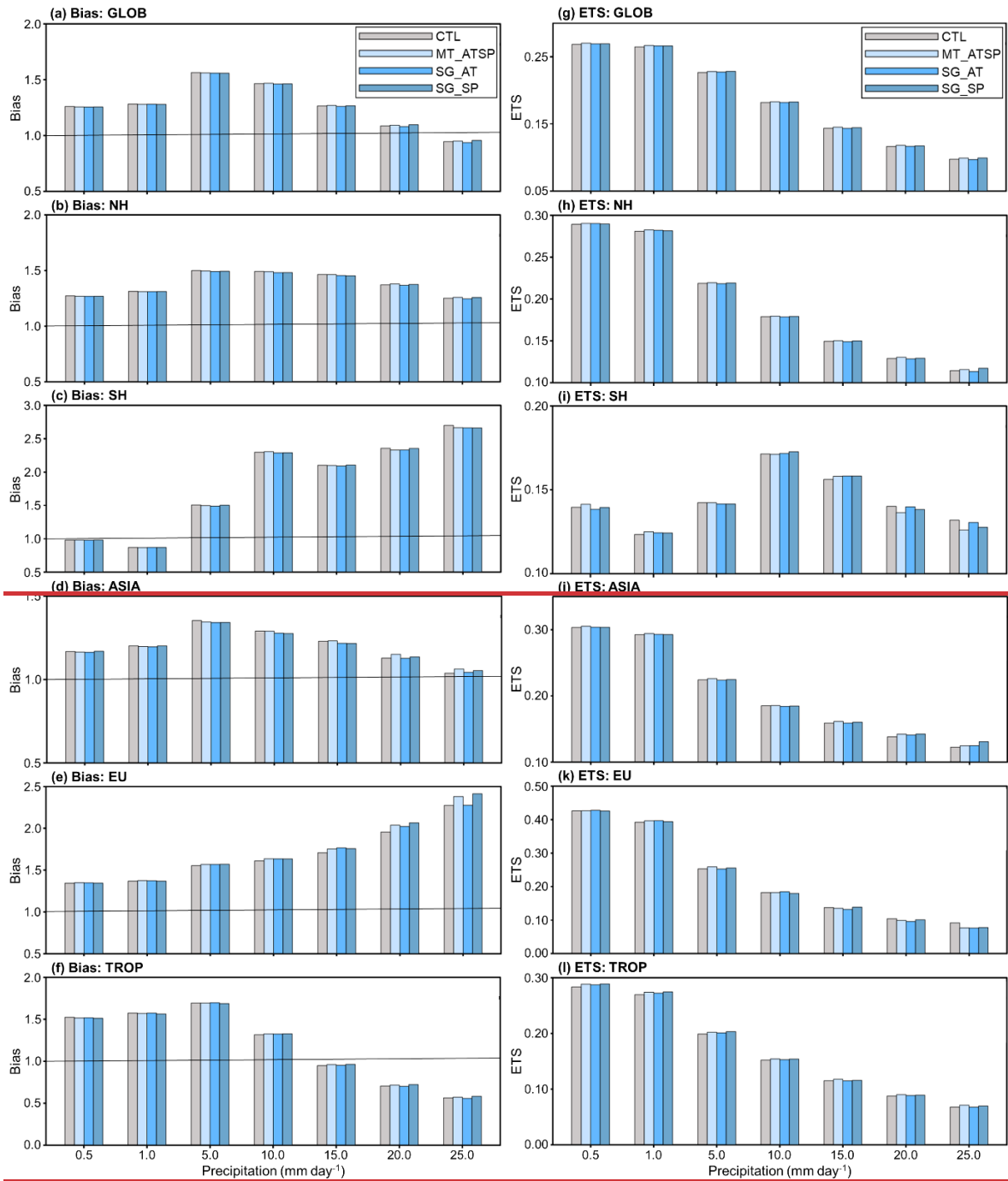
853 overestimates precipitation at the 5.0 mm day<sup>-1</sup> threshold and exhibits an FB close to 1 for  
854 heavier precipitation events (20.0 and 25.0 mm day<sup>-1</sup>) (Figure 7S2a), with regional  
855 variations (Figures 7S2b to 7S2f). Both the smallest FB (close to 1.0) and the largest FB (>  
856 2.5) are observed in the Southern Hemisphere for the lightest (0.5 mm day<sup>-1</sup>) and heaviest  
857 (25.0 mm day<sup>-1</sup>) precipitation events, respectively (Figure 7S2c).

858 Unlike FB, ETS is higher (indicating better skill in predicting precipitation events) at  
859 lower precipitation thresholds while ETS decreases as the precipitation intensity thresholds  
860 increase in the global domain (Figure 7S2g) and in the Northern Hemisphere (Figure 7S2h),  
861 including Asia (Figure 7S2j), Europe (Figure 7S2k), and tropical areas (Figure 7S2l). In the  
862 Southern Hemisphere, CTL shows the highest ETS skill at the precipitation threshold of 10.0  
863 mm day<sup>-1</sup> and the lowest at 1.0 mm day<sup>-1</sup> (Figure 7S2i). The different model performance  
864 patterns (in both FB and ETS) between the Northern and Southern Hemispheres across the  
865 range of precipitation intensity thresholds may be attributed to different weather regimes  
866 associated with cyclones and monsoons (Dare and Ebert, 2017), along with additional  
867 impacts from seasonal variations.

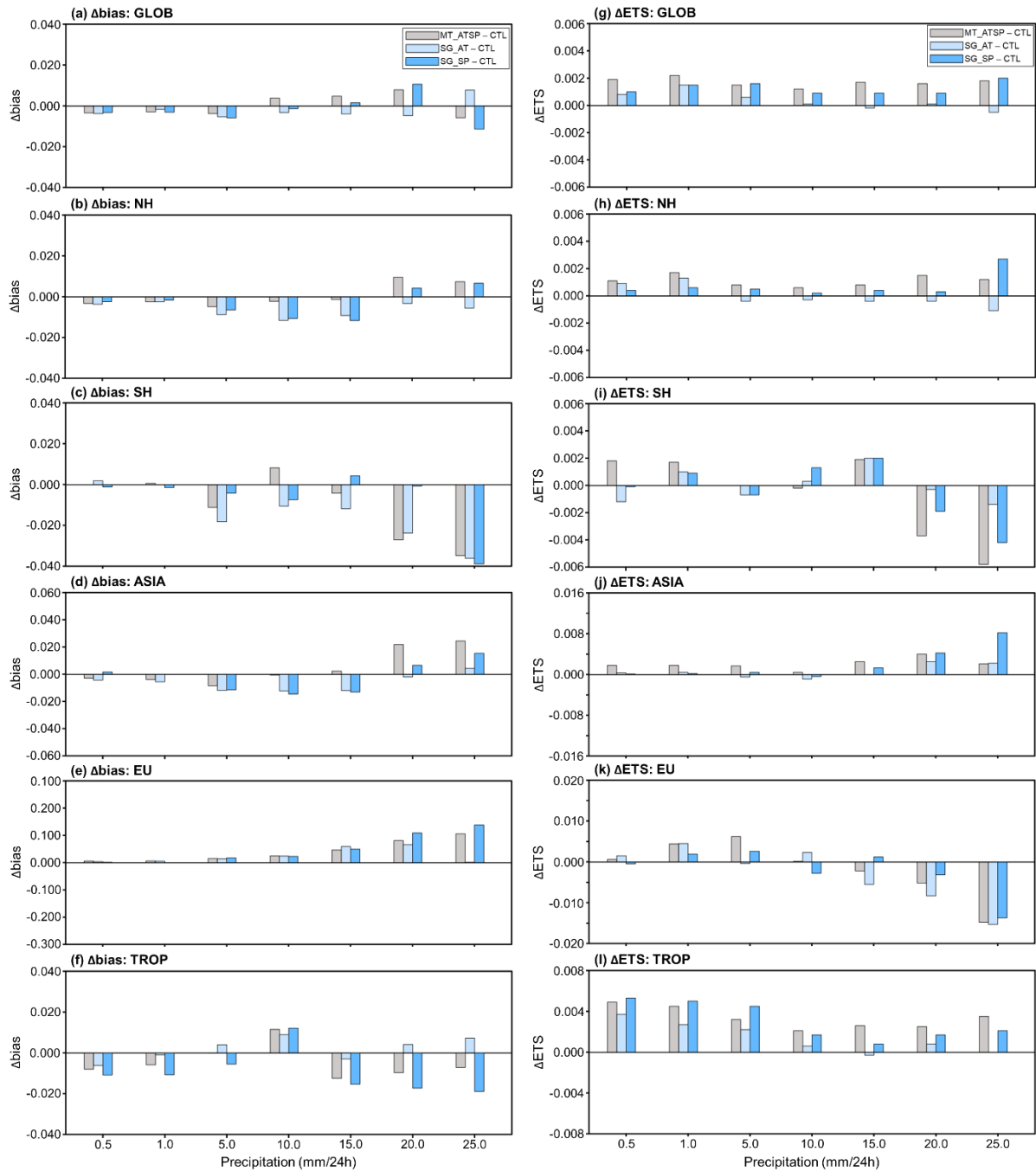
868 Overall, soil moistureSM DA improves the prediction of precipitation events (i.e., better  
869 ETS; Figure 7g) while its contribution to precipitation frequency (FB) remains neutral  
870 (Figure 7a). MT\_ATSP demonstrates higher ETS skill than CTL (by up to 1.8%) and single-  
871 sensor soil moistureSM DA (by up to 2.4% and 0.6% relative to SG\_AT and SG\_SP,  
872 respectively) (Figure 7g). The impacts of MT\_ATSP on the globally-averaged FB are  
873 marginal, showing negligible improvements at the 0.5, 1.0, 5.0, and 25.0 mm day<sup>-1</sup>  
874 thresholds and slight overpredictions at the 10.0, 15.0, and 20.0 mm day<sup>-1</sup> thresholds (Figure

875 7a, [Figure S2a](#)). Similar [soil moisture](#) SM DA performance patterns are observed in the  
876 Northern Hemisphere (Figures 7b and 7h) and Asia (Figures 7d and 7j). In the Southern  
877 Hemisphere, MT\_ATSP slightly improves FB for heavy precipitation events (precipitation  
878 thresholds  $\geq 2015.0$  mm day<sup>-1</sup>) while relatively obvious improvements in ETS by MT\_ATSP  
879 are witnessed at lower thresholds ( $\leq 1.0$  mm day<sup>-1</sup>) (Figures 7c and 7i). ~~Multi-sensor SM DA~~  
880 ~~enhances both FB and ETS across the range of precipitation thresholds in tropical areas~~  
881 ~~(Figures 7f and 7l, respectively). Compared to CTL and SG\_AT, multi-sensor soil moisture~~  
882 ~~DA enhances ETS across precipitation thresholds in tropical areas, although it is slightly less~~  
883 ~~effective than SG\_SP at thresholds  $\leq 5.0$  mm day<sup>-1</sup> (Figure 7l). For FB, MT\_ATSP shows~~  
884 ~~improvements over CTL and SG\_AT in tropical areas, except at thresholds of 5.0 and 10.0~~  
885 ~~mm day<sup>-1</sup>, where SG\_SP performs better (Figure 7f). In contrast, MT\_ATSP# is generally~~  
886 ineffective in Europe (Figures 7e and 7k), except for ETS at precipitation thresholds of 5.0  
887 mm day<sup>-1</sup> or lower. The overprediction of precipitation in Europe (Figure 7e, [Figure S2e](#)),  
888 especially for heavy precipitation events ( $\geq 15.0$  mm day<sup>-1</sup>), may lead to a decrease in ETS  
889 (Figure 7k, [Figure S2k](#)).

890



891 **Figure 7.** FB (a to f) and ETS (g to l) of 24–72 h precipitation forecasts at the 00 UTC cycle  
 892 in July 2022, averaged across six domains [i.e., global domain (GLOB; a and g), Northern  
 893 Hemisphere (NH; b and h), Southern Hemisphere (SH; c and i), Aisa (ASIA; d and j), Europe  
 894 (EU; e and k), and tropical area (TROP; f and l)]. The skill metrics are computed for seven  
 895 conventional thresholds (i.e., 0.5, 1.0, 5.0, 10.0, 15.0, 20.0, and 25.0 mm day<sup>-1</sup>).  
 896  
 897



898  
899  
900  
901  
902  
903  
904

**Figure 7.** Differences in frequency bias ( $\Delta FB = |FB_{EXP} - 1| - |FB_{CTL} - 1|$ ; a to f) and equitable threat score ( $\Delta ETS = ETS_{EXP} - ETS_{CTL}$ ; g to l) between EXP (MT\_ATSP, SG\_AT, and SG\_SP) and CTL, averaged over 24-72 h precipitation forecasts from the 00 UTC cycle in July 2022, for six domains [i.e., global domain (GLOB; a and g), Northern Hemisphere (NH; b and h), Southern Hemisphere (SH; c and i), Asia (ASIA; d and j), Europe (EU; e and k), and tropical area (TROP; f and l)]. The skill metrics are computed for seven conventional

905 thresholds (i.e., 0.5, 1.0, 5.0, 10.0, 15.0, 20.0, and 25.0 mm day<sup>-1</sup>). Negative  $\Delta$ FB and  
906 positive  $\Delta$ ETS values indicate improvements from soil moisture DA.

## 909 **8. Discussion**

### 910 **8.1. ASCAT data assimilation**

911 The experimental results indicate that SMAP DA slightly outperforms ASCAT DA in  
912 enhancing near-surface atmospheric analyses and forecasts. While many factors may affect  
913 the overall performance of each experiment, one factor may be related to errors resulting  
914 from subsurface scattering, which are not accounted for in the ASCAT soil moisture<sup>SM</sup> data  
915 used in this study, as discussed by Wagner et al. (2024). The current TU Wien change  
916 detection algorithm (Wagner et al., 1999, 2010), used to retrieve soil moisture<sup>SM</sup> from  
917 ASCAT backscatter observations, is based on the assumption of a positive linear relationship  
918 between soil backscatter and wetness. However, Wagner et al. (2024) demonstrated that this  
919 assumption fails when coarse fragments (e.g., stones and rocks) or discontinuities exist in the  
920 soil profile, as they increase subsurface scattering contributions to total backscatter signals  
921 under dry soil conditions. This eventually reverses the relationship between backscatter  
922 signals and soil moisture content, deteriorating the quality of soil moisture<sup>SM</sup> data retrieved  
923 with the current algorithm in many arid and semiarid regions. This phenomenon partly  
924 explains why ASCAT DA exhibits better performance in croplands than in barren or sparsely  
925 vegetated areas, as shown in Figure 3, which is consistent with results from soil moisture<sup>SM</sup>  
926 data evaluation studies (e.g., Dorigo et al., 2010).

927 Soil moisture<sup>SM</sup> bias correction methods used to remove systematic discrepancies  
928 between observations and models may also influence the ASCAT soil moisture<sup>SM</sup> DA

929 performance. Kumar et al. (2015) and Kwon et al. (2022, 2024) have shown that different  
930 bias correction methods can substantially impact soil moisture<sup>SM</sup> DA performance. In  
931 SMAP DA, soil moisture<sup>SM</sup> temporal variability information is directly assimilated (i.e.,  
932 anomaly correction method). In contrast, ASCAT DA employs the CDF matching method  
933 because it does not satisfy the underlying assumption of the anomaly correction method (see  
934 Section 3.3). It is a known issue that rescaling-based bias correction, such as CDF matching,  
935 causes a significant loss of information (Kumar et al., 2015). Meanwhile, Text S1 and Figures  
936 ~~S31-S53~~ suggest that employing the anomaly correction method in soil moisture<sup>SM</sup> DA  
937 worsens the atmospheric analysis within land-atmosphere coupled systems when the  
938 underlying assumptions of the anomaly correction approach are not met. Rather than relying  
939 on CDF matching and anomaly correction methods, a more robust and appropriate bias  
940 correction approach is required for improving ASCAT soil moisture<sup>SM</sup> DA.

941

## 942 **8.2. Soil moisture observation error**

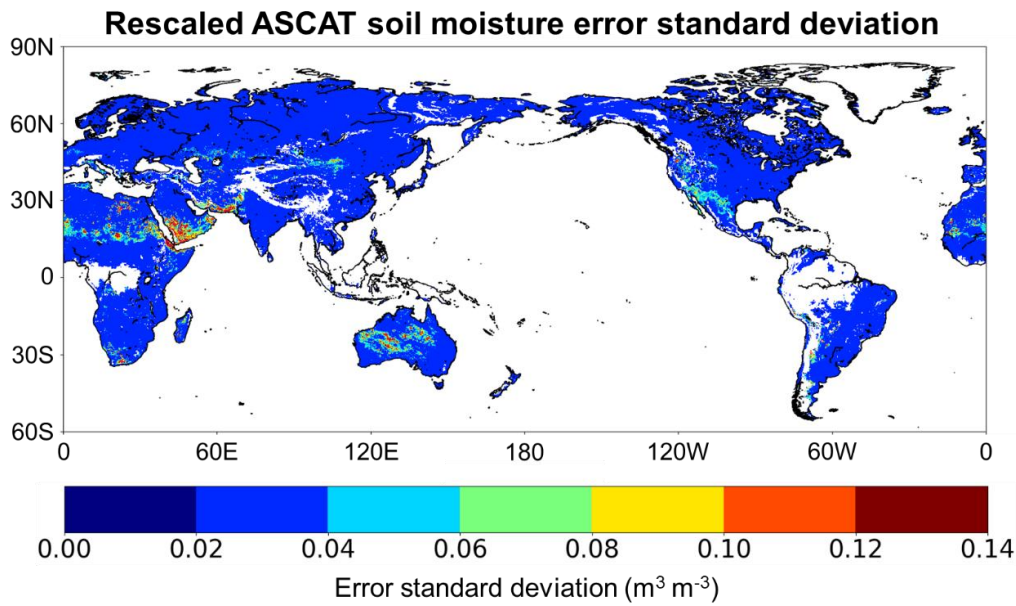
943 The effectiveness of the combined assimilation of multiple soil moisture<sup>SM</sup> products  
944 from different sources (i.e., radar backscatter and radiometer brightness temperature  
945 observations) in enhancing the soil moisture<sup>SM</sup> analysis skill has been demonstrated in  
946 previous studies (e.g., Blyverket et al., 2019; Draper et al., 2012; Kolassa et al., 2017;  
947 Renzullo et al., 2014). Our experimental results also show that, compared to single-sensor  
948 soil moisture<sup>SM</sup> DA, simultaneous assimilation of the ASCAT and SMAP soil moisture<sup>SM</sup>  
949 retrievals within the KIM-LIS coupled system has a synergistic impact, improving the  
950 analyses and forecasts of atmospheric variables including specific humidity, air temperature,

951 and precipitation. However, the superiority of individual single-sensor soil moisture<sup>SM</sup>  
952 retrieval products and their combined performance within the DA system depend on the  
953 region and time period (Figure 6). Specifically, locally reduced benefits of SMAP or ASCAT  
954 are observed in the multi-sensor soil moisture<sup>SM</sup> DA experiment when their performance  
955 impacts are opposite (Figure 6). This may be attributed to the use of uniform observation  
956 error standard deviations for the soil moisture<sup>SM</sup> retrievals across space and time, which is  
957 unrealistic and does not adequately reflect the actual and relative retrieval skill of each soil  
958 moisture<sup>SM</sup> product. Especially, underestimated soil moisture<sup>SM</sup> observation errors can  
959 degrade the soil moisture<sup>SM</sup> and atmospheric analyses by over-relying on less reliable soil  
960 moisture<sup>SM</sup> data within the DA framework.

961 One key advantage of simultaneously assimilating individual soil moisture<sup>SM</sup> products,  
962 rather than a preprocessed multi-sensor-derived soil moisture<sup>SM</sup> product, is the flexibility to  
963 handle individual soil moisture<sup>SM</sup> sensors separately within a single DA system while  
964 achieving comparable performance (Kolassa et al., 2017). However, this advantage can be  
965 more effectively utilized by accurately specifying the relative errors of the soil moisture<sup>SM</sup>  
966 retrievals in space and time, enabling the optimal combination of models and diverse soil  
967 moisture<sup>SM</sup> products.

968 Several recent studies (e.g., Wu et al., 2021; Kim et al., 2023; Kim et al., 2025) have  
969 made efforts to estimate spatially or spatiotemporally distributed errors in satellite-based soil  
970 moisture<sup>SM</sup> retrievals using TCA-based methods and machine learning (ML) algorithms. A  
971 map of spatially distributed (but time-invariant) error standard deviations from Kim et al.  
972 (2025) [see Figure S64, which is Figure 5a in Kim et al. (2025)] exhibits that the SMAP soil

973 [moisture<sup>SM</sup>](#) data have errors greater than  $0.05 \text{ m}^3 \text{ m}^{-3}$  in many areas, particularly in forests.  
974 Excluding forested areas where [soil moisture<sup>SM</sup>](#) retrievals are masked out during [quality](#)  
975 [control<sup>QC</sup>](#) (see Section 3.4) and thus not assimilated, the error standard deviations of SMAP  
976 [soil moisture<sup>SM</sup>](#) are still above  $0.02 \text{ m}^3 \text{ m}^{-3}$  (the uniformly applied error value in this study)  
977 in some savanna regions of South America and Africa, grasslands in North America, and  
978 croplands in South Asia (Figure S64;) [see Figure S43c for land cover types] [map generated](#)  
979 [in this study using the MODIS-IGBP global land-cover classification \(Friedl et al., 2002\)](#). As  
980 a result, this leads to degradation in the 2-m specific humidity and air temperature analysis in  
981 the regions, as noted in the SMAP [soil moisture<sup>SM</sup>](#) DA (SG\_SP) results shown in Figure 6.  
982 Meanwhile, in ASCAT [soil moisture<sup>SM</sup>](#) DA, the spatially distributed [soil moisture<sup>SM</sup>](#)  
983 observation error standard deviation ( $\text{m}^3 \text{ m}^{-3}$ ) (Figure 8) is applied after locally rescaling the  
984 uniformly specified 10% [soil wetness index<sup>SWI</sup>](#) observation error using the ratio of the  
985 standard deviations of modeled and observed [soil moisture<sup>SM</sup>](#) time series (see Section 4.2).  
986 However, the spatial pattern of the ASCAT observation error standard deviations in Figure 8  
987 does not completely match that of the TCA/ML-based ASCAT fMSE computed by Kim et al.  
988 (2023) (see their Figure 4f), which was derived using other satellite [soil moisture<sup>SM</sup>](#) data as  
989 triplet components. Notably, the ASCAT errors used in the current study appear to be  
990 relatively underestimated in dry areas of Africa and Asia (Figure 8), where the 2-m  
991 atmospheric analyses are degraded by ASCAT [soil moisture<sup>SM</sup>](#) DA (SG\_AT in Figure 6).  
992



993 **Figure 8.** ASCAT soil moisture (~~SM~~) error standard deviations used for ASCAT soil  
 994 moistureSM data assimilation (DA) in this study. The spatially distributed ASCAT soil  
 995 moistureSM errors ( $\text{m}^3 \text{m}^{-3}$ ) are derived by rescaling the constant 10% soil wetness index  
 996 (~~SWI~~) using the ratio of the standard deviations of the Noah land surface model (LSM) and  
 997 ASCAT soil moistureSM time series.  
 998  
 999

1000 The use of pre-generated spatial or spatiotemporal observation error estimates (e.g., Kim  
 1001 et al., 2025) can potentially maximize the benefits of each soil moistureSM product in multi-  
 1002 sensor soil moistureSM DA systems. One critical issue, however, is that bias correction of  
 1003 soil moistureSM observations, an essential procedure in soil moistureSM DA, may  
 1004 substantially alter their error characteristics, especially when rescaling-based methods like  
 1005 CDF matching are employed. To effectively apply spatially and temporally varying  
 1006 observation error estimates in multi-sensor soil moistureSM DA, a refined approach is  
 1007 needed to propagate error estimates from original soil moistureSM retrievals to bias-corrected  
 1008 soil moistureSM values.  
 1009

## 1010 9. Conclusions

1011 This study develops and evaluates the NASA LIS-based multi-sensor [soil moisture<sup>SM</sup>](#)  
1012 DA framework as part of the Korean Integrated Model (KIM) weather prediction system. We  
1013 aim to investigate the impact of simultaneously assimilating satellite-based near-surface [soil](#)  
1014 [moisture<sup>SM</sup>](#) retrievals from C-band active radar (ASCAT) and L-band passive radiometer  
1015 (SMAP) observations on the weather prediction performance of the KIM-LIS-based land-  
1016 atmosphere weakly coupled DA system. The ASCAT and SMAP [soil moisture<sup>SM</sup>](#) data are  
1017 assimilated individually and jointly into the Noah LSM within the KIM-LIS system, and their  
1018 relative and combined efficiencies in improving the global [soil moisture<sup>SM</sup>](#) analysis and  
1019 atmospheric analysis/forecast skills are evaluated. [Soil moisture<sup>SM</sup>](#) DA is conducted using  
1020 the 1-D [dimensional](#) EnKF while atmospheric DA is implemented using the hybrid 4D<sub>En</sub>Var  
1021 method with 4DIAU. The experiments are performed in the global domain based on 6-hour  
1022 cycling runs, which include analysis and forecast, followed by 5-day predictions at 00 UTC  
1023 and 12 UTC cycles.

1024 TCA-based evaluations indicate that assimilating either ASCAT or SMAP [soil](#)  
1025 [moisture<sup>SM</sup>](#) data results in an overall positive effect on the global [soil moisture<sup>SM</sup>](#) analysis  
1026 skill of the Noah LSM (i.e., 4.0% and 10.5% improvements, respectively, in the global mean  
1027 performance). Both single-sensor [soil moisture<sup>SM</sup>](#) DA cases (i.e., SG\_AT and SG\_SP)  
1028 enhance the [soil moisture<sup>SM</sup>](#) performance across land cover types, with the greatest  
1029 performance gains observed in croplands. [It should be noted that although this study employs](#)  
1030 [the TCA method as an alternative global-scale soil moisture evaluation approach, it has](#)  
1031 [limitations, particularly in constructing TCA triplets for the multi-sensor soil moisture DA](#)

1032 experiment without violating underlying assumptions. Therefore, we applied TCA only to the  
1033 single-sensor DA experiments, and the overall benefit of assimilating both sensors  
1034 simultaneously can only be inferred from the single-sensor results and the atmospheric  
1035 evaluation. Future studies should address this limitation to enable a more complete and robust  
1036 assessment of the impact of multi-sensor soil moisture DA by implementing instrumental  
1037 variable (IV)-based methods for estimating cross-correlated soil moisture errors, which  
1038 require only two independent soil moisture datasets (Dong et al., 2020).

1039 Domain-averaged vertical profile RMSD metrics of the resulting atmospheric variables  
1040 show that better specific humidity and air temperature analyses in the lower atmosphere are  
1041 achieved with SMAP DA and ASCAT DA, respectively. Compared to the single-sensor soil  
1042 moisture<sup>SM</sup> DA experiments, assimilating the ASCAT and SMAP soil moisture<sup>SM</sup>  
1043 retrievals together (MT\_ATSP) yields balanced skill enhancements, improving both specific  
1044 humidity and air temperature analyses. Evaluations indicate that soil moisture<sup>SM</sup> DA within  
1045 the KIM-LIS coupled system is particularly effective for the 2-m air temperature analysis and  
1046 forecast, especially in the multi-sensor soil moisture<sup>SM</sup> DA experiment. The synergistic  
1047 benefits of simultaneously assimilating both soil moisture<sup>SM</sup> products are regionally  
1048 dependent, yielding the greatest advantage when both soil moisture<sup>SM</sup> products have a  
1049 positive impact.

1050 In offline land DA systems, soil moisture<sup>SM</sup> DA typically reduces the uncertainty in  
1051 modeled surface soil moisture<sup>SM</sup> arising mainly from errors in precipitation forcing data.  
1052 Our experiments demonstrate that, in a land-atmosphere coupled system, precipitation  
1053 forecast skill can also be gained from soil moisture<sup>SM</sup> DA through land-atmosphere

1054 interaction processes, particularly when multiple soil moistureSM products from diverse  
1055 sources are utilized together. Specifically, MT\_ATSP improves the prediction of precipitation  
1056 events, as evaluated using the ETS metric, across the range of precipitation intensity  
1057 thresholds.

1058 ~~To conclude,~~ This study suggests that simultaneously assimilating the ASCAT and  
1059 SMAP soil moistureSM products within the KIM-LIS coupled system can leverage their  
1060 complementary advantages, as demonstrated for the estimates of specific humidity, air  
1061 temperature, and precipitation. The findings obtained in this study are promising for three  
1062 main reasons. First, clear synergistic local skill improvements from multi-sensor DA are  
1063 evident, particularly in regions and periods where both single-sensor experiments show  
1064 positive impacts. Second, the magnitude of atmospheric forecast skill improvements from  
1065 both single- and multi-sensor soil moisture DA, relative to CTL, is comparable to  
1066 improvements reported in previous studies (e.g., Draper and Reichle, 2019; Lin and Pu, 2019;  
1067 Muñoz-Sabater et al., 2019; Reichle et al., 2023), with multi-sensor DA yielding slightly  
1068 better (though not statistically significant) performance. Achieving consistent improvements  
1069 across the globe remains challenging due to factors discussed in Section 8, which can cause  
1070 local skill degradations in atmospheric estimates. Finally, as emphasized above, simultaneous  
1071 assimilation of ASCAT and SMAP produces a more balanced improvement across  
1072 atmospheric variables than single-sensor DA. These results highlight the value of assimilating  
1073 soil moisture observations from multiple sensors, even if trade-offs remain for certain  
1074 variables in regions or periods where single-sensor impacts conflict.

1075 To conclude, a key aspect of this study is the joint assimilation of individual radar- and  
1076 radiometer-based soil moisture products. Compared to assimilating pre-blended soil moisture  
1077 data, this approach is advantageous because (1) it accounts for the relative uncertainties of  
1078 both sensors, which vary across space and time; (2) it provides a flexible framework for  
1079 incorporating various combinations of soil moisture data sources within DA systems; and (3)  
1080 it is more suitable for near-real time operational forecast systems, the focus of this study,  
1081 since soil moisture data blending processes may increase latency and thereby reduce data  
1082 availability for operational use. However, it is acknowledged that overall domain-averaged  
1083 improvements in atmospheric estimates through multi-sensor soil moisture DA, relative to  
1084 single-sensor DA, are still marginal and statistically insignificant. ¶The following issues  
1085 remain to be addressed in future studies to enhance future performance. First, the impact of  
1086 subsurface scattering on the quality of the ASCAT soil moisture<sub>SM</sub> product under dry soil  
1087 conditions needs to be considered in QC procedures. Second, an alternative soil moisture<sub>SM</sub>  
1088 bias correction method, especially for ASCAT data, should be explored. Lastly, more realistic  
1089 spatially or spatiotemporally distributed estimates of soil moisture<sub>SM</sub> observation errors are  
1090 required to maximize the benefits of multi-sensor soil moisture<sub>SM</sub> DA. In addition, as  
1091 discussed in several previous studies, addressing biases in the soil moisture-latent heat flux  
1092 coupling in LSMs (Crow et al., 2023; Kwon et al., 2024; Lei et al. 2018), accounting for the  
1093 background error covariance between atmospheric and land variables during DA (Kwon et al.,  
1094 2024), and assimilating screen-level observations (de Rosnay et al., 2013; Lin and Pu, 2020)  
1095 can improve the positive impacts of soil moisture DA on atmospheric forecast in coupled  
1096 systems.

1097 -

1098

1099 **Acknowledgments**

1100 ~~This work was supported by the Korea Meteorological Administration R&D project~~  
 1101 ~~"Development of a Next-Generation Data Assimilation System by the Korea Institute of~~  
 1102 ~~Atmospheric Prediction Systems (KIAPS)" (KMA2020-02211). We sincerely thank the~~  
 1103 ~~scientists of the NASA LIS team for their considerable efforts in developing the LIS~~  
 1104 ~~framework and making it publicly available. We would also like to express our gratitude to~~  
 1105 ~~the research teams of ECMWF, ASCAT, SMAP, AMSR2, SMOS, and NOAA CPC for~~  
 1106 ~~sharing the data used in this study.~~

1107 **Appendix A: Abbreviations**

<u>AMSR2</u>	<u>Advanced Microwave Scanning Radiometer 2</u>
<u>AMSU-A</u>	<u>Advanced Microwave Sounding Unit-A</u>
<u>AMVs</u>	<u>Atmospheric Motion Vectors</u>
<u>ASCAT</u>	<u>Advanced SCATterometer</u>
<u>ATMS</u>	<u>Advanced Technology Microwave Sounder</u>
<u>CDF</u>	<u>Cumulative distribution function</u>
<u>CDR</u>	<u>Climate Data Record</u>
<u>CPC</u>	<u>Climate Prediction Center</u>
<u>CrIS</u>	<u>Cross-track Infrared Sounder</u>
<u>CTL</u>	<u>Control case serving as a baseline experiment</u>
<u>DA</u>	<u>Data assimilation</u>
<u>DCA</u>	<u>Dual Channel Algorithm</u>
<u>EASE</u>	<u>Equal Area Scalable Earth</u>
<u>ECMWF</u>	<u>European Centre for Medium-Range Weather Forecasts</u>
<u>EnKF</u>	<u>Ensemble Kalman filter</u>
<u>ERA5</u>	<u>Fifth generation of the ECMWF atmospheric reanalysis</u>
<u>ESA CCI</u>	<u>European Space Agency Climate Change Initiative</u>
<u>ESME</u>	<u>Estimated Soil Moisture Error</u>
<u>ETS</u>	<u>Equitable threat score</u>
<u>EUMETSAT</u>	<u>European Organisation for the Exploitation of Meteorological Satellites</u>

<a href="#"><u>FAO</u></a>	<a href="#"><u>Food and Agriculture Organization</u></a>
<a href="#"><u>FB</u></a>	<a href="#"><u>Frequency bias</u></a>
<a href="#"><u>fMSE</u></a>	<a href="#"><u>Fractional mean-square error</u></a>
<a href="#"><u>GLDAS</u></a>	<a href="#"><u>Global Land Data Assimilation System</u></a>
<a href="#"><u>GPS-RO</u></a>	<a href="#"><u>Global Positioning System Radio Occultation</u></a>
<a href="#"><u>Hybrid 4DEnVar</u></a>	<a href="#"><u>Hybrid four-dimensional ensemble variational</u></a>
<a href="#"><u>IASI</u></a>	<a href="#"><u>Infrared Atmosphere Sounding Interferometer</u></a>
<a href="#"><u>IFS</u></a>	<a href="#"><u>Integrated Forecasting System</u></a>
<a href="#"><u>IGBP</u></a>	<a href="#"><u>International Geosphere-Biosphere Programme</u></a>
<a href="#"><u>KIAPS</u></a>	<a href="#"><u>Korea Institute of Atmospheric Prediction Systems</u></a>
<a href="#"><u>KIM</u></a>	<a href="#"><u>Korean Integrated Model</u></a>
<a href="#"><u>KPOP</u></a>	<a href="#"><u>KIM Package of Observation Processing</u></a>
<a href="#"><u>KVAR</u></a>	<a href="#"><u>KIM VARiational data assimilation</u></a>
<a href="#"><u>LETKF</u></a>	<a href="#"><u>Local ensemble transform Kalman filter</u></a>
<a href="#"><u>LIS</u></a>	<a href="#"><u>Land Information System</u></a>
<a href="#"><u>LPRM</u></a>	<a href="#"><u>Land Parameter Retrieval Model</u></a>
<a href="#"><u>LSM</u></a>	<a href="#"><u>Land surface model</u></a>
<a href="#"><u>LST</u></a>	<a href="#"><u>Local solar time</u></a>
<a href="#"><u>L2</u></a>	<a href="#"><u>Level 2</u></a>
<a href="#"><u>MetOp</u></a>	<a href="#"><u>Meteorological Operational</u></a>
<a href="#"><u>MHS</u></a>	<a href="#"><u>Microwave Humidity Sounder</u></a>
<a href="#"><u>MODIS</u></a>	<a href="#"><u>Moderate resolution imaging spectroradiometer</u></a>
<a href="#"><u>MT_ATSP</u></a>	<a href="#"><u>Multi-sensor soil moisture data assimilation experiment</u></a>
<a href="#"><u>NASA</u></a>	<a href="#"><u>National Aeronautics and Space Administration</u></a>
<a href="#"><u>NCEP</u></a>	<a href="#"><u>National Centers for Environmental Prediction</u></a>
<a href="#"><u>NOAA</u></a>	<a href="#"><u>National Oceanic and Atmospheric Administration</u></a>
<a href="#"><u>NSIDC</u></a>	<a href="#"><u>National Snow and Ice Data Center</u></a>
<a href="#"><u>NWP</u></a>	<a href="#"><u>Numerical weather prediction</u></a>
<a href="#"><u>RFI</u></a>	<a href="#"><u>Radio Frequency Interference</u></a>
<a href="#"><u>RMSD</u></a>	<a href="#"><u>Root mean square difference</u></a>
<a href="#"><u>SG_AT</u></a>	<a href="#"><u>Single-sensor data assimilation experiment using the ASCAT soil moisture data</u></a>
<a href="#"><u>SG_SP</u></a>	<a href="#"><u>Single-sensor data assimilation experiment using the SMAP soil moisture data</u></a>
<a href="#"><u>SMAP</u></a>	<a href="#"><u>Soil Moisture Active Passive</u></a>
<a href="#"><u>SMOS</u></a>	<a href="#"><u>Soil Moisture and Ocean Salinity</u></a>
<a href="#"><u>SMOS-IC</u></a>	<a href="#"><u>SMOS-INRA-CESBIO</u></a>
<a href="#"><u>SRTM</u></a>	<a href="#"><u>Shuttle Radar Topography Mission</u></a>
<a href="#"><u>STATSGO</u></a>	<a href="#"><u>State Soil Geographic</u></a>
<a href="#"><u>TCA</u></a>	<a href="#"><u>Triple collocation analysis</u></a>
<a href="#"><u>TU Wien</u></a>	<a href="#"><u>Vienna University of Technology</u></a>
<a href="#"><u>UTC</u></a>	<a href="#"><u>Coordinated Universal Time</u></a>
<a href="#"><u>VV</u></a>	<a href="#"><u>Vertical transmit vertical receive</u></a>

<u>WMO</u>	<u>World Meteorological Organization</u>
<u>4DIAU</u>	<u>Four-dimensional incremental analysis update</u>

1108  
1109  
1110  
1111  
1112  
1113  
1114  
1115  
1116  
1117  
1118  
1119  
1120  
1121  
1122  
1123  
1124  
1125  
1126  
1127  
1128

**Code and Data availability**

The NASA Land Information System (LIS) framework is publicly available at <https://github.com/NASA-LIS/LISF>. Satellite-based soil moisture ~~(SM)~~ data assimilated in this study, i.e., Soil Moisture Active Passive (SMAP) and Advanced SCATterometer (ASCAT), can be obtained from <https://n5eil01u.ecs.nsidc.org/SMAP/SPL2SMP.009/> and <https://eoportal.eumetsat.int>, respectively. Other global ~~SM~~ soil moisture products, used as TCA triplet components to evaluate soil moisture~~SM~~ estimates, can be downloaded from <https://www.earthdata.nasa.gov/sensors/amsr2> for the Advanced Microwave Scanning Radiometer 2 (AMSR2) and <https://ib.remote-sensing.inrae.fr/index.php/smos-ic-v2-product-documentation> for the Soil Moisture and Ocean Salinity (SMOS) mission. Integrated Forecasting System (IFS) analysis data can be obtained from the European Centre for Medium-Range Weather Forecasts (ECMWF) in accordance with their data policy. The National Oceanic and Atmospheric Administration (NOAA) Climate Prediction Center (CPC) gauge-based global daily precipitation data can be downloaded from <https://psl.noaa.gov/data/gridded/data.cpc.globalprecip.html>. The Korean Integrated Model (KIM) software is not yet publicly available and cannot be distributed due to the Korean government's security policy. All experimental data generated in this work will be available from the authors upon request.

1129

1130 **Author contribution**

1131 YK: conceptualization, methodology, investigation, formal analysis, writing (original draft),  
1132 writing (review and editing). SJ: data curation, methodology, writing (review and editing).  
1133 HK: data curation, methodology, validation, writing (review and editing). KHS: validation,  
1134 writing (review and editing). IHK: supervision, methodology, writing (review and editing).  
1135 EK: validation, writing (review and editing). SC: validation, writing (review and editing)

1136

1137 **Competing interests**

1138 The contact author has declared that none of the authors has any competing interests.

1139

1140 **Acknowledgments**

1141 This work was supported by the Korea Meteorological Administration R&D project  
1142 "Development of a Next-Generation Data Assimilation System by the Korea Institute of  
1143 Atmospheric Prediction Systems (KIAPS)" (KMA2020-02211). We sincerely thank the  
1144 scientists of the NASA LIS team for their considerable efforts in developing the LIS  
1145 framework and making it publicly available. We would also like to express our gratitude to  
1146 the research teams of ECMWF, ASCAT, SMAP, AMSR2, SMOS, and NOAA CPC for  
1147 sharing the data used in this study.

1148

1149 **References**

1150

1151 Al-Yaari, A., Wigneron, J.-P., Dorigo, W., Colliander, A., Pellarin, T., Hahn, S., Mialon, A.,  
1152 Richaume, P., Fernandez-Moran, R., Fan, L., Kerr, Y.H., De Lannoy, G., 2019.

1153 Assessment and inter-comparison of recently developed/reprocessed microwave  
1154 satellite soil moisture products using ISMN ground-based measurements. *Remote Sens.*  
1155 *Environ.* 224, 289–303. <https://doi.org/10.1016/j.rse.2019.02.008>.

1156 Assouline, S., 2013. Infiltration into soils: conceptual approaches and solutions. *Water*  
1157 *Resour. Res.* 49, 1755–1772. <http://dx.doi.org/10.1002/wrcr.20155>.

1158 Azimi, S., Dariane, A.B., Modanesi, S., Bauer-Marschallinger, B., Bindlish, R., Wagner, W.,  
1159 Massari, C., 2020. Assimilation of Sentinel 1 and SMAP – based satellite soil moisture  
1160 retrievals into SWAT hydrological model: the impact of satellite revisit time and  
1161 product spatial resolution on flood simulations in small basins. *J. Hydrol.* 581, 124367.  
1162 <https://doi.org/10.1016/j.jhydrol.2019.124367>.

1163 Bartalis, Z., Wagner, W., Naeimi, V., Hasenauer, S., Scipal, K., Bonekamp, H., Figa, J.,  
1164 Anderson, C., 2007. Initial soil moisture retrievals from the METOP-A Advanced  
1165 Scatterometer (ASCAT). *Geophys. Res. Lett.* 34, L20401.  
1166 <https://doi.org/10.1029/2007GL031088>.

1167 Baugh, C., de Rosnay, P., Lawrence, H., Jurlina, T., Drusch, M., Zsoter, E., Prudhomme, C.,  
1168 2020. The impact of SMOS soil moisture data assimilation within the operational  
1169 Global Flood Awareness System (GloFAS). *Remote Sens.* 12, 1490.  
1170 <https://doi.org/10.3390/rs12091490>.

1171 [Beljaars, A.C.M., Viterbo, P., Miller, M.J., Betts, A. K., 1996. The anomalous rainfall over](#)  
1172 [the United States during July 1993: Sensitivity to land surface parameterization and soil](#)  
1173 [moisture anomalies. \*Mon. Weather Rev.\* 124, 362–383. \[https://doi.org/10.1175/1520-\]\(https://doi.org/10.1175/1520-0493\(1996\)124<0362:TAROTU>2.0.CO;2\)](#)  
1174 [0493\(1996\)124<0362:TAROTU>2.0.CO;2.](#)

1175 Ben Bouallègue, Z., Clare, M.C.A., Magnusson, L., Gascón, E., Maier-Gerber, M., Janoušek,  
1176 M., Rodwell, M., Pinault, F., Dramsch, J.S., Lang, S.T.K., Raoult, B., Rabier, F.,  
1177 Chevallier, M., Sandu, I., Dueben, P., Chantry, M., Pappenberger, F., 2024. A first  
1178 statistical assessment of machine learning-based weather forecasts in an operational-  
1179 like context. *B. Am. Meteorol. Soc.* 105, E864–E883. [https://doi.org/10.1175/BAMS-](https://doi.org/10.1175/BAMS-D-23-0162.1)  
1180 [D-23-0162.1.](#)

1181 [Bhuiyan, H., McNairn, H., Powers, J., Friesen, M., Pacheco, A., Jackson, T. J., Cosh, M. H.,](#)  
1182 [Colliander, A., Berg, A., Rowlandson, T., Bullock, P., Magagi, R., 2018. Assessing](#)  
1183 [SMAP soil moisture scaling and retrieval in the carman \(Canada\) study site. \*Vadose\*](#)  
1184 [Zone J. 17, 180132. \[https://doi.org/10.2136/vzj2018.07.0132.\]\(https://doi.org/10.2136/vzj2018.07.0132\)](#)

1185 Blyverket, J., Hamer, P.D., Bertino, L., Albergel, C., Fairbairn, D., Lahoz, W.A., 2019. An  
1186 evaluation of the EnKF vs. EnOI and the assimilation of SMAP, SMOS and ESA CCI  
1187 soil moisture data over the contiguous US. *Remote Sens.* 11, 478.  
1188 <https://doi.org/10.3390/rs11050478>.

1189 Bolten, J.D., Crow, W.T., Zhan, X., Jackson, T.J., Reynolds, C.A., 2010. Evaluating the  
1190 utility of remotely sensed soil moisture retrievals for operational agricultural drought  
1191 monitoring, *IEEE J. Sel. Top. Appl. Earth Obs. Remote Sens.* 3, 57–66.  
1192 <https://doi.org/10.1109/JSTARS.2009.2037163>.

1193 [Bosilovich, M.G., Sun, W.-Y., 1999 Numerical simulation of the 1993 Midwestern flood:](#)  
1194 [Land–atmosphere interactions. \*J. Climate\* 12, 1490–1505.](#)  
1195 [\[https://doi.org/10.1175/1520-0442\\(1999\\)012<1490:NSOTMF>2.0.CO;2.\]\(https://doi.org/10.1175/1520-0442\(1999\)012<1490:NSOTMF>2.0.CO;2\)](#)

- 1196 Brocca, L., Melone, F., Moramarco, T., Wagner, W., Naeimi, V., Bartalis, Z., Hasenauer, S.,  
 1197 2010. Improving runoff prediction through the assimilation of the ASCAT soil  
 1198 moisture product. *Hydrol. Earth Syst. Sci.* 14, 1881–1893.  
 1199 <http://dx.doi.org/10.5194/hess-14-1881-2010>.
- 1200 Catalano, F., Alessandri, A., De Felice, M., Zhu, Z., Myneni, R.B., 2016. Observationally  
 1201 based analysis of land–atmosphere coupling. *Earth Syst. Dynam.* 7, 251–266.  
 1202 <https://doi.org/10.5194/esd-7-251-2016>.
- 1203 Chan, S., Dunbar, R.S., 2021. Soil Moisture Active Passive (SMAP) mission: Level 2 passive  
 1204 soil moisture product specification document. JPL D-72547, NASA Jet Propulsion  
 1205 Laboratory, California, United States.  
 1206 [https://nsidc.org/sites/default/files/d7254720smap2012\\_sm\\_p20psd20\\_version2080\\_fin](https://nsidc.org/sites/default/files/d7254720smap2012_sm_p20psd20_version2080_final.pdf)  
 1207 [al.pdf](https://nsidc.org/sites/default/files/d7254720smap2012_sm_p20psd20_version2080_final.pdf).
- 1208 Chan, S.K., Bindlish, R., O’Neill, P., Jackson, T., Njoku, E., Dunbar, S., Chaubell, J.,  
 1209 Piepmeier, J., Yueh, S., Entekhabi, D., Colliander, A., Chen, F., Cosh, M.H., Caldwell,  
 1210 T., Walker, J., Berg, A., McNairn, H., Thibeault, M., Martínez-Fernández, J., Uldall, F.,  
 1211 Seyfried, M., Bosch, D., Starks, P., Holifield Collins, C., Prueger, J., van der Velde, R.,  
 1212 Asanuma, J., Palecki, M., Small, E.E., Zreda, M., Calvet, J., Crow, W.T., Kerr, Y.,  
 1213 2018. Development and assessment of the SMAP enhanced passive soil moisture  
 1214 product. *Remote Sens. Environ.* 204, 931–941.  
 1215 <https://doi.org/10.1016/j.rse.2017.08.025>.
- 1216 Chaubell, M.J., Yueh, S.H., Dunbar, R.S., Colliander, A., Chen, F., Chan, S.K., Entekhabi, D.,  
 1217 Bindlish, R., O’Neill, P.E., Asanuma, J., Berg, A.A., Bosch, D.D., Caldwell, T., Cosh,  
 1218 M.H., Collins, C.H., Martínez-Fernández, J., Seyfried, M., Starks, P.J., Su, Z.,  
 1219 Thibeault, M., Walker, J., 2020. Improved SMAP dual-channel algorithm for the  
 1220 retrieval of soil moisture. *IEEE Trans. Geosci. Remote Sens.* 58, 3894–3905.  
 1221 <https://doi.org/10.1109/tgrs.2019.2959239>.
- 1222 Chen, M., Shi, W., Xie, P., Silva, V.B.S., Kousky, V.E., Higgins, R.W., Janowiak, J.E., 2008.  
 1223 Assessing objective techniques for gauge-based analyses of global daily precipitation. *J.*  
 1224 *Geophys. Res.* 113, D04110. <https://doi.org/10.1029/2007JD009132>.
- 1225 Cho, E., Kwon, Y., Kumar, S.V., Vuyovich, C.M., 2023. Assimilation of airborne gamma  
 1226 observations provides utility for snow estimation in forested environments. *Hydrol.*  
 1227 *Earth Syst. Sci.* 27, 4039–4056. <https://doi.org/10.5194/hess-27-4039-2023>.
- 1228 Colliander, A., Jackson, T.J., Bindlish, R., Chan, S., Das, N., Kim, S. B. et al., 2017.  
 1229 Validation of SMAP surface soil moisture products with core validation sites. *Remote*  
 1230 *Sens. Environ.* 191, 215–231. <https://doi.org/10.1016/j.rse.2017.01.021>.
- 1231 Cook, B.I., Bonan, G.B., Levis, S., 2006. Soil moisture feedbacks to precipitation in southern  
 1232 *Africa. J. Climate* 19, 4198–4206. <https://doi.org/10.1175/JCLI3856.1>.
- 1233 Crow, W.T., Van den Berg, M.J., 2010. An improved approach for estimating observation  
 1234 and model error parameters in soil moisture data assimilation. *Water Resour. Res.* 46,  
 1235 W12519. <https://doi.org/10.1029/2010WR009402>.
- 1236 Crow, W.T., Kim, H., Kumar, S., 2023. Systematic modelling errors undermine the  
 1237 application of land data assimilation systems for hydrological and weather forecasting.  
 1238 *J. Hydrometeor.* 25, 3–26. <https://doi.org/10.1175/JHM-D-23-0069.1>.

- 1239 Dare, R.A., Ebert, E.E., 2017. Latitudinal variations in the accuracy of model-generated  
1240 forecasts of precipitation over Australia and south-east Asia. *J. South. Hemisph. Earth*  
1241 *Syst. Sci.* 67, 46–63. <https://doi.org/10.1071/ES17005>.
- 1242 Das, N.N., Entekhabi, D., Dunbar, R.S., Chaubell, M.J., Colliander, A., Yueh, S., Jagdhuber,  
1243 T., Chen, F., Crow, W., O’Neill, P.E., Walker, J.P., Berg, A., Bosch, D.D., Caldwell,  
1244 T., Cosh, M.H., Collins, C.H., Lopez-Baeza, E., Thibeault, M., 2019. The SMAP and  
1245 Copernicus Sentinel-1A/B microwave active passive high resolution surface soil  
1246 moisture product. *Remote Sens. Environ.* 233, 111380.  
1247 <https://doi.org/10.1016/j.rse.2019.111380>.
- 1248 Dee, D.P., Da Silva, A.M., 1998. Data assimilation in the presence of forecast bias. *Quart. J.*  
1249 *Roy. Meteor. Soc.* 124, 269–295. <https://doi.org/10.1002/qj.49712454512>.
- 1250 [de Rosnay, P., Drusch, M., Vasiljevic, D., Balsamo, G., Albergel, C., Isaksen, L., 2013. A](#)  
1251 [simplified extended Kalman filter for the global operational soil moisture analysis at](#)  
1252 [ECMWF. \*Q. J. Roy. Meteor. Soc.\* 139, 1199–1213. <https://doi.org/10.1002/qj.2023>.](#)
- 1253 [de Rosnay, P., Browne, P., de Boissésou, E., Fairbairn, D., Hirahara, Y. et al., 2022. Coupled](#)  
1254 [data assimilation at ECMWF: current status, challenges and future developments. \*Q. J.\*](#)  
1255 [\*Roy. Meteor. Soc.\* 148, 2672–2702. <https://doi.org/10.1002/qj.4330>.](#)
- 1256 Dirmeyer, P., Halder, S., 2016. Sensitivity of numerical weather forecasts to initial soil  
1257 moisture variations in CFSv2. *Wea. Forecasting* 31, 1973–1983.  
1258 <https://doi.org/10.1175/WAF-D-16-0049.1>.
- 1259 Dobson, M.C., Ulaby, F.T., 1986. Active microwave soil moisture research. *IEEE Trans.*  
1260 *Geosci. Remote Sens.* GE-24, 23–36. <https://doi.org/10.1109/TGRS.1986.289585>.
- 1261 [Dong, J., Wei, L., Chen, X., Duan, Z., Lu, Y., 2020. An instrument variable based algorithm](#)  
1262 [for estimating cross-correlated hydrological remote sensing errors. \*J. Hydrol.\* 581,](#)  
1263 [124413. <https://doi.org/10.1016/j.jhydrol.2019.124413>.](#)
- 1264 Dorigo, W.A., Scipal, K., Parinussa, R.M., Liu, Y.Y., Wagner, W., De Jeu, R.A.M., Naeimi,  
1265 V., 2010. Error characterisation of global active and passive microwave soil moisture  
1266 datasets. *Hydrol. Earth Syst. Sci.* 14, 2605–2616. [https://doi.org/10.5194/hess-14-2605-](https://doi.org/10.5194/hess-14-2605-2010)  
1267 2010.
- 1268 Dorigo, W., Wagner, W., Albergel, C., Albrecht, F., Balsamo, G., Brocca, L., Chung, D., Ertl,  
1269 M., Forkel, M., Gruber, A., Haas, E., Hamer, P.D., Hirschi, M., Ikonen, J., de Jeu, R.,  
1270 Kidd, R., Lahoz, W., Liu, Y.Y., Miralles, D., Mistelbauer, T., Nicolai-Shaw, N.,  
1271 Parinussa, R., Pratola, C., Reimer, C., van der Schalie, R., Seneviratne, S.I., Smolander,  
1272 T., Lecomte, P., 2017. ESA CCI soil moisture for improved Earth system  
1273 understanding: state-of-the art and future directions. *Remote Sens. Environ.* 203, 185–  
1274 215. <https://doi.org/10.1016/j.rse.2017.07.001>.
- 1275 Draper, C.S., Mahfouf, J.-F., Walker, J.P., 2011. Root-zone soil moisture from the  
1276 assimilation of screen-level variables and remotely sensed soil moisture. *J. Geophys.*  
1277 *Res.* 116, D02127. <https://doi.org/10.1029/2010JD013829>.
- 1278 Draper, C.S., Reichle, R.H., De Lannoy, G.J.M., Liu, Q., 2012. Assimilation of passive and  
1279 active microwave soil moisture retrievals. *Geophys. Res. Lett.* 39, L04401.  
1280 <https://doi.org/10.1029/2011GL050655>.

- 1281 Draper, C., Reichle, R., de Jeu, R., Naeimi, V., Parinussa, R., Wagner, W., 2013. Estimating  
1282 root mean square errors in remotely sensed soil moisture over continental scale  
1283 domains. *Remote Sens. Environ.* 137, 288–298.  
1284 <https://doi.org/10.1016/j.rse.2013.06.013>.
- 1285 Draper, C., Reichle, R.H., 2019. Assimilation of satellite soil moisture for improved  
1286 atmospheric reanalyses. *Mon. Weather Rev.* 147, 2163–2188.  
1287 <https://doi.org/10.1175/MWR-D-18-0393.1>.
- 1288 Drusch, M., Viterbo, P., 2007. Assimilation of screen-level variables in ECMWF’s Integrated  
1289 Forecast System: A study on the impact on the forecast quality and analyzed soil  
1290 moisture. *Mon. Weather Rev.* 135, 300–314. <https://doi.org/10.1175/MWR3309.1>.
- 1291 ECMWF, 2017. IFS Documentation CY43R3 - Part II: Data assimilation. European Centre  
1292 for Medium-Range Weather Forecasts, Reading, UK, 103 pp.  
1293 <https://doi.org/10.21957/v61kmv92i>.
- 1294 Ek, M.B., Mitchell, K.E., Lin, Y., Rogers, E., Grunmann, P., Koren, V., Gayno, G., Tarpley,  
1295 J.D., 2003. Implementation of Noah land surface model advances in the National  
1296 Centers for Environmental Prediction operational mesoscale Eta model. *J. Geophys.*  
1297 *Res.* 108, 8851. <https://doi.org/10.1029/2002JD003296>.
- 1298 Entekhabi, D., Njoku, E.G., O’Neill, P.E., Kellogg, K.H., Crow, W.T., Edelstein, W.N., 2010.  
1299 The soil moisture active passive (SMAP) mission. *Proc. IEEE* 98, 704–716.  
1300 <https://doi.org/10.1109/JPROC.2010.2043918>.
- 1301 Evensen, G., 1994. Sequential data assimilation with a nonlinear quasi-geostrophic model  
1302 using Monte Carlo methods to forecast error statistics. *J. Geophys. Res.* 99, 10143–  
1303 10162. <https://doi.org/10.1029/94JC00572>.
- 1304 [Fairbairn, D., de Rosnay, P., Weston, P., 2024. Evaluation of an adaptive soil moisture bias  
1305 correction approach in the ECMWF land data assimilation system. \*Remote Sens.\* 16,  
1306 493. <https://doi.org/10.3390/rs16030493>.](https://doi.org/10.3390/rs16030493)
- 1307 Farr, T.G., Rosen, P.A., Caro, E., Crippen, R., Duren, R., Hensley, S., Kobrick, M., Paller, M.,  
1308 Rodriguez, E., Roth, L., Seal, D., Shaffer, S., Shimada, J., Umland, J., Werner, M.,  
1309 Oskin, M., Burbank, D., Alsdorf, D., 2007. The shuttle radar topography mission. *Rev.*  
1310 *Geophys.* 45, RG2004. <https://doi.org/10.1029/2005RG000183>.
- 1311 Federico, S., Torcasio, R.C., Popova, J., Sokol, Z., Pop, L., Lagasio, M., Lynn, B.H., Puca, S.,  
1312 Dietrich, S., 2024. Improving the lightning forecast with the WRF model and lightning  
1313 data assimilation: Results of a two-seasons numerical experiment over Italy. *Atmos.*  
1314 *Res.* 304, 107382. <https://doi.org/10.1016/j.atmosres.2024.107382>.
- 1315 Ferguson, C.R., Agrawal, S., Beauharnois, M.C., Xia, G., Burrows, D.A., Bosart, L.F., 2020.  
1316 Assimilation of satellite-derived soil moisture for improved forecasts of the great plains  
1317 low-level jet. *Mon. Weather Rev.* 148, 4607–4627. [https://doi.org/10.1175/MWR-D-  
1318 20-0185.1](https://doi.org/10.1175/MWR-D-20-0185.1).
- 1319 [Findell, K.L., Eltahir, E.A.B., 2003. Atmospheric controls on soil moisture–boundary layer  
1320 interactions. Part I: Framework development. \*J. Hydrometeor.\* 4, 552–569.  
1321 \[https://doi.org/10.1175/1525-7541\\(2003\\)004<0552:ACOSML>2.0.CO;2\]\(https://doi.org/10.1175/1525-7541\(2003\)004<0552:ACOSML>2.0.CO;2\).](https://doi.org/10.1175/1525-7541(2003)004<0552:ACOSML>2.0.CO;2)
- 1322 Friedl, M.A., McIver, D.K., Hodges, J.C.F., Zhang, X.Y., Muchoney, D., Strahler, A.H.,  
1323 Woodcock, C.E., Gopal, S., Schneider, A., Cooper, A., Baccini, A., Gao, F., Schaaf, C.,

1324 2002. Global land cover mapping from MODIS: algorithms and early results. *Remote*  
1325 *Sens. Environ.* 83, 287–302. [https://doi.org/10.1016/S0034-4257\(02\)00078-0](https://doi.org/10.1016/S0034-4257(02)00078-0).

1326 [Fuentes, I., Padarian, J., Vervoort, R.W., 2022. Towards near real-time national-scale soil](#)  
1327 [water content monitoring using data fusion as a downscaling alternative. \*J. Hydrol.\* 609,](#)  
1328 [127705. <https://doi.org/10.1016/j.jhydrol.2022.127705>.](#)

1329 Gaspari, G., Cohn, S.E., 1999. Construction of correlation functions in two and three  
1330 dimensions. *Q. J. Roy. Meteor. Soc.* 125, 723–757.  
1331 <https://doi.org/10.1002/qj.49712555417>.

1332 Gavahi, K., Abbaszadeh, P., Moradkhani, H., 2022. How does precipitation data influence the  
1333 land surface data assimilation for drought monitoring? *Sci. Total Environ.* 831, 154916.  
1334 <https://doi.org/10.1016/j.scitotenv.2022.154916>.

1335 Gentine, P., Polcher, J., Entekhabi, D., 2011. Harmonic propagation of variability in surface  
1336 energy balance within a coupled soil–vegetation–atmosphere system. *Water Resour.*  
1337 *Res.* 47, W05525. <http://dx.doi.org/10.1029/2010WR009268>.

1338 Gruber, A., Su, C.-H., Zwieback, S., Crow, W., Dorigo, W., Wagner, W., 2016. Recent  
1339 advances in (soil moisture) triple collocation analysis. *Int. J. Appl. Earth Obs.* 45, 200–  
1340 211. <https://doi.org/10.1016/j.jag.2015.09.002>.

1341 Hersbach, H., Bell, B., Berrisford, P., Hirahara, S., Horányi, A., Muñoz-Sabater, J., Nicolas,  
1342 J., Peubey, C., Radu, R., Schepers, D., et al., 2020. The ERA5 global reanalysis, *Q. J.*  
1343 *Roy. Meteorol. Soc.* 146, 1999–2049. <https://doi.org/10.1002/qj.3803>.

1344 [Hohenegger, C., Brockhaus, P., Bretherton, C.S., Schär, C., 2009. The soil moisture–](#)  
1345 [precipitation feedback in simulations with explicit and parameterized convection. \*J.\*](#)  
1346 [Climate 22, 5003–5020. <https://doi.org/10.1175/2009JCLI2604.1>.](#)

1347 Hong, S.-Y., Kwon, Y.C., Kim, T.-H., Kim, J.-E.E., Choi, S.-J., Kwon, I.-H., Kim, J., Lee,  
1348 E.-H., Park, R.-S., and Kim, D.-I., 2018. The Korean Integrated Model (KIM) system  
1349 for global weather forecasting. *Asia-Pac. J. Atmos. Sci.* 54, 267–292.  
1350 <https://doi.org/10.1007/s13143-018-0028-9>.

1351 [Huang, S., Zhang, X., Wang, C., Chen, N., 2023. Two-step fusion method for generating 1](#)  
1352 [km seamless multi-layer soil moisture with high accuracy in the Qinghai-Tibet plateau.](#)  
1353 [ISPRS J. Photogramm. 197, 346–363. <https://doi.org/10.1016/j.isprsjprs.2023.02.009>.](#)

1354 [Huang, S., Zhang, X., Chen, N., Ma, H., Fu, P., Dong, J., Gu, X., Nam, W.-H., Xu, L., Rab,](#)  
1355 [G., Niyogi, D., 2022. A novel fusion method for generating surface soil moisture data](#)  
1356 [with high accuracy, high spatial resolution, and high spatiotemporal continuity. \*Water\*](#)  
1357 [Resour. Res. 58, e2021WR030827. <https://doi.org/10.1029/2021WR030827>.](#)

1358 Jalilvand, E., Tajrishy, M., Hashemi, S.A.G.Z., Brocca, L., 2019. Quantification of irrigation  
1359 water using remote sensing of soil moisture in a semi-arid region. *Remote Sens.*  
1360 *Environ.* 231, 111226. <https://doi.org/10.1016/j.rse.2019.111226>.

1361 [Jiang, M., Qiu, T., Wang, T., Zeng, C., Zhang, B., Shen, H., 2025. Seamless global daily soil](#)  
1362 [moisture mapping using deep learning based spatiotemporal fusion. \*Int. J. Appl. Earth\*](#)  
1363 [Obs. 139, 104517. <https://doi.org/10.1016/j.jag.2025.104517>.](#)

1364 Jun, S., Park, J.-H., Choi, H.-J., Lee, Y.-H., Lim, Y.-J., Boo, K.-O., Kang, H.-S., 2021.  
1365 Impact of soil moisture data assimilation on analysis and medium-range forecasts in an

1366 operational global data assimilation and prediction system. *Atmosphere* 12, 1089.  
1367 <https://doi.org/10.3390/atmos12091089>.

1368 Kang, J.-H., Chun, H.-W., Lee, S., Ha, J.-H., Song, H.-J., Kwon, I.-H., Han, H.-J., Jeong, H.,  
1369 Kwon, H.-N., Kim, T.-H., 2019. Development of an observation processing package  
1370 for data assimilation in KIAPS. *Asia-Pac. J. Atmos. Sci.* 54, 303–318.  
1371 <https://doi.org/10.1007/s13143-018-0030-2>.

1372 Keppenne, C.L., 2000. Data assimilation into a primitive-equation model with a parallel  
1373 ensemble Kalman filter. *Mon. Weather Rev.* 128, 1971–1981.  
1374 [https://doi.org/10.1175/1520-0493\(2000\)128<1971:DAIAPE>2.0.CO;2](https://doi.org/10.1175/1520-0493(2000)128<1971:DAIAPE>2.0.CO;2).

1375 Kerr, Y.H., Waldteufel, P., Richaume, P., Wigneron, J.P., Ferrazzoli, P., Mahmoodi, A., Al  
1376 Bitar, A., Cabot, F., Gruhier, C., Juglea, S.E., Leroux, D., Mialon, A., Delwart, S.,  
1377 2012. The SMOS soil moisture retrieval algorithm. *IEEE Trans. Geosci. Remote Sens.*  
1378 50, 1384–1403. <https://doi.org/10.1109/TGRS.2012.2184548>.

1379 Khaki, M., Awange, J., 2019. The application of multi-mission satellite data assimilation for  
1380 studying water storage changes over South America. *Sci. Total Environ.* 647, 1557–  
1381 1572. <https://doi.org/10.1016/j.scitotenv.2018.08.079>.

1382 [Khaki, M., Hendricks Franssen, H.-J., Han, S.C., 2020. Multi-mission satellite remote  
1383 sensing data for improving land hydrological models via data assimilation. \*Sci. Rep.\* 10,  
1384 18791. <https://doi.org/10.1038/s41598-020-75710-5>.](https://doi.org/10.1038/s41598-020-75710-5)

1385 [Khaki, M., Hoteit, I., Kuhn, M., Forootan, E., Awange, J., 2019. Assessing data assimilation  
1386 frameworks for using multi-mission satellite products in a hydrological context. \*Sci.  
1387 Total Environ.\* 647, 1031–1043. <https://doi.org/10.1016/j.scitotenv.2018.08.032>.](https://doi.org/10.1016/j.scitotenv.2018.08.032)

1388 Kim, H., Parinussa, R., Konings, A.G., Wagner, W., Cosh, M.H., Lakshmi, V., Zohaib, M.,  
1389 Choi, M., 2018. Global-scale assessment and combination of SMAP with ASCAT  
1390 (active) and AMSR2 (passive) soil moisture products. *Remote Sens. Environ.* 204,  
1391 260–275. <https://doi.org/10.1016/j.rse.2017.10.026>.

1392 Kim, H., Wigneron, J.-P., Kumar, S., Dong, J., Wagner, W., Cosh, M.H., Bosch, D.D.,  
1393 Collins, C.H., Starks, P.J., Seyfried, M., Lakshmi, V., 2020. Global scale error  
1394 assessments of soil moisture estimates from microwave-based active and passive  
1395 satellites and land surface models over forest and mixed irrigated/dryland agriculture  
1396 regions. *Remote Sens. Environ.* 251, 112052. <https://doi.org/10.1016/j.rse.2020.112052>.

1397 Kim, H., Lakshmi, V., Kwon, Y., Kumar, S.V., 2021a. First attempt of global-scale  
1398 assimilation of subdaily scale soil moisture estimates from CYGNSS and SMAP into a  
1399 land surface model. *Environ. Res. Lett.* 16, 074041. [https://doi.org/10.1088/1748-  
1400 9326/ac0ddf](https://doi.org/10.1088/1748-9326/ac0ddf).

1401 Kim, H., Lee, S., Cosh, M.H., Lakshmi, V., Kwon, Y., McCarty, G.W., 2021b. Assessment  
1402 and combination of SMAP and Sentinel-1A/B-derived soil moisture estimates with  
1403 land surface model outputs in the Mid-Atlantic Coastal Plain, USA. *IEEE Trans. Geosci.  
1404 Remote Sens.* 59, 991–1011. <https://doi.org/10.1109/TGRS.2020.2991665>.

1405 Kim, H., Crow, W., Li, X., Wagner, W., Hahn, S., Lakshmi, V., 2023. True global error maps  
1406 for SMAP, SMOS, and ASCAT soil moisture data based on machine learning and  
1407 triple collocation analysis. *Remote Sens. Environ.* 298, 113776.  
1408 <https://doi.org/10.1016/j.rse.2023.113776>.

- 1409 Kim, S., Kim, H., Kwon, Y., Nguyen, H.H., 2025. A stand-alone framework for predicting  
 1410 spatiotemporal errors in satellite-based soil moisture using tree-based models and deep  
 1411 neural networks. *Gisci. Remote Sens.* (minor revision).
- 1412 Kolassa, J., Reichle, R.H., Draper, C.S., 2017. Merging active and passive microwave  
 1413 observations in soil moisture data assimilation. *Remote Sens. Environ.* 191, 117–130.  
 1414 <https://doi.org/10.1016/j.rse.2017.01.015>.
- 1415 Koo, M.-S., Baek, S., Seol, K.-H., Cho, K., 2017. Advances in land modeling of KIAPS  
 1416 based on the Noah land surface model. *Asia-Pac. J. Atmos. Sci.* 53, 361–373.  
 1417 <https://doi.org/10.1007/s13143-017-0043-2>.
- 1418 Koster, R.D., Dirmeyer, P.A., Guo, Z., Bonan, G., Chan, E., Cox, P., Gordon, C.T., Kanae, S.,  
 1419 Kowalczyk, E., Lawrence, D., Liu, P., Lu, C.-H., Malyshev, S., Mcavaney, B., Mitchell,  
 1420 K., Mocko, D., Oki, T., Oleson, K., Pitman, A., Sud, Y.C., Taylor, C.M., Verseghy, D.,  
 1421 Vasic, R., Xue, Y., Yamada, T., 2004. Regions of strong coupling between soil  
 1422 moisture and precipitation. *Science* 305, 1138–1140.  
 1423 <https://doi.org/10.1126/science.1100217>.
- 1424 Koster, R.D., Guo, Z., Yang, R., Dirmeyer, P.A., Mitchell, K., Puma, M.J., 2009. On the  
 1425 nature of soil moisture in land surface models. *J. Clim.* 22, 4322–4335.  
 1426 <https://doi.org/10.1175/2009JCLI2832.1>.
- 1427 Koster, R.D., Mahanama, S.P.P., Yamada, T.J., Balsamo, G., Berg, A.A., Boisserie, M.,  
 1428 Dirmeyer, P.A., Doblas-Reyes, F.J., Drewitt, G., Gordon, C.T., Guo, Z., Jeong, J.-H.,  
 1429 Lawrence, D.M., Lee, W.-S., Li, Z., Luo, L., Malyshev, S., Merryfield, W.J.,  
 1430 Seneviratne, S.I., Stanelle, T., van den Hurk, B.J.J.M., Vitart, F., Wood, E.F., 2010.  
 1431 Contribution of land surface initialization to subseasonal forecast skill: first results  
 1432 from a multi-model experiment. *Geophys. Res. Lett.* 37, L02402.  
 1433 <https://doi.org/10.1029/2009GL041677>.
- 1434 Kumar, S.V., Peters-Lidard, C.D., Tian, Y., Houser, P.R., Geiger, J., Olden, S., Lighty, L.,  
 1435 Eastman, J.L., Dotu, B., Dirmeyer, P., Adams, J., Mitchell, K., Wood, E.F., Sheffield,  
 1436 J., 2006. Land information system: an interoperable framework for high resolution land  
 1437 surface modeling. *Environ. Modell. Softw.* 21, 1402–1415.  
 1438 <https://doi.org/10.1016/j.envsoft.2005.07.004>.
- 1439 Kumar, S.V., Reichle, R.H., Peters-Lidard, C.D., Koster, R.D., Zhan, X., Crow, W.T.,  
 1440 Eylander, J.B., Houser, P.R., 2008a. A land surface data assimilation framework using  
 1441 the land information system: Description and applications. *Adv. Water Resour.* 31,  
 1442 1419–1432. <https://doi.org/10.1016/j.advwatres.2008.01.013>.
- 1443 Kumar, S., Peters-Lidard, C., Tian, Y., Reichle, R.H., Geiger, J., Alonge, C., Eylander, J.,  
 1444 Houser, P., 2008b. An integrated hydrologic modeling and data assimilation framework.  
 1445 *Computer* 41, 52–59. <https://doi.org/10.1109/MC.2008.475>.
- 1446 Kumar, S.V., Reichle, R.H., Koster, R.D., Crow, W.T., Peters-Lidard, C.D., 2009. Role of  
 1447 subsurface physics in the assimilation of surface soil moisture observations. *J.*  
 1448 *Hydrometeorol.* 10, 1534–1547. <https://doi.org/10.1175/2009JHM1134.1>.
- 1449 Kumar, S.V., Peters-Lidard, C.D., Mocko, D., Reichle, R., Liu, Y., Arsenault, K.R., Xia, Y.,  
 1450 Ek, M., Riggs, G., Livneh, B., Cosh, M., 2014. Assimilation of remotely sensed soil

1451 moisture and snow depth retrievals for drought estimation. *J. Hydrometeorol.* 15, 2446–  
1452 2469, <https://doi.org/10.1175/JHM-D-13-0132.1>.

1453 Kumar, S.V., Peters-Lidard, C.D., Santanello, J.A., Reichle, R.H., Draper, C.S., Koster, R.D.,  
1454 Nearing, G., Jasinski, M.F., 2015. Evaluating the utility of satellite soil moisture  
1455 retrievals over irrigated areas and the ability of land data assimilation methods to  
1456 correct for unmodeled processes. *Hydrol. Earth Syst. Sci.* 19, 4463–4478.  
1457 <https://doi.org/10.5194/hess-19-4463-2015>.

1458 Kumar, S.V., Dong, J., Peters-Lidard, C.D., Mocko, D., Gómez, B., 2017. Role of forcing  
1459 uncertainty and background model error characterization in snow data assimilation.  
1460 *Hydrol. Earth Syst. Sci.* 21, 2637–2647. <https://doi.org/10.5194/hess-21-2637-2017>.

1461 Kumar, S.V., Dirmeyer, P.A., Peters-Lidard, C.D., Bindlish, R., Bolten, J., 2018. Information  
1462 theoretic evaluation of satellite soil moisture retrievals. *Remote Sens. Environ.* 204,  
1463 392–400. <https://doi.org/10.1016/j.rse.2017.10.016>.

1464 Kumar, S.V., Jasinski, M., Mocko, D.M., Rodell, M., Borak, J., Li, B., Beaudoin, H.K.,  
1465 Peters-Lidard, C.D., 2019. NCA-LDAS land analysis: Development and performance  
1466 of a multisensory, multivariate land data assimilation system for the national climate  
1467 assessment. *J. Hydrometeorol.* 20, 1571–1593. <https://doi.org/10.1175/JHM-D-17-0125.1>.

1469 Kwon, I.-H., Song, H.-J., Ha, J.-H., Chun, H.-W., Kang, J.-H., Lee, S., Lim, S., Jo, Y., Han,  
1470 H.-J., Jeong, H., Kwon, H.-N., Shin, S., Kim, T.-H., 2018. Development of an  
1471 operational hybrid data assimilation system at KIAPS. *Asia-Pac. J. Atmos. Sci.* 54,  
1472 319–335. <https://doi.org/10.1007/s13143-018-0029-8>.

1473 Kwon, Y., Forman, B.A., Ahmad, J.A., Kumar, S.V., Yoon, Y., 2019. Exploring the utility of  
1474 machine learning-based passive microwave brightness temperature data assimilation  
1475 over terrestrial snow in High Mountain Asia. *Remote Sens.* 11, 2265.  
1476 <https://doi.org/10.3390/rs11192265>.

1477 Kwon, Y., Yoon, Y., Forman, B.A., Kumar, S.V., Wang, L., 2021. Quantifying the  
1478 observational requirements of a space-borne LiDAR snow mission. *J. Hydrol.* 601,  
1479 126709. <https://doi.org/10.1016/j.jhydrol.2021.126709>.

1480 Kwon, Y., Kumar, S.V., Navari, M., Mocko, D.M., Kemp, E.M., Wegiel, J.W., Geiger, J.V.,  
1481 Bindlish, R., 2022. Irrigation characterization improved by the direct use of SMAP soil  
1482 moisture anomalies within a data assimilation system. *Environ. Res. Lett.* 17, 084006.  
1483 <https://doi.org/10.1088/1748-9326/ac7f49>.

1484 Kwon, Y., Jun, S., Kim, E., Seol, K.-H., Hong, S., Kwon, I.-H., Kang, J.-H., Kim, H., 2024.  
1485 Improving weather forecast skill of the Korean Integrated Model by assimilating Soil  
1486 Moisture Active Passive soil moisture anomalies. *Q. J. Roy. Meteor. Soc.* 150, 5305–  
1487 5336. <https://doi.org/10.1002/qj.4871>.

1488 Laiolo, P., Gabellani, S., Campo, L., Silvestro, F., Delogu, F., Rudari, R., Pulvirenti, L., Boni,  
1489 G., Fascetti, F., Pierdicca, N., Crapolicchio, R., Hasenauer, S., Puca, S., 2016. Impact  
1490 of different satellite soil moisture products on the predictions of a continuous  
1491 distributed hydrological model. *Int. J. Appl. Earth Obs.* 48, 131–145.  
1492 <https://doi.org/10.1016/j.jag.2015.06.002>.

- 1493 [Lamichhane, M., Mehan, S., Mankin, K.R., 2025. Surface soil moisture prediction using](#)  
1494 [multimodal remote sensing data fusion and machine learning algorithms in semi-arid](#)  
1495 [agricultural region. \*Sci. Remote Sens.\* 12, 100255.](#)  
1496 [https://doi.org/10.1016/j.srs.2025.100255.](https://doi.org/10.1016/j.srs.2025.100255)
- 1497 Lee, S., Song, H.-J., Chun, H.-W., Kwon, I.-H., Kang, J.-H., Lim, S., 2020. All-sky  
1498 microwave humidity sounder assimilation in the Korean Integrated Model forecast  
1499 system. *Q. J. Roy. Meteor. Soc.* 146, 3570-3586. [https://doi.org/10.1002/qj.3862.](https://doi.org/10.1002/qj.3862)
- 1500 [Lei, F., Crow, W.T., Holmes, T.R.H., Hain, C., Anderson, M.C., 2018. Global investigation](#)  
1501 [of soil moisture and latent heat flux coupling strength. \*Water Resour. Res.\* 54, 8196–](#)  
1502 [8215. \[https://doi.org/10.1029/2018WR023469.\]\(https://doi.org/10.1029/2018WR023469\)](#)
- 1503 Li, S., Zhang, L., Ma, R., Yan, M., Tian, X., 2020. Improved ET assimilation through  
1504 incorporating SMAP soil moisture observations using a coupled process model: A  
1505 study of U.S. arid and semiarid regions. *J. Hydrol.* 590, 125402.  
1506 [https://doi.org/10.1016/j.jhydrol.2020.125402.](https://doi.org/10.1016/j.jhydrol.2020.125402)
- 1507 Lievens, H., De Lannoy, G.J.M., Al Bitar, A., Drusch, M., Dumedah, G., Hendricks Franssen,  
1508 H.-J., Kerr, Y.H., Tomer, S.K., Martens, B., Merlin, O., Pan, M., Roundy, J.K.,  
1509 Vereecken, H., Walker, J.P., Wood, E.F., Verhoest, N.E.C., Pauwels, V.R.N., 2016.  
1510 Assimilation of SMOS soil moisture and brightness temperature products into a land  
1511 surface model. *Remote Sens. Environ.* 180, 292–304.  
1512 [https://doi.org/10.1016/j.rse.2015.10.033.](https://doi.org/10.1016/j.rse.2015.10.033)
- 1513 [Lin, X., Huang, S., Li, J., Huang, Q., Shi, H., She, D., Leng, G., Wei, X., Guo, W., Liu, Y.,](#)  
1514 [Luo, J., 2023. Feedback dynamics between precipitation, temperature, and soil](#)  
1515 [moisture in China and their possible driving mechanisms under a changing](#)  
1516 [environment. \*Atmos. Res.\* 294, 106983.](#)  
1517 [https://doi.org/10.1016/j.atmosres.2023.106983.](https://doi.org/10.1016/j.atmosres.2023.106983)
- 1518 [Lin, L.-F., Pu, Z., 2019. Examining the impact of SMAP soil moisture retrievals on short-](#)  
1519 [range weather prediction under weakly and strongly coupled data assimilation with](#)  
1520 [WRF-Noah. \*Mon. Weather Rev.\* 147, 4345–4366. \[0017.1.\]\(https://doi.org/10.1175/MWR-D-19-</a></a><br/>1521 <a href=\)](#)
- 1522 Lin, L.-F., Pu, Z., 2020. Improving near-surface short-range weather forecasts using strongly  
1523 coupled land–atmosphere data assimilation with GSI-EnKF. *Mon. Weather Rev.* 148,  
1524 2863–2888. [https://doi.org/10.1175/MWR-D-19-0370.1.](https://doi.org/10.1175/MWR-D-19-0370.1)
- 1525 Liu, Q., Reichle, R.H., Bindlish, R., Cosh, M.H., Crow, W.T., de Jeu, R., De Lannoy, G.J.M.,  
1526 Huffman, G.J., Jackson, T.J., 2011. The contributions of precipitation and soil moisture  
1527 observations to the skill of soil moisture estimates in a land data assimilation system. *J.*  
1528 *Hydrometeorol.* 12, 750–765. [https://doi.org/10.1175/JHM-D-10-05000.1.](https://doi.org/10.1175/JHM-D-10-05000.1)
- 1529 Lodh, A., Routray, A., Dutta, D., George, J.P., Mitra, A.K., 2022. Improving the prediction of  
1530 monsoon depressions by assimilating ASCAT soil moisture in NCUM-R modeling  
1531 system. *Atmos. Res.* 272, 106130. [https://doi.org/10.1016/j.atmosres.2022.106130.](https://doi.org/10.1016/j.atmosres.2022.106130)
- 1532 [Long, D., Bai, L., Yan, L., Zhang, C., Yang, W., Lei, H., Quan, J., Meng, X., Shi, C., 2019.](#)  
1533 [Generation of spatially complete and daily continuous surface soil moisture of high](#)  
1534 [spatial resolution. \*Remote Sens. Environ.\* 233, 111364.](#)  
1535 [https://doi.org/10.1016/j.rse.2019.111364.](https://doi.org/10.1016/j.rse.2019.111364)

1536 Lorenc, A.C., Bowler, N.E., Clayton, A.M., Pring, S.R., Fairbairn, D., 2015. Comparison of  
1537 hybrid-4DEnVar and hybrid-4DVar data assimilation methods for global NWP. *Mon.*  
1538 *Weather Rev.* 143, 212–229. <https://doi.org/10.1175/MWR-D-14-00195.1>.

1539 Manco, I., De Lucia, C., Repola, F., Fedele, G., Mercogliano, P., 2023. A comparative  
1540 performance study of WRF, COSMO and ICON atmospheric models for the Italian  
1541 peninsula at very high resolution. *Tethys* 20, 1–20.  
1542 <https://doi.org/10.3369/tethys.2023.20.01>.

1543 Miller, D.A., White, R.A., 1998. A conterminous United States multilayer soil characteristics  
1544 dataset for regional climate and hydrology modelling. *Earth Interact.* 2, 1–26.  
1545 [https://doi.org/10.1175/1087-3562\(1998\)002<0001:ACUSMS>2.3.CO;2](https://doi.org/10.1175/1087-3562(1998)002<0001:ACUSMS>2.3.CO;2).

1546 [Min, X., Shangguan, Y., Li, D., Shi, Z., 2022. Improving the fusion of global soil moisture](#)  
1547 [datasets from SMAP, SMOS, ASCAT, and MERRA2 by considering the non-zero](#)  
1548 [error covariance. \*Int. J. Appl. Earth Obs.\* 113, 103016.](#)  
1549 <https://doi.org/10.1016/j.jag.2022.103016>.

1550 [Muñoz-Sabater, J., Lawrence, H., Albergel, C., de Rosnay, P., Isaksen, L., Mecklenburg, S. et](#)  
1551 [al., 2019. Assimilation of SMOS brightness temperatures in the ECMWF integrated](#)  
1552 [forecasting system. \*Q. J. Roy. Meteor. Soc.\* 145, 2524–2548.](#)  
1553 <https://doi.org/10.1002/QJ.3577>.

1554 Nair, A.S., Indu, J., 2018. A coupled land surface and radiative transfer models based on  
1555 relief correction for a reliable land data assimilation over mountainous terrain. *IEEE*  
1556 *Geosci. Remote Sens. Lett.* 15, 1657–1661.  
1557 <https://doi.org/10.1109/LGRS.2018.2854908>.

1558 Nair, A.S., Indu, J., 2019. Improvement of land surface model simulations over India via data  
1559 assimilation of satellite-based soil moisture products. *J. Hydrol.* 573, 406–421.  
1560 <https://doi.org/10.1016/j.jhydrol.2019.03.088>.

1561 Nearing, G., Yatheendradas, S., Crow, W., Zhan, X., Liu, J., Chen, F., 2018. The efficiency  
1562 of data assimilation. *Water Resour. Res.* 54, 6374–6392.  
1563 <https://doi.org/10.1029/2017WR020991>.

1564 Nguyen, H.H., Kim, H., Crow, W., Yueh, S., Wagner, W., Lei, F., Wigneron, J.-P.,  
1565 Colliander, A., Frappart, F., 2025. From theory to hydrological practice: Leveraging  
1566 CYGNSS data over seven years for advanced soil moisture monitoring. *Remote Sens.*  
1567 *Environ.* 316, 114509. <https://doi.org/10.1016/j.rse.2024.114509>.

1568 O'Neill, P.E., Chan, S., Njoku, E.G., Jackson, T., Bindlish, R., Chaubell, J., 2021. SMAP L2  
1569 radiometer half-orbit 36 km EASE-grid soil moisture, version 8 [Data Set]. Boulder,  
1570 Colorado USA. NASA National Snow and Ice Data Center Distributed Active Archive  
1571 Center. <https://doi.org/10.5067/LPJ8F0TAK6E0>. Date Accessed 06-01-2023.

1572 Orth, R., Seneviratne, S.I., 2013. Propagation of soil moisture memory to streamflow and  
1573 evapotranspiration in Europe. *Hydrol. Earth Syst. Sci.* 17, 3895–3911.  
1574 <https://doi.org/10.5194/hess-17-3895-2013>.

1575 [Pal, J.S., Eltahir, E.A.B., 2003. A feedback mechanism between soil-moisture distribution](#)  
1576 [and storm tracks. \*Q. J. Roy. Meteor. Soc.\* 129, 2279–2297.](#)  
1577 <https://doi.org/10.1256/qj.01.201>.

1578 Paloscia, S., Pampaloni, P., 1988. Microwave polarization index for monitoring vegetation  
1579 growth. *IEEE Trans. Geosci. Remote Sens.* 26, 617–621.  
1580 <https://doi.org/10.1109/36.7687>.

1581 Peters-Lidard, C.D., Houser, P.R., Tian, Y., Kumar, S.V., Geiger, J., Olden, S., Lighty, L.,  
1582 Doty, B., Dirmeyer, P., Adams, J., Mitchell, K., Wood, E.F., Sheffield, J., 2007. High-  
1583 performance Earth system modeling with NASA/GSFC's land information system.  
1584 *Innov. Syst. Softw. Eng.* 3, 157–165. <https://doi.org/10.1007/s11334-007-0028-x>.

1585 Pipunic, R.C., Walker, J.P., Western, A.W., Trudinger, C.M., 2013. Assimilation of multiple  
1586 data types for improved heat flux prediction: a one-dimensional field study. *Remote*  
1587 *Sens. Environ.* 136, 315–329. <http://dx.doi.org/10.1016/j.rse.2013.05.015>.

1588 Polichtchouk, I., van Niekerk, A., Wedi, N., 2023. Resolved gravity waves in the  
1589 extratropical stratosphere: Effect of horizontal resolution increase from O(10) to O(1)  
1590 km. *J. Atmos. Sci.* 80, 473–486. <https://doi.org/10.1175/JAS-D-22-0138.1>.

1591 Reichle, R.H., McLaughlin, D.B., Entekhabi, D., 2002a. Hydrologic data assimilation with  
1592 the ensemble Kalman filter. *Mon. Weather Rev.* 130, 103–114.  
1593 [https://doi.org/10.1175/1520-0493\(2002\)130<0103:HDAWTE>2.0.CO;2](https://doi.org/10.1175/1520-0493(2002)130<0103:HDAWTE>2.0.CO;2).

1594 Reichle, R.H., Walker, J.P., Koster, R.D., Houser, P.R., 2002b. Extended versus ensemble  
1595 Kalman filtering for land data assimilation. *J. Hydrometeorol.* 3, 728–740.  
1596 [https://doi.org/10.1175/1525-7541\(2002\)003<0728:EVEKFF>2.0.CO;2](https://doi.org/10.1175/1525-7541(2002)003<0728:EVEKFF>2.0.CO;2).

1597 Reichle, R.H., Koster, R.D., 2004. Bias reduction in short records of satellite soil moisture.  
1598 *Geophys. Res. Lett.* 31, L19501. <https://doi.org/10.1029/2004GL020938>.

1599 Reichle, R.H., Koster, R.D., Liu, P., Mahanama, S.P.P., Njoku, E.G., Owe, M., 2007.  
1600 Comparison and assimilation of global soil moisture retrievals from the advanced  
1601 microwave scanning radiometer for the earth observing system (AMSR-E) and the  
1602 scanning multichannel microwave radiometer (SMMR). *J. Geophys. Res. Atmos.* 112,  
1603 D09108. <https://doi.org/10.1029/2006JD008033>.

1604 Reichle, R.H., Crow, W.T., Koster, R.D., Sharif, H.O., Mahanama, S.P.P., 2008.  
1605 Contribution of soil moisture retrievals to land data assimilation products. *Geophys.*  
1606 *Res. Lett.* 35, L01404. <https://doi.org/10.1029/2007GL031986>.

1607 Reichle, R.H., Zhang, S.Q., Kolassa, J., Liu, Q., Todling, R., 2023. A weakly-coupled land  
1608 surface analysis with SMAP radiance assimilation improves GEOS medium-range  
1609 forecasts of near-surface air temperature and humidity. *Q. J. Roy. Meteor. Soc.* 149,  
1610 1867–1889. <https://doi.org/10.1002/qj.4486>.

1611 Renzullo, L.J., van Dijk, A.I.J.M., Perraud, J.-M., Collins, D., Henderson, B., Jin, H., Smith,  
1612 A.B., McJannet, D.L., 2014. Continental satellite soil moisture data assimilation  
1613 improves root-zone moisture analysis for water resources assessment. *J. Hydrol.* 519,  
1614 2747–2762. <https://doi.org/10.1016/j.jhydrol.2014.08.008>.

1615 Reynolds, C.A., Jackson, T.J., Rawls, W.J., 2000. Estimating soil water-holding capacities by  
1616 linking the Food and Agriculture Organization Soil map of the world with global pedon  
1617 databases and continuous pedotransfer functions. *Water Resour. Res.* 36, 3653–3662.  
1618 <https://doi.org/10.1029/2000WR900130>.

- 1619 Ricker, M., Behrens, A., Staneva, J., 2024. The operational CMEMS wind wave forecasting  
 1620 system of the Black Sea. *J. Oper. Oceanogr.* 1–22.  
 1621 <https://doi.org/10.1080/1755876X.2024.2364974>.
- 1622 Rodell, M., Houser, P.R., Jambor, U., Gottschalk, J., Mitchell, K., Meng, C.-J., Arsenault,  
 1623 K., Cosgrove, B., Radakovich, J., Bosilovich, M., Entin, J.K., Walker, J.P., Lohmann,  
 1624 D., Toll, D., 2004. The Global Land Data Assimilation System. *Bull. Am. Meteorol.*  
 1625 *Soc.* 85, 381–394. <https://doi.org/10.1175/BAMS-85-3-381>.
- 1626 Sacchetti, D., Cassola, F., Corazza, M., Pedemonte, L., Tizzi, M., Drofa, O., Davolio, S.,  
 1627 2024. The ARPAL atmospheric operational modeling chain and its applications:  
 1628 description and validation. *Bull. Atmos. Sci. Technol.* 5, 1.  
 1629 <https://doi.org/10.1007/s42865-024-00064-z>.
- 1630 Santanello Jr., J.A., Kumar, S.V., Peters-Lidard, C.D., Lawston, P.M., 2016. Impact of soil  
 1631 moisture assimilation on land surface model spinup and coupled land–atmosphere  
 1632 prediction. *J. Hydrometeorol.* 17, 517–540. <https://doi.org/10.1175/JHM-D-15-0072.1>.
- 1633 Schaake, J.C., Koren, V.I., Duan, Q.Y., Mitchell, K., Chen, F., 1996. A simple water balance  
 1634 model (SWB) for estimating runoff at different spatial and temporal scales. *J. Geophys.*  
 1635 *Res.* 101, 7461–7475. <https://doi.org/10.1029/95JD02892>.
- 1636 Schmugge, T.J., O'Neill, P.E., Wang, J.R., 1986. Passive microwave soil moisture research.  
 1637 *IEEE Trans. Geosci. Remote Sens.* GE-24, 1.  
 1638 <http://dx.doi.org/10.1109/TGRS.1986.289584>.
- 1639 Scipal, K., Holmes, T., De Jeu, R., Naeimi, V., Wagner, W., 2008. A possible solution for the  
 1640 problem of estimating the error structure of global soil moisture data sets. *Geophys.*  
 1641 *Res. Lett.* 35, L24403, <https://doi.org/10.1029/2008GL035599>.
- 1642 Seo, E., Lee, M.-I., Reichle, R.H., 2021. Assimilation of SMAP and ASCAT soil moisture  
 1643 retrievals into the JULES land surface model using the Local Ensemble Transform  
 1644 Kalman Filter. *Remote Sens. Environ.* 253, 112222.  
 1645 <https://doi.org/10.1016/j.rse.2020.112222>.
- 1646 Shellito, P.J., Small, E.E., Cosh, M.H., 2016. Calibration of Noah soil hydraulic property  
 1647 parameters using surface soil moisture from SMOS and Basinwide in situ observations.  
 1648 *J. Hydrometeorol.* 17, 2275–2292. <https://doi.org/10.1175/JHM-D-15-0153.1>.
- 1649 Shellito, P.J., Small, E.E., Livneh, B., 2018. Controls on surface soil drying rates observed by  
 1650 SMAP and simulated by the Noah land surface model. *Hydrol. Earth Syst. Sci.* 22,  
 1651 1649–1663. <https://doi.org/10.5194/hess-22-1649-2018>.
- 1652 Shin, Y., Jung, Y., 2014. Development of irrigation water management model for reducing  
 1653 drought severity using remotely sensed soil moisture footprints *J. Irrig. Drain. Eng.* 140,  
 1654 04014021. [https://doi.org/10.1061/\(ASCE\)IR.1943-4774.0000736](https://doi.org/10.1061/(ASCE)IR.1943-4774.0000736).
- 1655 Shin, S., Kang, J.-S., Jo, Y., 2016. The local ensemble transform Kalman filter (LETKF) with  
 1656 a global NWP model on the cubed sphere. *Pure Appl. Geophys.* 173, 2555–2570,  
 1657 <https://doi.org/10.1007/s00024-016-1269-0>.
- 1658 Shin, S., Kang, J.-H., Chun, H.-W., Lee, S., Sung, K., Cho, K., Jo, Y., Kim, J.-E., Kwon, I.-  
 1659 H., Lim, S., Kang, J.-S., 2018. Real data assimilation using the Local Ensemble  
 1660 Transform Kalman Filter (LETKF) system for a global nonhydrostatic NWP model on

- 1661 the cubed-sphere. *Asia-Pac. J. Atmos. Sci.* 54, 351–360.  
1662 <https://doi.org/10.1007/s13143-018-0022-2>.
- 1663 [Singh, A., Gaurav, K., 2023. Deep learning and data fusion to estimate surface soil moisture](#)  
1664 [from multi-sensor satellite images. \*Sci. Rep.\* 13, 2251. \[https://doi.org/10.1038/s41598-\]\(https://doi.org/10.1038/s41598-023-28939-9\)](#)  
1665 [023-28939-9.](#)
- 1666 Song, H.-J., Kwon, I.-H., 2015. Spectral transformation using a cubed-sphere grid for a three-  
1667 dimensional variational data assimilation system. *Mon. Weather Rev.* 143, 2581–2599.  
1668 <https://doi.org/10.1175/MWR-D-14-00089.1>.
- 1669 Song, H.-J., Shin, S., Ha, J.-H., Lim, S., 2017. The advantages of hybrid 4D-EnVar in the  
1670 context of the forecast sensitivity to initial conditions. *J. Geophys. Res. Atmos.* 122,  
1671 12226–12244. <https://doi.org/10.1002/2017JD027598>.
- 1672 Stoffelen, A., 1998. Toward the true near-surface wind speed: error modeling and calibration  
1673 using triple collocation. *J. Geophys. Res.* 103, 7755–7766.  
1674 <https://doi.org/10.1029/97JC03180>.
- 1675 Tangdamrongsub, N., Han, S.-C., Yeo, I.-Y., Dong, J., Steele-Dunne, S.C., Willgoose, G.,  
1676 Walker, J.P., 2020. Multivariate data assimilation of GRACE, SMOS, SMAP  
1677 measurements for improved regional soil moisture and groundwater storage estimates.  
1678 *Adv. Water Resour.* 135, 103477. <https://doi.org/10.1016/j.advwatres.2019.103477>.
- 1679 Torcasio, R.C., Mascitelli, A., Realini, E., Barindelli, S., Tagliaferro, G., Puca, S., Dietrich,  
1680 S., Federico, S., 2023. The impact of global navigation satellite system (GNSS) zenith  
1681 total delay data assimilation on the short-term precipitable water vapor and  
1682 precipitation forecast over Italy using the Weather Research and Forecasting (WRF)  
1683 model. *Nat. Hazards Earth Syst. Sci.* 23, 3319–3336. [https://doi.org/10.5194/nhess-23-](https://doi.org/10.5194/nhess-23-3319-2023)  
1684 [3319-2023.](#)
- 1685 Tuttle, S., Salvucci, G., 2016. Empirical evidence of contrasting soil moisture–precipitation  
1686 feedbacks across the United States. *Science* 352, 825–828.  
1687 <https://doi.org/10.1126/science.aaa7185>.
- 1688 van den Hurk, B., Doblas-Reyes, F., Balsamo, G., Koster, R.D., Seneviratne, S.I., Camargo Jr,  
1689 H., 2012. Soil moisture effects on seasonal temperature and precipitation forecast  
1690 scores in Europe. *Climate Dyn.* 38, 349–362. [https://doi.org/10.1007/s00382-010-](https://doi.org/10.1007/s00382-010-0956-2)  
1691 [0956-2.](#)
- 1692 [van der Schalie, R., de Jeu, R., Rodríguez-Fernández, N., Al-Yaari, A., Kerr, Y., Wigneron,](#)  
1693 [J.-P., Parinussa, R., Drusch, M., 2018. The Effect of three different data fusion](#)  
1694 [approaches on the quality of soil moisture retrievals from multiple passive microwave](#)  
1695 [sensors. \*Remote Sens.\* 10, 107. <https://doi.org/10.3390/rs10010107>.](#)
- 1696 Wagner, W., Lemoine, G., Rott, H., 1999. A method for estimating soil moisture from ERS  
1697 scatterometer and soil data. *Remote Sens. Environ.* 70, 191–207.  
1698 [https://doi.org/10.1016/S0034-4257\(99\)00036-X](https://doi.org/10.1016/S0034-4257(99)00036-X).
- 1699 Wagner, W., Bartalis, Z., Naeimi, V., Park, S.-E., Figa-Saldaña, J., Bonekamp, H., 2010.  
1700 Status of the MetOp ASCAT soil moisture product. *IEEE Int. Geosci. Remote. Se.*  
1701 *Proceedings.* 25-30 July 2010, 276–279.  
1702 <https://doi.org/10.1109/IGARSS.2010.5653358>.

1703 Wagner, W., Hahn, S., Kidd, R., Melzer, T., Bartalis, Z., Hasenauer, S., Figa-Saldaña, J., De  
1704 Rosnay, P., Jann, A., Schneider, S., Komma, J., Kubu, G., Brugger, K., Aubrecht, C.,  
1705 Züger, J., Gangkofner, U., Kienberger, S., Brocca, L., Wang, Y., Blöschl, G., Eitzinger,  
1706 J., Steinnocher, K., Zeil, P., Rubel, F., 2013. The ASCAT soil moisture product: A  
1707 review of its specifications, validation results, and emerging applications.  
1708 Meteorologische Zeitschrift 22, 5–33. <https://doi.org/10.1127/0941-2948/2013/0399>.

1709 Wagner, W., Lindorfer, R., Hahn, S., Kim, H., Vreugdenhil, M., Gruber, A., Fischer, M.,  
1710 Trnka, M., 2024. Global scale mapping of subsurface scattering signals impacting  
1711 ASCAT soil moisture retrievals. IEEE Trans. Geosci. Remote Sens. 62, 4509520.  
1712 <https://doi.org/10.1109/TGRS.2024.3429550>.

1713 Wanders, N., Karssenbergh, D., de Roo, A., de Jong, S.M., Bierkens, M.F.P., 2014. The  
1714 suitability of remotely sensed soil moisture for improving operational flood forecasting,  
1715 Hydrol. Earth Syst. Sci. 18, 2343–2357. <https://doi.org/10.5194/hess-18-2343-2014>.

1716 [Wang, Y., Mao, J., Jin, M., Hoffman, F.M., Shi, X., Wullschleger, S.D., Dai, Y., 2021. Development of observation-based global multilayer soil moisture products for 1970 to 2016. Earth Syst. Sci. Data 13, 4385–4405. https://doi.org/10.5194/essd-13-4385-2021.](#)

1717  
1718

1719 Whitaker, J.S., Hamill, T.M., 2012. Evaluating methods to account for system errors in  
1720 ensemble data assimilation. Mon. Weather Rev. 140, 3078–3089.  
1721 <https://doi.org/10.1175/MWR-D-11-00276.1>.

1722 WMO, 2008. Recommendations for the verification and intercomparison of QPFs and PQPFs  
1723 from operational NWP models. WWRP 2009-1, World Meteorological Organization  
1724 (WMO), Switzerland.

1725 Wu, K., Ryu, D., Nie, L., Shu, H., 2021. Time-variant error characterization of SMAP and  
1726 ASCAT soil moisture using Triple Collocation Analysis. Remote Sens. Environ. 256,  
1727 112324. <https://doi.org/10.1016/j.rse.2021.112324>.

1728 Xie, P., Yatagai, A., Chen, M., Hayasaka, T., Fukushima, Y., Liu, C., Yang, S., 2007. A  
1729 gauge-based analysis of daily precipitation over East Asia. J. Hydrometeorol. 8, 607–  
1730 626. <https://doi.org/10.1175/JHM583.1>.

1731 [Xie, Q., Jia, L., Menenti, M., Hu, G., 2022. Global soil moisture data fusion by Triple Collocation Analysis from 2011 to 2018. Sci. Data 9, 687. https://doi.org/10.1038/s41597-022-01772-x.](#)

1732  
1733

1734 Xu, T., Chen, F., He, X., Barlage, M., Zhang, Z., Liu, S., He, X., 2021. Improve the  
1735 performance of the Noah-MP-Crop model by jointly assimilating soil moisture and  
1736 vegetation phenology data. J. Adv. Model. Earth Sy. 13, e2020MS002394.  
1737 <https://doi.org/10.1029/2020MS002394>.

1738 [Yang, L., Sun, G., Zhi, L., Zhao, J., 2018. Negative soil moisture-precipitation feedback in dry and wet regions. Sci. Rep. 8, 4026. https://doi.org/10.1038/s41598-018-22394-7.](#)

1739  
1740 [Yin, J., Hain, C.R., Zhan, X., Dong, J., Ek, M., 2019. Improvements in the forecasts of near-surface variables in the Global Forecast System \(GFS\) via assimilating ASCAT soil moisture retrievals. J. Hydrol. 578, 124018. https://doi.org/10.1016/j.jhydrol.2019.124018.](#)

1741  
1742  
1743

1744 Yuan, X., Wood, E.F., Luo, L., Pan, M., 2011. A first look at Climate Forecast System  
1745 version 2 (CFSv2) for hydrological seasonal prediction. Geophys. Res. Lett. 38,  
1746 L13402. <https://doi.org/10.1029/2011GL047792>.

1747 ~~Yin, J., Hain, C.R., Zhan, X., Dong, J., Ek, M., 2019. Improvements in the forecasts of near-~~  
1748 ~~surface variables in the Global Forecast System (GFS) via assimilating ASCAT soil-~~  
1749 ~~moisture retrievals. J. Hydrol. 578, 124018.~~  
1750 ~~<https://doi.org/10.1016/j.jhydrol.2019.124018>.~~

1751 Zhang, H., Wang, S., Liu, K., Li, X., Li, Z., Zhang, X., Liu, B., 2022. Downscaling of  
1752 AMSR-E soil moisture over north China using random forest regression. ISPRS Int. J.  
1753 Geo Inf. 11, 101. <https://doi.org/10.3390/ijgi11020101>.

1754 Zheng, J., Yuan, X., Ji, P., 2024. The important role of reliable land surface model simulation  
1755 in high-resolution multi-source soil moisture data fusion by machine learning. J.  
1756 Hydrol. 630, 130700. <https://doi.org/10.1016/j.jhydrol.2024.130700>.